

UNIVERSITÀ DEGLI STUDI DI NAPOLI
"FEDERICO II"



SCUOLA POLITECNICA E DELLE SCIENZE DI BASE

Department of Industrial Engineering

Master's Degree Dissertation in
AEROSPACE AND ASTRONAUTIC ENGINEERING

DESIGN METHODOLOGIES FOR AIRCRAFT
NOISE ESTIMATION WITH PARAMETRIC
ANALYSIS

Author

Valerio Marciello

Thesis Advisors

Prof. Fabrizio Nicolosi

Prof. Francesco Marulo

Co-Advisors

Mario Di Stasio

Paul Traub

Dr. Sirka Fuhrmann

Academic Year 2019/2020

*To my mother,
whose loving spirit guides me
every day of my life,*

and

*to Maria Vittoria,
who makes everything wonderful
with her colorful mind.*

Acknowledgements

I would like to express my deep gratitude to Professor Nicolosi and Professor Marulo, my thesis advisors, for their constant guidance and for giving me an important opportunity for human and professional growth. I would also like to extend my thanks to the DAF research group for their essential advices on object-oriented programming.

I wish to thank Dr. Fuhrmann, Dr. Schaber, Mr. Traub, Mr. Schmier and every other member from the family of MTU Aero Engines, who welcomed me and collaborated with me in the realization of this work.

I wish to thank my friends, and in particular my fellow students, for enriching the years of our education with unforgettable memories.

A heartfelt thanks to Maria Vittoria Moxedano, for always seeing the best in me, even when I could not see it myself.

Finally, special thanks go to my family, for always encouraging me to pursue my aspirations without ever doubting my abilities, for always guaranteeing all the support I needed, and for never ceasing to watch over me.

Abstract

Analysis of scenario

A major challenge in the transport sector is to make economic growth compatible with environmental constraints, while remaining competitive and innovative. The loose integration of engine models into iterative design workflows has prevented aircraft manufacturers from implementing efficient, cost-effective solutions. The search for a new paradigm has led European programmes such as Clean Sky 2 to coordinate and finance research activities aimed at delivering a more sustainable aviation with reduced gas emissions and noise levels. Among these, the ADORNO project has originated from the partnership of the University of Naples with MTU Aero Engines and Lead Tech. Its objectives include the development of a computer method for the prediction of aircraft noise, allowing to consider acoustic emissions from the early stages of design processes. In order to accelerate the attainment of this goal, the candidate has completed an internship activity at the headquarters of MTU.

Statement of the problem

The new software had to comply with several constraints concerning compatibility with the development environments in use at MTU. The new code had to be written in C++, following the paradigms of object-oriented programming. It had to rely on methods capable of predicting the noise generated by moving turbofan aircraft, with reference to microphones placed at arbitrary positions, including both aerodynamic and propulsive sources as well as the effects of sound propagation in the atmosphere.

Adopted methodology

Based on a pre-existing MATLAB code developed at UNINA, the new program has been redesigned by the candidate and named ATTILA⁺⁺. The employed semi-empirical methods, provided by some ESDU Items, allow to calculate the aerodynamic noise starting from a few geometric data. The engine noise is calculated by external programs and given to the software as additional input. All contributions are adjusted for atmospheric attenuation, ground reflection and lateral attenuation.

Main results

The first version of ATTILA⁺⁺ has been completed in compliance with the technical requirements. In order to test its potential, a parametric analysis of the airframe noise has been conducted on a specific regional aircraft, with the main objective of identifying the geometric parameters with the greatest impact on the total noise level. Preliminary results have shown that efforts made to reduce aerodynamic noise are rewarded only in the approach conditions envisaged by the regulatory authority. It has been found that switching from single- to triple-slotted flaps can lead to an increase of + 3.2 dB in airframe noise and + 1.7 dB in the total effective perceived noise level (EPNL). Reducing the flap deflection by 10° has resulted in a reduction of 0.34 % in the total EPNL. Doubling the main wheels has increased the EPNL by 0.53 %, while halving their diameter has led to − 0.26 %. Lastly, the acoustic footprints left by the aircraft during take-off and landing have been reproduced.

Keywords

Airframe noise, object-oriented programming, sensitivity analysis.

Contents

1	Introduction	1
1.1	Background	1
1.2	Objective	4
1.3	Thesis outline	4
2	Elements of Aviation Acoustics and Noise Certification	5
2.1	Introduction to aviation acoustics	5
2.1.1	General definitions	5
2.1.2	Frequency and period	6
2.1.3	Wavefronts, wavelength, sound rays	7
2.1.4	Speed of sound	7
2.1.5	Sound fields	7
2.2	Frequency spectra	8
2.2.1	Fourier transform	8
2.2.2	Third octave bands	8
2.3	Fundamental sound metrics	10
2.3.1	Sound pressure	10
2.3.2	Effective sound pressure	10
2.3.3	Acoustic power	11
2.3.4	Power watt level	11
2.3.5	Sound intensity	11
2.3.6	Sound intensity level	12
2.3.7	Sound pressure level	12
2.4	Integral sound metrics	14
2.4.1	Overall sound pressure level	14
2.4.2	Noisiness level	14
2.4.3	Perceived noise level	14
2.4.4	Tone-corrected perceived noise level	15
2.4.5	Effective perceived noise level	17
2.5	Propagation and motion effects	19
2.5.1	Overview	19
2.5.2	Spreading effect	19

2.5.3	Doppler shift	19
2.5.4	Atmospheric attenuation of the sound	20
2.5.5	Ground reflection effect	21
2.6	Aircraft noise and noise certification	23
2.6.1	Noise pollution	23
2.6.2	Engine noise	23
2.6.3	Airframe noise	26
2.6.4	Noise certification	27
2.6.5	Certification of subsonic jet aircraft	28
3	Noise Prediction Method	30
3.1	Aircraft noise prediction	30
3.1.1	The ADORNO Project	30
3.1.2	Aircraft noise prediction Including performance	31
3.1.3	Additional requirements and technical needs	31
3.2	Methodologies implemented by ATTILA ⁺⁺	34
3.2.1	Introduction	34
3.2.2	Evaluation of airframe noise	34
3.2.3	Evaluation of ground reflection effect	37
3.2.4	Evaluation of atmospheric attenuation	38
3.2.5	Evaluation of lateral attenuation effect	39
3.2.6	Evaluation of engine noise	40
3.2.7	Noise metrics	42
3.3	Software architecture of ATTILA ⁺⁺	43
3.3.1	General overview	43
3.3.2	Description of the classes	44
3.3.3	Technical and user interfaces	50
3.4	Functional innovations of ATTILA ⁺⁺	64
3.4.1	Applied improvements	64
3.4.2	Future developments	67
4	Aircraft Noise Analysis	69
4.1	Test case specification	69
4.1.1	Introduction	69
4.1.2	Test case: the Airbus A220-300	69
4.1.3	Noise levels certified by EASA	71
4.1.4	Input data	72
4.2	Estimation of noise levels	79
4.2.1	Introduction	79
4.2.2	Aircraft noise prediction in Approach conditions	79

4.2.3	Aircraft noise prediction in Lateral conditions	82
4.2.4	Aircraft noise prediction in Flyover conditions	85
4.3	Sensitivity analysis of airframe noise	89
4.3.1	Overview	89
4.3.2	Effects of wing surface	90
4.3.3	Effects of flap surface	96
4.3.4	Effects of flap span	101
4.3.5	Effects of flap slots	106
4.3.6	Effects of flap deflection	110
4.3.7	Effects of wheel diameter	115
4.3.8	Effects of the number of main wheels	120
4.3.9	Effects of the angle of descent	124
4.4	Single-event noise contours	127
5	Conclusions	129
5.1	Discussion of results	129
5.2	Future developments	131
	Bibliography	132

List of Symbols

Symbol	Units (SI)	Description
\bar{A}	m	Distance between the receiver and the vertical plane tangent to trajectory.
A	Pa	Amplitude of sound waves.
b	m	Span.
\bar{B}	m	Distance between the trajectory and the orthogonal projection of the receiver on the vertical plane tangent to trajectory.
B	-	Number of fan blades.
BPR	rad s ⁻¹	Blade passing frequency.
c	m s ⁻¹	Speed of sound.
\bar{C}	m	Distance between trajectory and microphone.
d	m	Diameter of undeformed tyre of landing gear wheels.
DI	-	Directivity index.
$EPNL$	dB, EPNdB	Effective perceived noise level.
$EPNLnT$	dB, EPNdB	Effective perceived noise level (without tonal correction).
f	Hz	Frequency.
F	-	Spectrum function.
I	W m ⁻²	Sound intensity.
j	-	Imaginary unit.
l	m	Reference length.
m	m ⁻¹	Intensity attenuation coefficient.
M	-	Flight Mach number.
n	noy	Noisiness.
N	noy	Overall perceived noisiness.
N_{Eng}	-	Number of engines.
N_{MLG}	-	Number of main landing gear units.
N_{Slot}	-	Number of flap slots.
N_{Wheel}	-	Number of landing gear wheels.

Continued on next page

Continued from previous page

Symbol	Units (SI)	Description
$OASPL$	dB	Overall sound pressure level.
p'	Pa	Instantaneous sound pressure.
p	Pa	Effective sound pressure.
p_∞	Pa	Ambient pressure.
P	W	Acoustic power.
PNL	dB, PNdB	Perceived noise level.
$PNLT$	dB, PNdB	Tone-corrected perceived noise level.
PWL	dB	Power watt level.
Q	-	Complex reflection factor.
r	m	Distance between source and receiver.
R	J kg ⁻¹ K ⁻¹	Specific gas constant.
Re	-	Wave-related Reynolds number.
RH	%	Relative humidity of air.
RPM	min ⁻¹	Revolutions per minute.
s	m	Length of uncompressed landing gear struts.
S	m ²	Surface.
SEL	dBA	Sound exposure level.
SIL	dB	Sound intensity level.
SPL	dB	Sound pressure level.
Sr	-	Strouhal number.
t	s	Time.
T_p	s	Period.
T_∞	K	Ambient temperature.
x	m	X-coordinate.
y	m	Y-coordinate.
z	m	Z-coordinate.
Z_n	Pa s m ⁻¹	Normal surface impedance.
α	rad	Climb/Descent angle.
α_A	dB hm ⁻¹	Sound attenuation coefficient.
β	rad	Elevation angle.
γ	-	Specific heat ratio.
δ	rad	Deflection angle.
Δ	rad	Orientation of the vertical plane tangent to trajectory.
Δf	Hz	Bandwidth.
Δt	s	Time interval.

Continued on next page

Continued from previous page

Symbol	Units (SI)	Description
Δx	m	X-distance between source and receiver.
Δy	m	Y-distance between source and receiver.
Δz	m	Z-distance between source and receiver.
θ	rad	Polar emission angle.
λ	m	Wavelength.
μ_∞	Pa s	Dynamic viscosity.
ρ_∞	kg m ⁻³	Ambient density.
ϕ_f	rad	Azimuthal angle.
ϕ_{gr}	rad	Ground reflection angle.
ω	rad s ⁻¹	Angular frequency.
ω_{rotor}	rad s ⁻¹	Fan rotor angular speed.
ψ	rad	Phase shift.

Subscript	Description
a	Air.
Avg	Average.
C	Translational and rotational.
f	Flap.
gr	Ground.
h	Horizontal tail.
j	Jet.
Max	Maximum.
MLG	Main landing gear.
N	Nitrogen.
NLG	Nose landing gear.
O	Oxygen.
r	Receiver/Microphone.
Ref	Reference.
s	Source.
$S.L.$	Sea level.
v	Vertical tail.
w	Wing.

1

Introduction

1.1 Background

A major challenge in the transport sector is to make economic growth compatible with sustainability and environmental constraints, while remaining competitive and innovative. In this sense, the EU's **Horizon 2020** programme ^[1] aims to ensure that Europe produces world-class science, by combining research and innovation. The aeronautical sector will be a critical player in contributing to the key Societal Challenge “*smart, green and integrated transport*” defined in Horizon 2020 ^[2].

Launched in 2014 as part of the Commission's Horizon 2020 Research and Innovation Programme, **Clean Sky 2** ^[3] (CS2) is the largest European research programme developing innovative, cutting-edge technology aimed at reducing CO₂, gas emissions and noise levels produced by aircraft. Funded by the Horizon 2020 programme, Clean Sky 2 (Figure 1.1) contributes to strengthening European aero-industry collaboration, global leadership and competitiveness. According to Clean Sky 2 Joint Technical Programme ^[4], the results will be applicable to 75 % of the world fleet needing replacement up to 2050, and CS2 technology will be able to address aviation emissions totaling over 70 % of the worldwide civil air fleet.

With respect to energy efficiency and environmental performance, several high level objectives were established by the Advisory Council on Aviation Research in Europe (ACARE) in the renewed Strategic Research and Innovation Agenda (SRIA) ^[5]:

- A 75 % reduction in carbon dioxide (CO₂) emissions;
- A 90 % reduction in mono-nitrogen oxides (NO_x);
- A noise reduction of flying aircraft of 65 %;



Figure 1.1: Clean Sky 2 - Logo ^[3].

- Mitigate the environmental impact of the lifecycle of aircraft and related products by designing and manufacturing aircraft to be recyclable.

Nowadays, the problem of aircraft emissions is strongly felt, especially due to the increasing air traffic and the high common sensitivity to the issue of environmental pollution. In this context, Clean Sky 2 aims to contribute strongly to the ACARE SRIA, by coordinating and funding research activities to deliver significantly quieter and more environmentally friendly aircraft.

Among these, the **ADORNO** project ^[6] (Figure 1.2) was born from the partnership of the **University of Naples “Federico II”** ^[7] with the Germany’s leading engine manufacturer **MTU Aero Engines** ^[8], and **Lead Tech** ^[9], an engineering company which supplies a wide range of technical services such as software development and integrated logistic support. ADORNO focuses on the development of aircraft models for the engine platform of regional aircraft. The main objective is to provide aircraft requirements as well as trade factors for specific fuel consumption and engine drag for both a year 2014 reference aircraft and a CS2 target aircraft. The project also includes the development of a method for the prediction of aircraft noise that will be developed and integrated in the aircraft design chain.

The overall ADORNO work plan is divided into four *Work Packages* (WP):

- **WP1** - Management, dissemination and exploitation;
- **WP2** - Aircraft design and emissions assessment;
- **WP3** - Noise and emissions software;
- **WP4** - Advanced trade factor methodology.

The starting point for WP2 has been **JPAD** ^[10] (acronym of *Java toolchain of Programs for Aircraft Design*), the analysis and pre-design software developed by

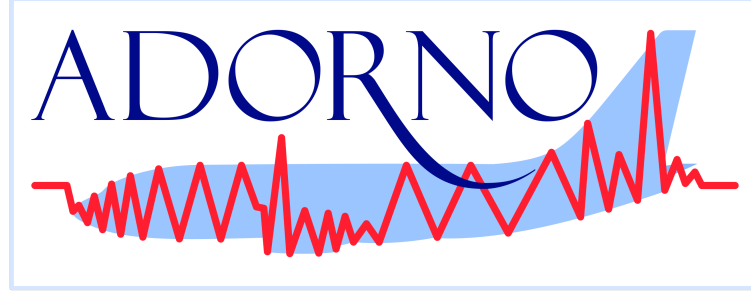


Figure 1.2: ADORNO Project - Logo ^[6].

the DAF research group of the University of Naples “Federico II”. JPAD is conceived as an ecosystem of interconnected modules aimed at providing a reliable, fast and efficient tool to support the design, the analysis and the optimization of transport aircraft. One of the modules of JPAD was therefore the basis for the development of a software for the assessment of emissions (F. Nicolosi et al., 2020) ^[11].

With reference to Work Package 3, the development of a tool for the evaluation of the acoustic emissions of a transport aircraft has been carried on. The software, named **ATTILA**, was originally developed at the University of Naples by the vibro-acoustics research group for the estimation of the noise produced by a turbofan-powered civil aircraft (C. Casale et al., 2019) ^[12].

Preliminary aircraft design can aspire to define a new frontier of innovation in terms of configurations and technologies suitable for the ever-increasing need for more green and efficient aircraft with reduced operating costs. In general, the design of aeronautical products is a complex multi-disciplinary process with requirements and constraints on the air transport system as a whole, and all the individual components to be produced. A major issue, which has prevented aircraft manufacturers from implementing efficient and cost-effective design processes, is the loose integration of engine models into iterative aircraft design workflows. This requires on one hand a novel design paradigm accelerating the integration of aircraft and engine models, taking account of design and certification requirements. On the other hand, it requires human-centric methods supporting the analysis of large data-driven scenarios and the decision-making process (F. Nicolosi et al., 2020) ^[11]. For these important reasons, many other efforts will be made as part of the project to improve the two aforementioned programs. In fact, in addition to constituting useful stand-alone tools for assessing the environmental impact of commercial aircraft, they would also give the opportunity to involve the problem of gas and acoustic emissions in the multi-disciplinary design optimization (MDO) processes.

In order to accelerate the activities concerning the development of a preliminary version of ATTILA compatible with MTU’s IT-framework, the author of this dissertation carried out a three-month internship at MTU Munich, from 7 January 2020 to 6 April 2020, as a representative of the University of Naples.

1.2 Objective

The aim of this thesis work is to present a computer program capable of providing a reasonable estimate of the noise generated by an aircraft, also in the preliminary design phases. First, both the technical and functional characteristics of the code will be extensively explored, being representative of the work carried out by the candidate in the context of the ADORNO project. Subsequently, by conducting a parametric analysis on a regional aircraft (the Airbus A220-300), we intend to search for the design parameters that have the greatest impact on the acoustic emissions, with reference only to aerodynamic noise. The main objective, beyond the results that will be presented, is to show the potential of the program that aims to become a valid stand-alone software for assessing the acoustic emissions of an aircraft and, at the same time, an instrument that allows to take into account the problem of noise emissions from the early stages of the aircraft design process.

1.3 Thesis outline

Chapter 1 has given a general overview of the European context in which the ADORNO project is inserted, as well as the objectives of this dissertation.

Chapter 2 will lay the theoretical foundations for understanding the problem of aircraft noise. In particular, the meaning of the main acoustic metrics used in the field of noise certification will be explained. The work of Prof. G.J.J. Ruijgrok (2004) ^[13] and Prof. S. Farokhi (2020) ^[14] have been the main source of information for its realization.

Chapter 3 will be entirely dedicated to the computer program ATTILA⁺⁺. The software architecture will be described, and the main functional characteristics currently implemented will be listed, together with the technical requirements already met and the objectives regarding future code developments. The methodologies used by the program will also be briefly described.

Chapter 4 will contain a software application which consists of a detailed sensitivity analysis conducted on the Airbus A220-300. The variations in the noise levels, consequent to the assigned percentage variations of some parameters of interest, will be presented in the form of charts and synoptic tables. The primary effect of the trajectory on noise recorded at ground level will also be briefly discussed. Finally, the reader will be offered reproductions of the acoustic footprints left by the aircraft during the take-off and landing phases.

2

Elements of Aviation Acoustics and Noise Certification

2.1 Introduction to aviation acoustics

2.1.1 General definitions

Sound is a physical disturbance in the air, produced by a *sound source*. If the disturbance reaches a listener, *a sound is heard*. A *noise* can be defined as sound that is unwanted by the observer.

This definition, proposed by Prof. G.J.J. Ruijgrok (2004) ^[13], emphasizes the fact that noise is basically a subjective phenomenon, and the level of annoyance is influenced even by personal feelings and by the attitude towards the source. Obviously such a definition does not allow to objectively quantify a sound, nor to compare two or more sounds with a different nature. At the same time, the growing number of noise sources in our technological society has led us to the need to control and reduce the sound levels to which we are subjected in our daily lives.

From a physical point of view, sound is a vibration that propagates as an acoustic wave through a transmission medium. The region in which the wave travels is called *sound field*. In a space where the sound waves can propagate freely without reflection they are called *free progressive waves*, travelling in a *free field*.

A multitude of metrics for the evaluation of sound levels is used today, and some of them are adopted by the certification authorities in the context of the limitation of noise emissions. In aeronautical engineering there are two main problems to deal with:

- Interior noise;
- Exterior noise.

In both cases, the problem is complex and, according to Prof. Ruijgrok (2004) ^[13], its solution should be divided into three consecutive logical phases:

- i. Determination of the noise produced by the aircraft (the *source*);
- ii. Evaluation of the propagation effects on the noise, which travels through the atmosphere and may be influenced by the presence of obstacles and ground surface;
- iii. The effect on the *receivers* of noise, typically a human being or a microphone.

Moreover, we deal with many types of aircraft which all have their own noise radiation characteristics, and which are heard under various environmental conditions.

A specific treatment of this theme would go beyond the objectives of this thesis, so the purpose of this first chapter is exclusively to lay the essential theoretical fundamentals of acoustic theory for understanding the restrictions that the *International Civil Aviation Organization* (ICAO) ^[15] prescribes for limiting the acoustic power that an aircraft can emit near airports. This document will focus exclusively on the problem of external noise.

2.1.2 Frequency and period

Since the acoustic pressure has a sinusoidal trend, it has all the typical characteristics of oscillatory phenomena. The time required to complete one cycle is called the *period*, T_P . The number of oscillations per second is the frequency f of the disturbance and is expressed in terms of cycles per seconds or *Hertz* (Hz). The frequency is the reciprocal of the period:

$$f = \frac{1}{T_P} \quad (2.1)$$

At low frequencies the air particles oscillate slowly producing low, bass tones. At high frequencies the air particles vibrate quickly giving high tones. The frequencies audible to the human ear range from about 20 Hz to 20000 Hz. The inaudible sounds with frequencies under 20 Hz are called *infrasounds*. Inaudible sounds over 20000 Hz are called *ultrasounds*.

2.1.3 Wavefronts, wavelength, sound rays

Wavefronts are the imaginary surfaces around the source which are the loci of all points where the wave has the same phase of the sinusoid. We call *wavelength*, λ , the distance between two consecutive wavefronts which correspond to the same phase on the wave. The directions in which the wave propagates are identified by the *sound rays*, which are the imaginary curves directed normally to the wavefronts.

2.1.4 Speed of sound

The rate at which the pressure disturbance travels through the air is called *speed of sound*, c . In air we have that:

$$c = \sqrt{\gamma_a R_a T_\infty} \quad (2.2)$$

Where $\gamma_a = 1.4$ is the ratio of the *specific heats of air*, $R_a = 287.05 \text{ J kg}^{-1} \text{ K}^{-1}$ is the *specific gas constant* and T_∞ is the ambient temperature in Kelvin. It can be written:

$$c = f \lambda \quad (2.3)$$

2.1.5 Sound fields

As mentioned above, when the sound energy generated by a point source spreads spherically in all directions we speak of *free-field conditions*. A *free field* is a sound field in which the effects of obstacles are negligible in the space of interest. It is theoretically possible to consider a wavefront as spherical if its distance from the source is large in comparison with its dimensions. In that case it is also possible to consider as if the sound comes from a single point called the *acoustic center* of the source. It is also important to distinguish between the two parts in which a sound field is generally divided (G.J.J. Ruijgrok, 2004) ^[13]:

- i. The *far-field*, where the sound pressure can be expressed as inversely proportional to the distance;
- ii. The *near-field*, where the variation of the sound pressure with the distance is a complex function of the radiation characteristics of the source.

Prerequisites to be able to assume far-field conditions are to work at distances greater than the wavelength corresponding to the lowest frequency emitted by the source and, of course, to be in free-field conditions.

2.2 Frequency spectra

2.2.1 Fourier transform

The acoustic emission of a real source is usually distributed over a large range of frequencies. It is of fundamental importance to know how the frequency spectra vary with the distance and the angle of emission. In fact, the frequency content determines the perceived loudness since the sensitivity of the human ear depends on the sound frequency (G.J.J. Ruijgrok, 2004) ^[13]. It is possible to break down a sound signal into its frequency components by means of the *Fourier transform*. The *Fourier series* corresponding to the periodic function $f(t)$ can be expressed as:

$$f(t) = \sum_{k=0}^{\infty} A_k \cos\left(\frac{2\pi k t}{T_P}\right) + B_k \sin\left(\frac{2\pi k t}{T_P}\right) \quad (2.4)$$

Where t is the time, T_P is the period and A_k and B_k can be expressed as:

$$A_0 = \frac{1}{T_P} \int_0^{T_P} f(t) dt \quad (2.5)$$

$$A_k = \frac{2}{T_P} \int_0^{T_P} f(t) \cos\left(\frac{2\pi k t}{T_P}\right) dt \quad (2.6)$$

$$B_k = \frac{2}{T_P} \int_0^{T_P} f(t) \sin\left(\frac{2\pi k t}{T_P}\right) dt \quad (2.7)$$

Each contribution in equation 2.4 is called *harmonic*. It represents a distinct wave contribution when $f(t)$ expresses a sound signal.

2.2.2 Third octave bands

It is often used to divide the frequency range of interest into smaller ranges. A *frequency band* is an interval in the frequency domain, delimited by a *lower frequency* and an *upper frequency*. We talk about *constant percentage bandwidths* when the frequency interval increases as the frequency increases. The *center frequency* of a band f_i is the geometric mean of its limiting frequencies f_u and f_l :

$$f_i = \sqrt{f_u f_l} \quad (2.8)$$

On the basis of the ratio between the bandwidth and the center frequency, several constant percentage bandwidths can be defined. The procedures for describing aircraft noise generally require that the measurement data are expressed in *one-third-octave bands* (or *tertsbands*).

Table 2.1: One-third-octave bands.

Number	Pass band [Hz]	Number	Pass band [Hz]
1	1.25	23	200
2	1.6	24	250
3	2	25	315
4	2.5	26	400
5	3.15	27	500
6	4	28	630
7	5	29	800
8	6.3	30	1000
9	8	31	1250
10	10	32	1600
11	12.5	33	2000
12	16	34	2500
13	20	35	3150
14	25	36	4000
15	31.5	37	5000
16	40	38	6300
17	50	39	8000
18	63	40	10000
19	80	41	12500
20	100	42	16000
21	125	43	20000
22	160		

One-third-octave bands are characterized by the following relationship:

$$\frac{\Delta f}{f_i} = 2^{\frac{1}{6}} - 2^{-\frac{1}{6}} \quad (2.9)$$

Where Δf is the difference between f_u and f_l . This is equivalent to saying that the ratio between the two band limits, and between two consecutive band centers, is equal to $1/3$. The instrument needed to measure in third octave bands is a *constant percentage bandwidth* (CPB) analyzer. It is equipped with a suitable filter capable of recording only the energy associated with the frequencies belonging to each tertsubband. The nominal values of the central frequencies are listed in Table 2.1.

2.3 Fundamental sound metrics

2.3.1 Sound pressure

The instantaneous value of the fluctuating pressure disturbance on ambient pressure is called the *sound pressure*. The variation of the sound pressure is an oscillation which can be described, in the first instance, by the equation for simple harmonic motion. In the case of point sound sources, sound pressure can be expressed as an harmonic function of time t and distance r from the receiver:

$$p'(t) = \frac{A}{r} \cos \left[\omega \left(t - \frac{r}{c} \right) \right] \quad (2.10)$$

Where A is the wave amplitude at unitary distance from the source and ω is the angular frequency in rad s^{-1} , which is linked to the frequency f as follows:

$$\omega = 2\pi f \quad (2.11)$$

Equation 2.10 is only valid under the hypothesis of free far-field. Note that the wave amplitude decreases as the distance from the source increases, and this is because the acoustic energy emitted by the source spreads out in all directions. This effect is known as (*spherical*) *spreading effect*. Lastly, the time (r/c) is taken for the sound wave to cover the distance r .

2.3.2 Effective sound pressure

Effective sound pressure, p , is the most often used measure of the magnitude of a sound signal. It is defined as the root mean square value of the instantaneous sound pressures over one period of time:

$$p = \sqrt{\frac{1}{T_P} \int_0^{T_P} p'(t)^2 dt} \quad (2.12)$$

Equations 2.10 and 2.12, in addition to the hypothesis of free far-field, lead to:

$$p = \frac{A}{r\sqrt{2}} \quad (2.13)$$

If two or more independent sound sources produce pressure disturbances, each with a different frequency, and if they propagate simultaneously, the expression of the resulting effective sound pressure is the root mean-square of the single contributions:

$$p = \sqrt{\sum_{i=1}^n p_i^2} \quad (2.14)$$

This derives from equation 2.12 where p' is the sum of all the contributions.

If the sounds are at the same frequency, this result is not precise as it does not consider the possible phenomena of interference between the waves.

2.3.3 Acoustic power

The *acoustic power*, P , is the total sound energy emitted by the source per unit of time. It is characterized by a huge range of values, from 10^{-10} (human whisper) to values around 10^8 (rocket launch). A small propeller-driven airplane radiates 50 W, while a large jet transport at take-off produces around 103 W (G.J.J. Ruijgrok, 2004) ^[13].

2.3.4 Power watt level

In order to better manage the wide range of values that characterizes the acoustic power, it is common to refer to an equivalent logarithmic quantity, called *power watt level*, PWL , defined as:

$$PWL = 10 \log \left(\frac{P}{P_{Ref}} \right) \quad (2.15)$$

Where $P_{Ref} = 10^{-12}$ W is the reference power. The unit of PWL is *decibel* (dB). It follows from equation 2.15 that a doubling of the source power causes a change of 3 dB. Using the decibel scale leads to a range of power levels from 0 to 200 dB.

2.3.5 Sound intensity

The *sound intensity*, I , is the power per unit of area transmitted by a sound wave. In the case of a point source in a free field where the sound energy is spread uniformly in all directions, the intensity is constant and can be calculated as follows:

$$I(r) = \frac{P}{4 \pi r^2} \quad (2.16)$$

Where r is the distance from the point source. It can be demonstrated that, in the free field, the effective pressure and the sound intensity in the direction of propagation are linked by the following equation:

$$I = \frac{p^2}{\rho_{\infty} c} \quad (2.17)$$

Where ρ_{∞} is the air density, c is the speed of sound and $\rho_{\infty} c$ is called the *characteristic acoustic resistance* of the medium. In general, real sound sources have a three-dimensional extension and tend to be directional. This means that the energy propagated by the source is not necessarily the same in all directions. This is also typical for aircraft, which have a very marked directional pattern.

2.3.6 Sound intensity level

Similar to what happens for acoustic power, the sound intensity can also be expressed on a logarithmic scale. *Sound intensity level*, SIL , is defined as the following quantity expressed in dB:

$$SIL = 10 \log \left(\frac{I}{I_{Ref}} \right) \quad (2.18)$$

Where $I_{Ref} = 10^{-12} \text{ W m}^{-2}$ is a reference value. As previously mentioned, the aircraft (and more generally any three-dimensional source) have a marked directional pattern. In order to describe the directionality of a source it is possible to define the *directivity index*, DI , as the difference between the sound intensity level in a specified direction and the average sound intensity level, SIL_{Avg} , at a specified distance r :

$$DI(\theta, \phi_f) = SIL(\theta, \phi_f) - SIL_{Avg} \quad (2.19)$$

Where θ is the polar emission angle and ϕ_f is the azimuthal angle. Equation 2.16 leads to the following expression of SIL_{Avg} :

$$SIL_{Avg} = 10 \log \left(\frac{P}{I_{Ref} 4 \pi r^2} \right) \quad (2.20)$$

2.3.7 Sound pressure level

Sound pressure level, SPL , is defined as the following quantity expressed in dB:

$$SPL = 10 \log \left(\frac{p^2}{p_{Ref}^2} \right) \quad (2.21)$$

Where $p_{Ref} = 2 \cdot 10^{-5} \text{ Pa}$ is the reference pressure and has the meaning of an audibility threshold.

Sound pressure level is a function of frequency f , at the same way as the effective sound pressure p . If $SPL = 0 \text{ dB}$, it means that the effective sound pressure is equal to the reference pressure, so that values lower than p_{Ref} can also lead to negative SPL values. The threshold of pain stands at 140 dB.

It is important to note immediately that there is no proportion between the decibel scale and the magnitude of the auditory sensation. A change of 1 dB is the smallest amount to be perceptible by the human ear, and only a change of 3 dB may be well discernable (G.J.J. Ruijgrok, 2004) ^[13]. This is the reason why the value of the SPL is usually rounded off to the nearest whole number. From equations 2.17, 2.18 and 2.21:

$$SPL = SIL + 0.2 + 10 \log \left[\frac{\rho_{\infty} c}{(\rho_{\infty} c)_{S.L.}} \right] \quad (2.22)$$

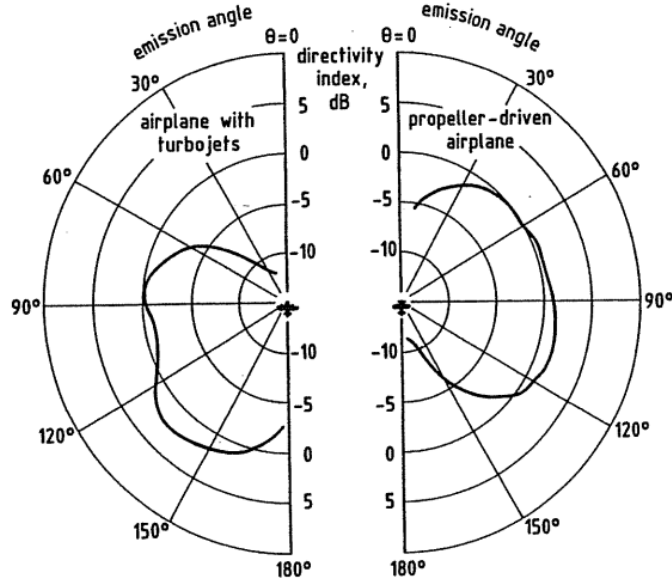


Figure 2.1: Typical directional patterns (G.J.J. Ruijgrok, 2004) ^[13].

Where $(\rho_{\infty} c)_{S.L.}$ is the characteristic acoustic resistance of air at sea level. Since the difference between SIL and SPL is constant and only depends on the reference height, it is possible to write (from equation 2.19):

$$DI(\theta, \phi_f) = SPL(\theta, \phi_f) - SPL_{Avg} \quad (2.23)$$

Where:

$$SPL_{Avg} = SIL_{Avg} + 0.2 + 10 \log \left[\frac{\rho_{\infty} c}{(\rho_{\infty} c)_{S.L.}} \right] \quad (2.24)$$

Figure 2.1 shows a typical example of directional pattern for a commercial turbojet and a propeller-driven aircraft (i.e. DI as θ changes). If two or more independent sound sources produce pressure disturbances at the same frequency, the expression of the resulting sound level does not simply consist of the arithmetic sum of the individual SPL values. This is due to the logarithmic nature of the sound pressure level:

$$SPL = 10 \log \left(\sum_{i=1}^n 10^{\frac{SPL_i}{10}} \right) \quad (2.25)$$

In case there are two similar sources (with the same SPL), the total level would be 3 dB higher than in the case of a single source.

2.4 Integral sound metrics

2.4.1 Overall sound pressure level

The *overall sound pressure level*, $OASPL$, is the logarithmic addition of all of the discrete spectral sound pressure levels into a single figure. Each SPL value can refer to a single frequency (or band), therefore the $OASPL$ gives the opportunity to have a single figure of merit that summarizes the level of acoustic energy contained by the entire sound signal:

$$OASPL = 10 \log \left(\sum_{i=1}^n 10^{\frac{SPL_i}{10}} \right) \quad (2.26)$$

In equation 2.26, n represents the number of considered one-third-octave bands.

2.4.2 Noisiness level

If two pure tones of equal frequency are compared, the ear will judge the sound with the highest SPL as the loudest. Several experiments have also made it clear that people are more sensitive to complex sounds containing high frequency components.

The results of this investigation led to the definition of noisiness (K.D. Kryter, 1960) ^[16]. *Noisiness*, n , is intended to measure sound as it is actually perceived by the human ear. The unit of measurement is *noy*, and the relationship linking the SPL in each tertsbands with the *noy* values is available in the form of the *equal noisiness curves* (Figure 2.2). These curves represent the sound levels (as the frequency changes), at which the listener perceives a constant intensity if subjected to a pure sound impulse. A mathematical formulation of *noy* table is provided by the certification authorities. ^{[17] [18] [19]}

The *overall perceived noisiness*, N , is defined as follows:

$$N = n_{Max} + 0.15 \sum_{i=17}^{40} n_i - n_{Max} \quad (2.27)$$

Where n_{Max} is the greatest *noy* value and i is the band number (with reference to Table 2.1). Note that only bands ranging from 50 Hz to 10000 Hz are considered, as they are the bands to which the human ear is sensitive.

2.4.3 Perceived noise level

The *perceived noise level*, PNL , can be obtained from the overall *noy* level N through the following definition:

$$PNL = 40 + \frac{10}{\log 2} \log N \quad (2.28)$$

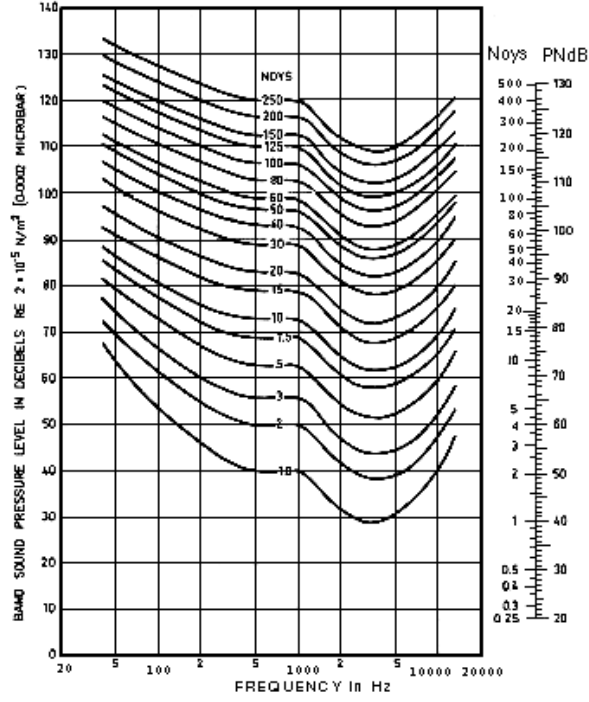


Figure 2.2: Equal noisiness curves (K.D. Kryter, 1960) ^[16].

PNL is expressed in dB. The perceived noise level is one of the most important metrics in the field of aircraft noise certification.

2.4.4 Tone-corrected perceived noise level

When the discrete frequency components of a sound signal have pronounced spectral irregularities, the noise perceived by the human ear increases. This led to the development of a procedure aimed at adjusting the perceived noise level, known as *tone correction*. ICAO ^[15] ^[17] describes this procedure that can be summarized in ten logical steps:

- i. Starting from the sound pressure level in the 80 Hz one-third-octave band (band number $i = 19$) and ending with that of 10000 Hz ($i = 40$), calculate the changes in *SPL* (*slopes*) as follows:

$$s_i = SPL_i - SPL_{i-1} \quad (2.29)$$

- ii. Encircle the values of the slopes s_i where the absolute value of their change is greater than 5:

$$|\Delta s_i| = |s_i - s_{i-1}| > 5 \quad (2.30)$$

iii. Encircle the values of SPL_i which meet one of the following conditions:

- The encircled value of the slope s_i is positive and algebraically greater than the slope s_{i-1} ;
- The encircled value of the slope s_{i+1} is zero or negative and the slope s_i is positive.

iv. Omit all SPL_i encircled in step iii and compute new adjusted SPL'_i as follows:

- For encircled sound pressure levels in bands from 19 to 39, let the new SPL be the arithmetic average of the preceding and following values:

$$SPL'_i = \frac{SPL_{i-1} + SPL_{i+1}}{2} \quad (2.31)$$

- If the SPL in the highest frequency band (band number $i = 40$) is encircled, calculate the adjusted value as:

$$SPL'_{40} = SPL_{39} + s_{39} \quad (2.32)$$

v. Compute new slopes s'_i on the basis of the adjusted set of SPL values, including one for the imaginary band with number $i = 41$ ($f_{41} = 12500$ Hz).

vi. For bands from 19 to 39, compute the arithmetic mean of three adjacent slopes:

$$\bar{s}_i = \frac{s'_i + s'_{i+1} + s'_{i+2}}{3} \quad (2.33)$$

vii. Compute final sound pressure levels SPL''_i as follows:

$$\begin{cases} SPL''_{19} = SPL_{19} \\ SPL''_i = SPL''_{i-1} + \bar{s}_{i-1} \end{cases} \quad 20 \leq i \leq 40 \quad (2.34)$$

viii. Calculate the differences F_i between the original sound pressure levels and the final adjusted values, keeping them only when greater than 3:

$$F_i = SPL_i - SPL''_i \quad (2.35)$$

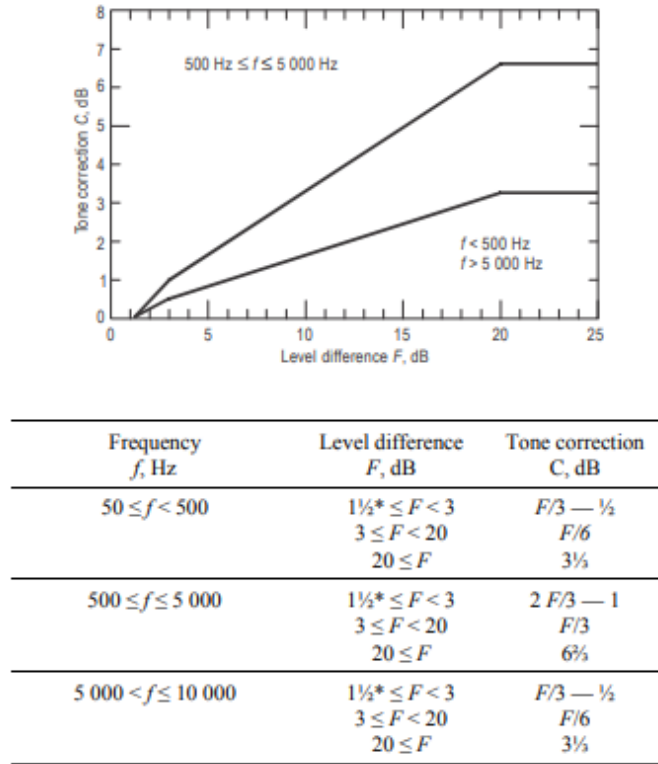


Figure 2.3: Tone correction factors (ICAO Annex 16, Volume I) [17].

- ix. Calculate the tone correction factors C_i by using the formulas of Figure 2.3.
- x. Determine the largest of the tone correction factors, C_{Max} , and calculate the *tone-corrected perceived noise level*, $PNLT$, as follows:

$$PNLT = PNL + C_{Max} \quad (2.36)$$

Since $PNLT$ is generally a function of time, this procedure must be repeated at any time when a sound level measurement has been made.

2.4.5 Effective perceived noise level

If the instantaneous tone-corrected perceived noise level is expressed in terms of continuous function of time, $PNLT(t)$, it is possible to define the *effective perceived noise level*, $EPNL$, as the time integral of $PNLT(t)$ over the noise event duration, normalized to a reference duration of 10 seconds:

$$EPNL = 10 \log \left(\frac{1}{T_0} \int_{t_1}^{t_2} 10^{\frac{PNLT(t)}{10}} dt \right) \quad (2.37)$$

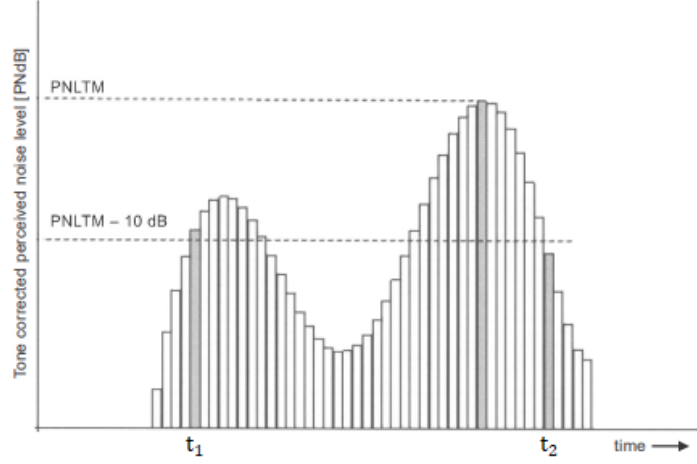


Figure 2.4: Example of noise time history (ICAO Annex 16, Volume I) [17].

Where $T_0 = 10$ s. The noise event is bounded by t_1 and t_2 which are, respectively, the time when $PNLT(t)$ is first equal to $PNLT_{Max} - 10$ and the time when $PNLT(t)$ is last equal to $PNLT_{Max} - 10$, being $PNLT_{Max}$ the maximum recorded value of $PNLT$ (see Figure 2.4).

For practical applications, it is convenient to express $PNLT$ as discrete values. In this case the $EPNL$ can be expressed as the following sum:

$$EPNL = 10 \log \left[\frac{1}{T_0} \sum_{i=i_1}^{i_2} 10^{\frac{PNLT_i}{10}} \Delta t \right] \quad (2.38)$$

Where the sample values should be taken at regular time intervals of $\Delta t = 0.5$ s. Substituting $T_0 = 10$ s and $\Delta t = 0.5$ s, $EPNL$ can be rewritten as:

$$EPNL = 10 \log \left[\sum_{i=i_1}^{i_2} 10^{\frac{PNLT_i}{10}} - 13 \right] \quad (2.39)$$

ICAO [17] also expresses the $EPNL$ in terms of a *duration factor*, D , as follows:

$$EPNL = D + PNLT_{Max} \quad (2.40)$$

2.5 Propagation and motion effects

2.5.1 Overview

Let us define a *propagation effect* any effect that causes an alteration of the sound energy level perceived by a receiver and that is due to the propagation of the waves through a medium and within the surrounding environment. In this paragraph we will analyze some of the main propagation effects, as well as the effects due to the source motion, that can affect the noise produced by a generic source.

2.5.2 Spreading effect

The first example of propagation effect is the *spherical spreading effect*, already discussed in section 2.3.1. It is due to the diffusion of acoustic energy on spherical wave fronts with a radius equal to the distance from the source. From equations 2.13 and 2.21 it follows that the difference between the *SPL* values measured at distances r_1 and r_2 from the source is equal to:

$$\Delta SPL = SPL_2 - SPL_1 = 20 \log \left(\frac{r_1}{r_2} \right) \quad (2.41)$$

The previous relationship is called the *inverse-distance law* (G.J.J. Ruijgrok, 2004) ^[13]. It is also possible to take into account the difference in ambient pressure between positions 1 and 2. Since the total squared effective pressure is the algebraic sum of all contributions, it is possible to adjust equation 2.41 as follows:

$$\Delta SPL = SPL_2 - SPL_1 = 20 \log \left(\frac{r_1}{r_2} \right) + 20 \log \left(\frac{p_{\infty,2}}{p_{\infty,1}} \right) \quad (2.42)$$

Where $p_{\infty,1}$ and $p_{\infty,2}$ are the ambient pressures at positions 1 and 2.

2.5.3 Doppler shift

When the acoustic source is moving, its radiation characteristics may be significantly different from those of the airplane at rest on the ground. This is primarily connected to the *Doppler effect*. It consists of a change in observed frequency of a moving source caused by a time rate of change in the distance between source and receiver (G.J.J. Ruijgrok, 2004) ^[13]. It is possible to demonstrate that, for a subsonic motion:

$$\frac{f'}{f} = \frac{1}{1 - M \cos \theta} \quad (2.43)$$

Where M is the Mach number at which the source is moving, and θ is called the *emission angle*. It is the angle formed by the line of sight between the source and the observer, and the trajectory of the moving source. The original frequency f

is increased or decreased to the value of f' , depending on whether the source is approaching or leaving. If the ratio between f' and f is greater than the characteristic ratio between two center band frequencies, then it means that the corresponding sound contribution has been shifted to an adjacent band.

2.5.4 Atmospheric attenuation of the sound

Atmospheric attenuation is the process by which sound energy is absorbed in travelling through the atmosphere. This effect is due primarily to the fact that atmospheric air, like all forms of fluid, exhibits some degree of internal friction: molecular translation, molecular rotation, and the internal vibrational relaxation of oxygen and nitrogen molecules. The rate at which sound energy is absorbed by the propagation medium is expressed by the *sound attenuation coefficient*, α_A , which is normally given in dB per 100 m. The decrease in sound pressure level can thus be written as:

$$\Delta SPL = - \frac{\alpha_A r}{100} \quad (2.44)$$

Where r is the distance between source and receiver. When the sound propagates in a homogeneous and quiescent atmosphere, the attenuation coefficient is primarily a function of the frequency f . In addition, also the ambient air temperature and the amount of water vapor in the atmosphere affect the magnitude of the sound absorption.

Coefficient α_A is relatively small except at high frequencies. A qualitative impression of the effect of frequency on α_A can be given by the *Reynolds number*, Re , of the wave motion (G.J.J. Ruijgrok, 2004) ^[13]:

$$Re = \frac{\rho_\infty c \lambda}{\mu_\infty} = \frac{\rho_\infty c^2}{\mu_\infty f} \quad (2.45)$$

Where c is the sound speed, ρ_∞ the air density, λ the wavelength and μ_∞ the coefficient of dynamic viscosity, which determines the shear stress between air layers moving at different velocities. Since the Reynolds number inversely indicates the relative importance of the viscous forces with respect to the pressure forces, it is possible to notice that, at high frequencies, the effect of absorption will be more relevant.

Additional effects are related to temperature gradients and relative wind. According to equation 2.2, the speed of sound is proportional to the square root of the absolute temperature. Since the atmospheric air temperature changes with altitude, so does the speed of sound, which means that the sound rays show a certain curvature in accordance with Snell's law of refraction. In the same way, if there is a vertical wind gradient, it will modify the propagation speed of the pressure waves making it further variable with the altitude.

2.5.5 Ground reflection effect

A major problem in the interpretation of results from noise measurements are the effects of ground reflected sounds, which must be removed from the measured levels before the free-field noise characteristics become visible. On the contrary, these effects must be taken into consideration, in addition to the free-field noise, to obtain a reliable prediction of the sound level resulting from an experimental test. It is possible to define the *ground effect* as the difference between the measured sound pressure level at a given emission angle and the sound pressure level (at the same emission angle) which would occur in the free-field (G.J.J. Ruijgrok, 2004) ^[13].

Let r_1 denote the distance traveled by the direct ray, and r_2 that of the indirect ray. Angle ϕ_{gr} is the angle to the horizontal subtended by the reflected wave. Let us ignore the small displacement of the source during the time interval between the reception of the two signals. The geometric representation of source and receiver is shown in Figure 2.5.

At a given frequency, the sound pressure at the receiver position is the sum of the sound pressures caused by the direct ray and the reflected ray. The amplitude and phase of the reflected wave are modified by a complex *reflection factor*, Q :

$$p'_r(t) = \frac{A}{r_1} e^{\frac{j\omega r_1}{c}} + \frac{Q A}{r_2} e^{\frac{j\omega r_2}{c}} \quad (2.46)$$

$$Q = |Q| e^{j\psi} \quad (2.47)$$

Where A is the amplitude of the sound pressure at unitary distance. The module of Q is the ratio of direct and reflected wave magnitudes, and ψ is the phase change. Equations 2.12, 2.21 and 2.46 lead to:

$$\Delta SPL = 10 \log \left[1 + \left(\frac{r_1}{r_2} \right)^2 |Q|^2 + 2 \frac{r_1}{r_2} |Q| \cos \left(\omega \frac{\Delta r}{c} + \psi \right) \right] \quad (2.48)$$

Where $\Delta r = r_2 - r_1$. If the previous expression is integrated over one-third-octave bands:

$$\begin{aligned} \Delta SPL_i = SPL_i - SPL_{Free-field,i} = 10 \log & \left\{ 1 + \left(\frac{r_1}{r_2} \right)^2 |Q_i|^2 + \right. \\ & \left. + 2 \frac{r_1}{r_2} |Q_i| \frac{\sin \left(\pi \frac{\Delta r}{\lambda_i} \frac{\Delta f_i}{f_i} \right)}{\pi \frac{\Delta r}{\lambda_i} \frac{\Delta f_i}{f_i}} \cos \left[2 \pi \frac{\Delta r}{\lambda_i} \sqrt{1 + \frac{1}{4} \left(\frac{\Delta f_i}{f_i} \right)^2} + \psi_i \right] \right\} \end{aligned} \quad (2.49)$$

Where the subscript refers to the considered one-third-octave band, f_i is the band center, Δf_i is the width of the band and λ_i is the wavelength.

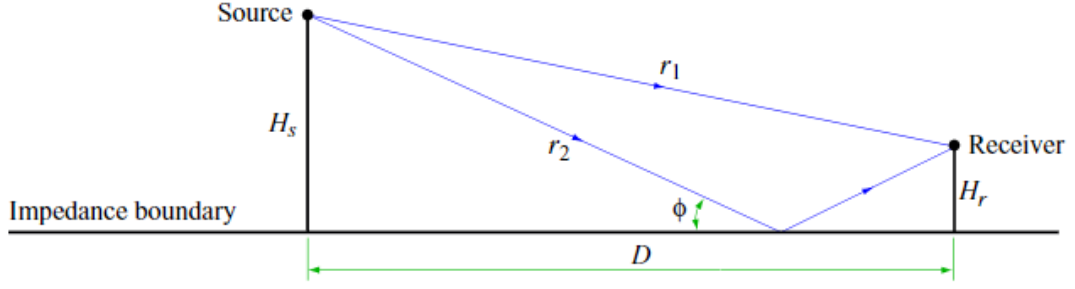


Figure 2.5: Representation of source-receiver geometry (ESDU item no. 94035) [20].

An expression for Q_i follows from the requirement that the complex ratio between the sound pressure at a point on the surface and the normal particle velocity at the surface equals the *normal surface impedance*, Z_n . Under the hypothesis of locally reactive ground surfaces (which means that lateral propagation through the ground can be ignored), it is possible to demonstrate that:

$$Q_i = \frac{\frac{Z_{n,i}}{\rho_\infty c} \sin \phi_{gr} - 1}{\frac{Z_{n,i}}{\rho_\infty c} \sin \phi_{gr} + 1} \quad (2.50)$$

Where Z_n is the *normal surface impedance* and its ratio to the characteristic resistance of the ambient air is called the *specific impedance of the surface*. The problem of quantifying the ground reflection effect is therefore reduced to the knowledge of soil impedance.

2.6 Aircraft noise and noise certification

2.6.1 Noise pollution

The high level of acoustic energy represents one of the current major problems concerning the environmental impact of an aircraft, since the exposure to loud noise is harmful to human physiological and psychological health and welfare. Communities in the vicinity of airports are mainly affected by aircraft noise during all flight phases near the runway. *Engine noise* is generally the most important contribution. Nevertheless, it is not possible to ignore the noise related to aerodynamics and turbulent flows, known as *airframe noise*, especially during the landing phases. However, there are other sources of noise, e.g. those from ground support vehicles, impacting on community noise. In summary, there are three aviation noise sources near airports (S. Farokhi, 2020) ^[14]:

- i. ***Engine noise***;
- ii. ***Airframe noise***;
- iii. ***Airport ground support equipment***, e.g. towing, baggage handling, maintenance/repair, refueling, food service.

In the next paragraphs we will discuss in detail the problem of aircraft noise. Later, the main regulations imposed by the authorities for aircraft certification will be presented.

2.6.2 Engine noise

High-performance gas turbine engines are very noisy machines. In order to maximize the energy transfer in turbomachinery, modern engines use high-speed wheels of rotating and stationary or counter-rotating blade rows. *Turbomachinery noise* is thus the dominating source of noise in the fore arc of the engine whereas *jet noise* dominates the aft arc (S. Farokhi, 2020) ^[14]. Figure 2.6 shows the noise sources in a separate-flow turbofan engine.

The majority of engine noise is due to *jet noise*. However, the new generation high bypass-ratio turbofans have made it possible to mitigate jet noise, making *fan noise* the most significant contribution. Since the energy transfer is unsteady, the blade wakes are unsteady with periodic vortex shedding structures. The pressure fluctuation in the exhaust jet due to this turbulent structure is the source of broadband jet noise. In his classical paper (1952) ^[21], Sir Lighthill showed that the acoustic power, P_j , in a (cold) subsonic turbulent jet is proportional to the 8th power of the jet speed, V_j :

$$P_j \propto V_j^8 \quad (2.51)$$

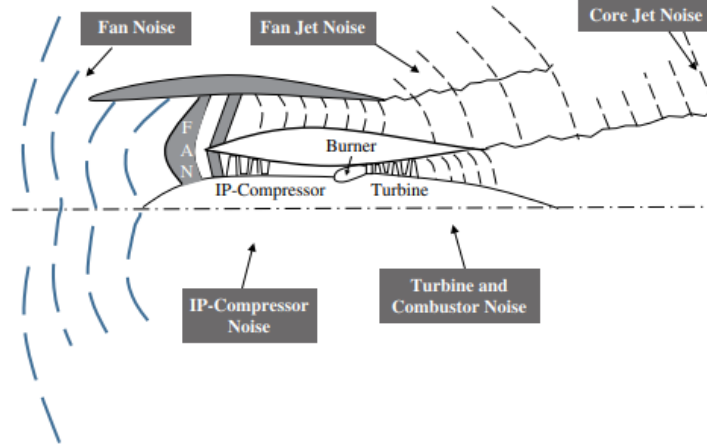


Figure 2.6: Noise sources in a separate-flow turbofan engine (S. Farokhi, 2020) ^[14].

Therefore, to reduce the power of the radiated noise from an aircraft exhaust, the jet speed needs to be reduced. Interestingly, propulsive efficiency is also improved with reduced exhaust speed. The development of high and ultra-high bypass ratio turbofan engines accomplishes both goals, i.e. higher propulsive efficiency and reduced jet noise, simultaneously (S. Farokhi, 2020) ^[14]. Modern fans often have relative tip speeds that are supersonic and therefore cause shock waves. Their associated discrete tone noise is at the *blade passing frequency*, BPF , which is the product between the number of blades, B , and the rotor angular speed, ω_{rotor} :

$$BPF = B \omega_{rotor} \quad (2.52)$$

However, upstream propagating shocks that are not perfectly periodic due to manufacturing tolerances or blade vibration can coalesce and generate the so-called *buzz-saw noise*. These characteristics are shown in Figure 2.7. The directivity of radiated sound from the inlet in the far-field typically has its maximum around 60° from the inlet axis. Instead, the angle from the jet axis where noise reaches its peak level is around 35° (S. Farokhi, 2020) ^[14].

In recent years, numerous efforts have been made to reduce engine noise. Prof. S. Farokhi (2020) ^[14] summarizes the main technologies developed for this purpose:

- One first technology uses wing shielding for engine noise mitigation during landing and take-off phases. It is possible to geometrically shield the emitted pressure waves by means of the lifting surfaces (e.g. the wing). This effect is known as the ***shielding effect***, and can be particularly efficient on fan noise. The shielding effect is strongly dependent on the aircraft configuration. Therefore, the attempt to mitigate noise by means of this effect presupposes an accurate study from the earliest design stages of the aircraft, but it is certainly a valid and strong option in the development of future quiet aviation, since it can easily lead to a reduction of several dB in the total *EPNL*.

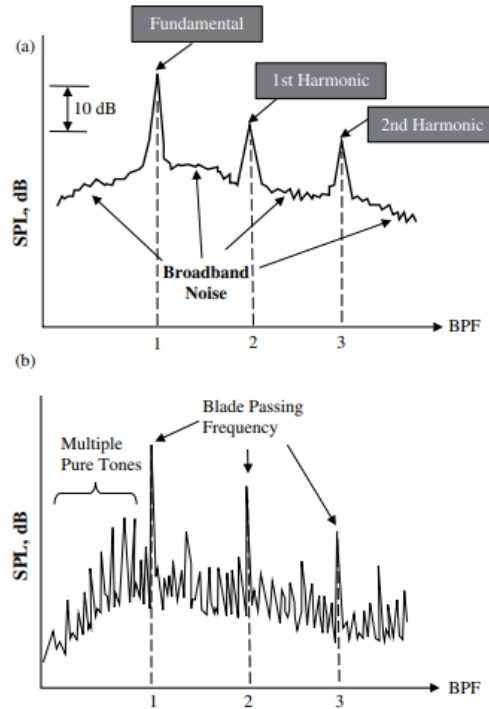


Figure 2.7: The effect of fan tip relative Mach number on its radiated noise: (a) spectra of a subsonic tip fan showing harmonics of BPF and fan broadband noise; (b) spectra of a supersonic tip fan showing *buzz-saw noise* (S. Farokhi, 2020) ^[14].

- The **fan bypass ratio** has played a decisive role in engine noise reduction in commercial aviation. First, the core jet speed is reduced, since its power is drained and supplied to a larger fan. Second, the fan nozzle velocity is lower than the core, which mitigates noise. The use of **acoustic liners** in the fan inlet and exit ducts has also proven effective in fan noise reduction. Acoustic liners are Helmholtz resonators, which may be integrated in an inlet duct or fan exit duct to attenuate fan noise at its dominant frequency. The modern fan blades, that use sweep and reduce thickness, contribute to the fan noise reduction as well. Introduction of *geared turbofan* (GTF) is a technology demonstrator for *ultra-high bypass* (UHB) turbofan engines that are designed with bypass ratios higher than 12. This feature alone is responsible for engine noise reduction of about 20 dB with respect to the cumulative noise level limited by the ICAO, which corresponds to a 50 % reduction in perceived noise.
- Jet noise is a perfect candidate for mitigation since it is proportional to V_j^8 . Beyond a reduction in jet speed, as in high bypass ratio turbofan engines, there are other means of reducing jet noise without paying a severe penalty on gross thrust thanks to the fact that it depends on many other parameters, predominantly on the nozzle pressure ratio and the jet Mach number. **Chevron nozzles** and special acoustic liners for high-temperature applications allow to achieve this goal, mitigating the exhaust noise and reducing the total *EPNL* up to 1 %.

- In the case of supersonic jet, there are different concepts currently under development although no solution is simple to apply, beyond the reduction of jet speed. Chevron nozzles for supersonic jets and fluid injection are only two examples of experimental techniques aimed at mitigating noise emissions of supersonic jets. Advanced propulsion system designs, such as *Variable-cycle engines* (VCE), are the strongest promise for supersonic civil transports. They are designed to operate efficiently under mixed flight conditions, such as subsonic, transonic and supersonic.

2.6.3 Airframe noise

Airframe noise is the noise caused by airflow over airplane surfaces. In other words, it is the far-field noise observed from an airplane when the propulsion system is inoperative. It is a form of aerodynamic noise, generated by the turbulence in the airflow over the outer surface of the airplane. During the approach and landing phases where the power setting is relatively low, the noise produced by the airframe contribute significantly to the total perceived noise. Therefore, airframe is an important source of noise that may impose a lower bound on the noise produced by the airplane, below which further engine noise reduction will not significantly lower the ground observed noise levels.

According to Prof. S. Farokhi (2020) ^[14], it is possible to break down the airframe noise into the following main contributions:

- Landing gear or undercarriage noise due to massively separated turbulent wake;
- Noise due to unsteady wakes originated from wing, flaps, slats, high-lift devices, and radiation from flap edges;
- Turbulent boundary layer formation and radiation from eddies on fuselage and wings;
- Panel vibration;
- Cavities, steps, wheel wells, interaction effects;

The level of airframe noise is dependent upon the aircraft configuration, with particular reference to the deflection of flaps and slats and the presence or absence of landing gears. The landing approach configuration with slats extended, flaps down and undercarriage lowered is therefore considerably noisier than the clean configuration (M.R. Fink, 1977) ^[22].

2.6.4 Noise certification

Nowadays, the increasing perception of the environmental impact of new technologies drives new needs that progress should face, particularly in terms of managing existing technologies and introducing new technologies specifically aimed at sustainability.

The introduction of boundary layer ingestion concepts and ultra-high-by-pass ratio turbofan was aimed at increasing the efficiency of the propulsive systems requiring a lower nominal power and a lower fuel consumption at the same time, consequently affecting the pollutant emitted.

On the other hand, new technologies (e.g. electric motors, piezoelectric actuators, etc.) are aimed at reducing noise emissions. Aircraft design is highly dependent on the regulations under which it must be certified to be operational. Airworthiness codes are constantly updated, and they must be able to merge technological improvements with increasing levels of safety.

The *International Civil Aviation Organization* (ICAO) ^[15] is a special agency charged with the execution of standardization activities on technical and operational aspects of civil aviation. It was established by the Chicago Convention on International Civil Aviation in 1944.

Through the requirements developed by ICAO, and to which all member states have to comply, safe and efficient international air traffic is maintained and enhanced worldwide. These standards and recommended practices are laid down in documents termed *Annexes to the Chicago Convention*. In particular, the *Standards and Recommended Practices for Aircraft Noise*, laid down in *Annex 16, Environmental Protection*, were adopted by the ICAO Council for the first time in 1971 for subsonic jet-powered civil airplanes.

Annex 16 consists of two Volumes, each divided in several Parts. Volume I (1988) deals with the requirements on noise emissions, and Volume II (1981) gives the provisions related to aircraft engine emissions. The noise certification standards contained in Annex 16 have been developed by the *Committee on Aircraft Noise* (CAN) instituted by ICAO in 1970. In 1983 CAN has been renamed *Committee on Aviation Environmental Protection* (CAEP).

Due to the development and application of noise reduction technology there has been a steady decrease in noise emissions from new type aircraft, through which the ICAO was able to establish more stringent noise requirements for completely new designs of aircraft. Moreover, similar standards have been formulated for other types of aircraft. The current noise level standards for subsonic jet airplanes are described in the Chapter 3 of Part II of Annex 16 - Volume I ^[17].

2.6.5 Certification of subsonic jet aircraft

When performing noise certification under Annex 16 - Volume I ^[17], the airplane must execute a series of landing and take-off maneuvers over the following three measurement stations (see also Figure 2.8):

- i. (**Approach**). On the approach to landing, at a point on the extended centerline of the runway and at a distance of 2000 m from the threshold;
- ii. (**Flyover**). On take-off, at a point on the extended centerline of the runway and at a distance of 6500 m from the start of take-off roll;
- iii. (**Lateral**). On take-off, at a point on a line parallel to and 450 m from the runway centerline where the noise level is the maximum during take-off.

The noise evaluation measure is the effective perceived noise level (*EPNL*), already defined in section 2.4.5. The noise levels at the three reference measurement points shall not exceed the values indicated in Figure 2.9. The noise limits are functions of the maximum certificated take-off mass of the airplane.

With regard to lateral noise, sufficient measurement points must be used to demonstrate that the maximum noise level has been determined. Also simultaneous measurements must be made at one test point at a symmetrical position on the other side of the runway.

The approach reference flight path must be calculated on the basis of a stabilized flight speed and following a -3° path. The mass of the airplane at the touchdown must be the maximum landing mass permitted in the approach configuration at which noise certification is requested.

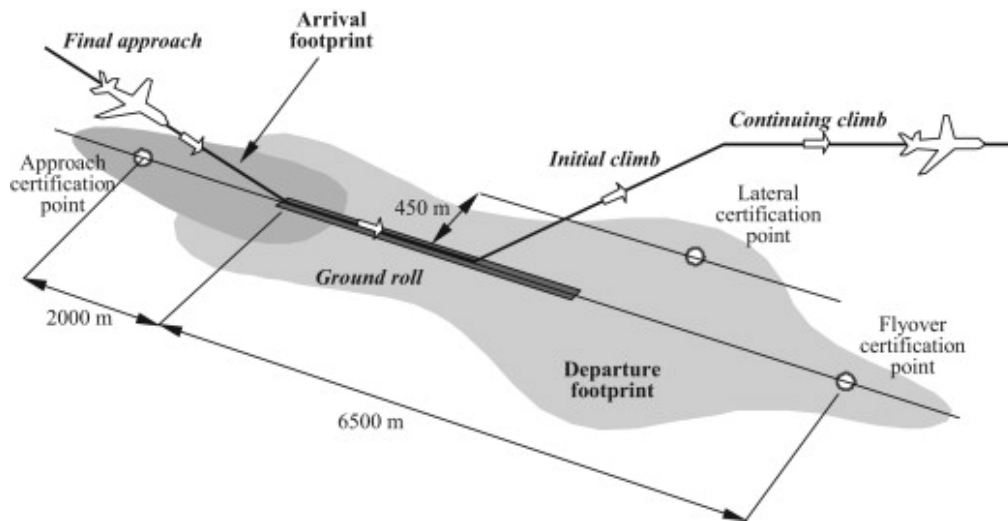


Figure 2.8: Annex 16 - Volume I, measuring locations (Credits: Prof. A. Filippone) ^[23].

M = Maximum take-off mass in 1 000 kg		0	20.2	28.6	35	48.1	280	385	400
Lateral full-power noise level (EPNdB) All aeroplanes		94		80.87 + 8.51 log M					103
Approach noise level (EPNdB) All aeroplanes		98		86.03 + 7.75 log M				105	
Flyover noise levels (EPNdB)	2 engines or less	89			66.65 + 13.29 log M				101
	3 engines	89		69.65 + 13.29 log M					104
	4 engines or more	89	71.65 + 13.29 log M						106

Figure 2.9: Allowable noise levels at the three measurement points (ICAO Annex 16) ^[17].

The take-off reference trajectory starts from the take-off roll and ends when at least the following height above the runway level is reached:

- Airplanes with one or two engines: 300 m;
- Airplanes with three engines: 260 m;
- Airplanes with four engines or more: 210 m.

After reaching the specified height, the thrust must not be reduced below that required to maintain a climb gradient of 4 % and a level flight in the case of a multi-engine airplane with one engine inoperative. The mass of the airplane must be the maximum take-off mass at which the noise certification is required.

In all cases, the noise certification reference flight procedures must be calculated under the following reference atmospheric conditions:

- Sea level atmospheric pressure of 101325 Pa;
- Ambient air temperature of 25°C;
- Relative humidity of 70%;
- Zero wind.

The regulations allow that the noise level goes beyond the limits at one or two measurement points if the sum of the excesses is not greater than 3 dB, and any excess at any single point is not greater than 2 dB.

3

Noise Prediction Method

3.1 Aircraft noise prediction

3.1.1 The ADORNO Project

ADORNO ^[6], acronym of *Aircraft Design and nOise RatiNg for regiOnal aircraft*, is a European project that focuses on the development of aircraft models for a regional aircraft engine platform. The main objective is to provide aircraft requirements as well as trade factors for specific fuel consumption and engine drag for both a year 2014 reference aircraft and a CS2 target aircraft. Three main partners are involved in the project:

- **University of Naples “Federico II”** ^[7], as the coordinator of the project;
- **MTU Aero Engines** ^[8], as the Topic Leader;
- **Lead Tech** ^[9], as participant.

The collaboration between MTU Aero Engines and the University of Naples aims to increase their knowledge about the problem of the environmental impact of transport aircraft. Lead Tech’s role is to provide technical support in software development, in particular as regards the drafting of technical documentation.

As already explained in the introduction to this dissertation, the overall ADORNO work plan is divided into four *Work Packages* (WP). WP3 concerns the development of a software for the prediction of aircraft noise that will be integrated into the aircraft design chain. The software is called **ATTILA** and will be introduced in the next paragraph.

3.1.2 Aircraft noise prediction Including performance

ATTILA, acronym of *Aircraft noise prediction Including performance*, is a software originally developed at UNINA by the vibro-acoustics research group for the estimation of the noise produced by an aircraft (C. Casale et al., 2019) ^[12].

It was originally coded in MATLAB ^[24] with the purpose of estimating the acoustic emissions of a turbofan civil aircraft with reference to the main certification tests required by ICAO regulation (i.e., Approach, Lateral, Flyover - see section 2.6). The metric used to quantify the noise emissions is the effective perceived noise level (*EPNL*). The tool also allows to estimate different noise metrics for each certification point and for each contribution to the overall aircraft noise, such as *SPL*, *OASPL*, *PNL* and *PNLT*, already introduced in Chapter 2.

To allow the use of ATTILA within MTU's IT-framework, the code architecture has undergone a complete redesign. Nonetheless, since the final tool should be also used by UNINA in order to carry out design and analysis tasks, the starting philosophy of a stand-alone application has been kept, to allow both MTU and UNINA to make use of the same software for preliminary noise estimations.

The redesign process of ATTILA has seen a strong collaboration between UNINA and MTU, to definitely set the specifications for the noise analysis tool. In order to accelerate the activities concerning the development of a preliminary version of the software compatible with MTU's IT-framework, the author of this dissertation carried out a three-month internship at MTU Munich, from 7 January 2020 to 6 April 2020, as a representative of the University of Naples.

The work described in this section has been successfully finalized mainly thanks to this close collaboration. The new tool, adapted to these specific requests and re-written in C++, has been renamed **ATTILA++**. To underline that the code is still far from its final form, in this chapter and in the following one we will refer to the version 0.8.1 of the software (**ATTILA++ v0.8.1**).

3.1.3 Additional requirements and technical needs

As mentioned above, the implementation to MTU's IT-framework has yielded to additional requirements to be fulfilled by the final noise tool. Two different usage scenarios can be distinguished. One regards the use within the aero-acoustic department (TEAT). In this case the software should accept input data in the form of *comma-separated values* files (*.csv*), while output data should be written in the form of text files (*.txt*). The second usage provides for an interface to the NPSS environment for pre-design applications ^[25]. In this case, the modules dedicated to the calculation of *SPL* and *PNLT* should be directly callable from an external application, and the results should be directly returned to the user.

Coordination with MTU has brought to the selection of C++ as the new programming language, and to the adoption of *object-oriented programming* (OOP) paradigms to redesign the software. NPSS, in fact, is written in C++, so the selection of this programming language would have for sure simplified the interface between the tools. In addition, OOP paradigms allow to more easily pursue several software engineering goals, such as reusability, extensibility, and flexibility, granting a reduction in time required to produce working code, enhancing code reliability, and easing maintenance tasks and further updates. Last but not least, a code written in C++ can be compiled on both Windows and Linux platforms, as long as cross-platform libraries have been used. In addition to easing the interface between the noise tool and MTU's internal framework of software, several more specific requirements were also set by MTU:

- i. The software must allow the user to define arbitrary flight paths, as well as arbitrary microphone locations, in order to guarantee the maximum freedom in terms of customization of calculation conditions.
- ii. The software must leave the user the opportunity to choose which contributions to include in the calculation of the total noise.
- iii. The software must let the user modify even parameters that are usually deemed constant, such as the ones related to gas properties, or the ones directly linked to measurements ruled by regulations. This would allow to avoid inconsistencies between one software and another, and would lead to an easier customizability of the calculation conditions, achieving greater flexibility to changes in terms of new requirements from local or national authorities.
- iv. Input data should be taken from external *.csv* files. The software should also be able to take as input additional external data already containing the contribution of one or more noise sources, to replace the calculation of the same with the data already provided by external tools.
- v. The software must exit clearly on errors, reporting events, exceptions and warnings in a log file. This would increase the stability of the software and allow an efficient diagnosis of the problems.
- vi. The necessary runtime for the calculation of *SPL* for a single noise source should not exceed an agreed threshold, in order to allow the usage of the noise tool for pre-design evaluations within the context of optimization processes.
- vii. The software should include a module for the evaluation of the *shielding effect*. This would of course improve the accuracy of noise estimations, including an additional effect which is usually taken into account at more advanced design stages than preliminary design. In addition, the estimation of engine noise shielding by lifting surfaces would enable the analysis of unconventional aircraft configuration, such as H-tail or U-tail layouts with over-horizontal-tail-mounted engines, or over-wing-mounted engines.

- viii. Additional noise metrics should be added to the ones already available in ATTILA, in order to enhance user capability to customize the output.
- ix. In case of embedded usage, the software should allow to create an input file from the set of input parameters, in order to ease an eventual subsequent use as a stand-alone tool.

Finally, although MTU has already its own tools for engine noise estimation, UNINA is also currently testing the theoretical model proposed by ESDU item no. 98008 ^[26] for fan/compressor noise estimation (valid for turbofan engines), in order to have its own tool estimating at least some of the engine noise components. In addition, the software could include a module for the evaluation of propeller noise, which would allow to extend the use of the software also to the case of propeller-driven aircraft. In any case, this function is not one of the main objectives agreed.

Requirements from i to iv, vi and ix have already been met in the new version of the software programmed in C⁺⁺, which will be presented in the next sections. The remaining requirements constitute one of the objectives to be achieved in the near future within ADORNO.

3.2 Methodologies implemented by ATTILA⁺⁺

3.2.1 Introduction

In this section we will introduce the methodologies and techniques on which ATTILA⁺⁺ (v0.8.1) is based, which can provide an estimate of the noise produced by an aircraft. Most of the theoretical knowledge used in the tool development has been provided by some ESDU documents.

ESDU ^[27] (originally an acronym of *Engineering Sciences Data Unit*) is an engineering advisory organization which provides validated engineering analysis tools in the fields of aerospace engineering, process engineering and structural engineering. Tools provided by ESDU cover a wide range of engineering disciplines. Its work is monitored, guided and validated by technical committees comprised of leading experts from industry, academia and government organizations from around the world. In particular, some ESDU papers will be briefly summarized in the next paragraphs. They provide a means of estimating the airframe noise and some main propagation effects. Furthermore, although at the moment the code is not provided with an integrated module for the engine noise prediction, ESDU item no. 98008 ^[26] for the estimation of the noise emitted by fans and compressors will be briefly described. UNINA is currently testing the methodologies proposed by the item, and the results that will be shown in the next chapter are obtained by means of them.

3.2.2 Evaluation of airframe noise

ESDU item no. 90023 ^[28] provides a methodology with which an airframe noise estimation can be carried out on the basis of the main geometric and architectural characteristics of the aircraft. This methodology does not replace an in-depth analysis of the aircraft's acoustic emissions, but can be useful in the pre-design phase to take into account the effects of the design parameters on the aircraft noise certification.

The theory used for the evaluation of airframe noise consists of a semi-empirical prediction method which has been developed from that proposed by Martin R. Fink (1977) ^[22] with changes to directivity and spectral functions based on recently available data. Geometry and operating conditions are required input data. Figure 3.1 shows the geometric representation of angles θ and ϕ_f at the base of the following discussion. Angle θ is known as polar emission angle and ϕ_f is the azimuthal angle. The airframe noise is calculated by summation for any selected combination of the following airframe components:

- i. Wing (conventional or delta);
- ii. Horizontal tail;

- iii. Vertical tail;
- iv. Flaps;
- v. Slats;
- vi. Main landing gear;
- vii. Nose landing gear.

Although the fuselage does produce some lift, most of the fluctuating lift and drag forces which generate the noise are associated with the components listed above. The contribution of noise from the fuselage may be considered negligible at a reception point in the far-field.

Radiation from clean airframes is assumed to be caused by convection of the turbulent boundary layers past the trailing edges of lifting surfaces. The resulting trailing edge noise radiation has been studied analytically, and functional dependence given by those analyses has been verified experimentally by Fink (1977) ^[22].

Noise contributions from the nose landing gear and main landing gear are calculated separately because generally each has a different size and therefore a different peak frequency (M.R. Fink, 1977) ^[22].

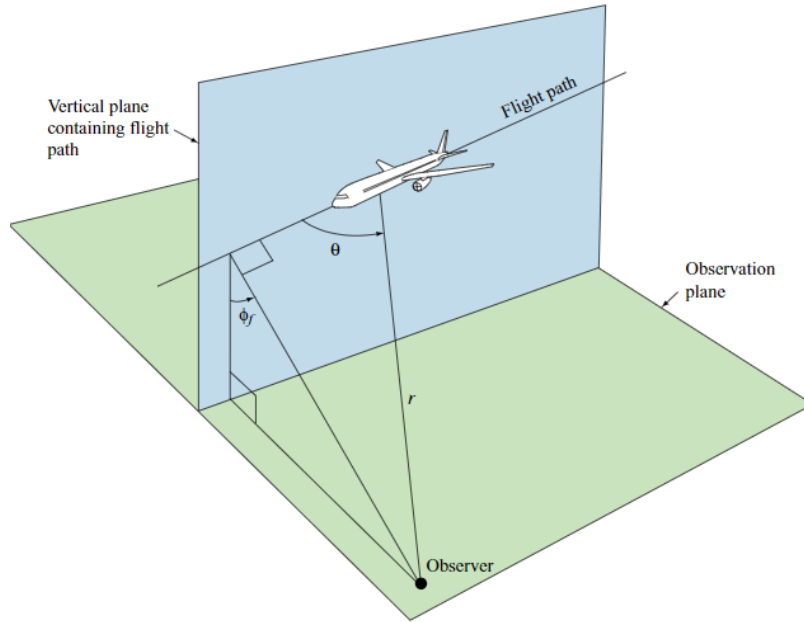


Figure 3.1: Representation of the airplane-microphone geometric configuration for the airframe noise estimation (ESDU item no. 90023) ^[28].

Noise from the trailing edge flaps is calculated regardless of whether the landing gear is extended or retracted. This would seem to be a questionable assumption. Extending the landing gear generates turbulence from wheels, struts, and open cavities. This turbulence is convected past the trailing edge flaps and would be expected to generate incidence fluctuation noise. This effect could be taken into account if the intensity, scale length, and lateral extent of the landing gear turbulent wake were known. However, this type of interaction noise is not considered by the procedure (M.R. Fink, 1977) [22].

Noise from leading edge slats was found to be representable as a sum of noise from the slat itself plus increased trailing edge noise from the wing. This is the only case for which an interaction effect is included in the calculations described in the ESDU document [28]. Some tests conducted by Fink (1977) [22] showed that neglecting all the other effects of interaction between noise sources does not preclude that the theoretical prediction is perfectly in agreement with the experimental results.

For each component, the sound pressure level at the reception point, adjusted for the difference in ambient pressures at aircraft and reception point locations, is given by equation 3.1, in accordance with 2.42:

$$SPL = 10 \log(p^2) + 10 \log\left(\frac{\rho_{\infty,s}^2 c_s^4}{p_{Ref}^2}\right) - 20 \log\left(\frac{p_{\infty,s}}{p_{\infty,r}}\right) \quad (3.1)$$

Where ρ_{∞} , c and p_{∞} are the air density, the sound speed and the ambient pressure. Subscript s refers to the source location, as well as subscript r refers to the microphone location. Here, the quantity p^2 represents the mean-square acoustic pressure divided by $\rho_{\infty,s}^2 c_s^4$, and p_{Ref} is the reference pressure.

The non-dimensional mean-square acoustic pressure is given by:

$$p^2 = \frac{P b_w^2 DI(\theta, \phi_f) F(Sr)}{4 \pi r^2 (1 - M \cos \theta)^4} \quad (3.2)$$

Where b_w is the wing span and P is the acoustic power divided by $\rho_s c_s^3 b_w^2$; Sr is the *Strouhal number*; F is the *spectrum function*; r is the distance between source and receiver; M is the Mach number; DI is the directivity index. The unsteady effects and the frequency dependence are taken into account by the Strouhal number:

$$Sr = \frac{f l (1 - M \cos \theta)}{M c_s} \quad (3.3)$$

Where l is a length scale characteristic of the airframe component, specified by ESDU item no. 90023 [28], and f is the frequency. For each of the structural components responsible for the production of airframe noise, different functions for the calculation of the Strouhal number Sr , the spectrum function F and the directivity index DI are shown in Appendix A of the ESDU item No. 90023 [28].

All these functions allow the calculation of the *OASPL* and the one-third-octave band *SPL* generated by any source at any reception position within a frequency range and over polar and azimuthal angular ranges set by the user.

The output values are for free-field and still, lossless atmospheric conditions. The method does not account for wind and temperature gradients and ignores any interaction effect between the airframe components. It is not suitable for use on propeller-driven airplanes, mainly because the installation effects associated with propellers are likely to be very different from those associated with the turbofan airplanes used to develop the prediction method. Wing incidence effects have been neglected in the derivation of the method. Although there are no explicit limits on take-off weights or airspeed, this prediction method has been validated for multi-engine turbofan airplanes with maximum take-off weights ranging from 42000 kg to 390000 kg and flying at airspeeds ranging from 70 m s⁻¹ to 145 m s⁻¹.

3.2.3 Evaluation of ground reflection effect

ESDU item no. 94035 ^[20] provides a way to estimate the ground reflection correction, which may be subtracted from a measured spectrum to give a free-field spectrum, or added to a free-field spectrum to give a measured spectrum. With reference to Figure 2.5, the direct wave between the source and receiver propagates over a path length r_1 , while the path length of the reflected wave is r_2 . Angle ϕ_{gr} is made by incident and reflected rays with ground. The theoretical approach used in ESDU item no. 94035 assumes that the sound waves propagate through a still, homogeneous atmosphere with a spherically divergent wave front. This implies zero mean wind and absence of temperature gradients. It is also assumed that the ground plane between source and receiver is flat, and that the sound source radiates equally strongly in the direction of the direct ray and in the direction of the reflected ray before it touches the ground. Both source and receiver are assumed to be stationary. The document provides a method for estimating ground impedance as the frequency changes, on the basis of some constant characteristics of the soil. In order to calculate the aforementioned constants, the ESDU document provides tables which refer to different types of soil:

- i. Snow;
- ii. Grass;
- iii. Sand or sandy soil;
- iv. Limestone chips, dirt roadway;
- v. Wet compacted soil;
- vi. Tarmac, concrete.

After the ground impedance has been evaluated, the reflection factor is calculated and adjusted for the interaction of a curved wave front with a surface of finite impedance. The latter effect is evaluated by using some asymptotic series reported in the ESDU document. The spectrum correction is calculated with a formula similar to 2.49, also taking into consideration the loss of coherence between direct and reflected rays due to the turbulence scattering. The effects of air turbulence on sound propagation can be quantified starting from a constant parameter which identifies the level of turbulence. The choice is among the following options:

- i. Perfectly still;
- ii. Normally still;
- iii. Moderately still;
- iv. Turbulent.

The resulting values assume a perfectly shaped filter, in such a way that some energy from outside the theoretical upper and lower limits of the frequency bands is included in the analyzed band levels. The effect of a practical filter is also taken into account by a further corrective step provided by the document.

3.2.4 Evaluation of atmospheric attenuation

ESDU item no. 78002 ^[29] gives a means of estimating the atmospheric attenuation due to gaseous absorption as the sound wave propagates through the atmosphere.

The attenuation over distance, $I(r)$, can be derived from the intensity attenuation coefficient as follows:

$$I(r) = I(0) e^{-mr} \quad (3.4)$$

Where $I(0)$ is the sound intensity at the origin. The *intensity attenuation coefficient*, m , represents the characteristic speed with which the intensity decreases as the distance increases. This leads to the following expression for the reduction of *SPL* due to atmospheric attenuation:

$$\Delta SPL = 10 \log \left[\frac{I(0)}{I(r)} \right] = 434.3 m r \quad (3.5)$$

Where distance r is expressed in m/100. Therefore, comparing equations 2.44 and 3.5, the atmospheric attenuation coefficient α_A can be expressed as:

$$\alpha_A = 434.3 (m_O + m_N + m_C) r \quad (3.6)$$

Where m_O is the attenuation coefficient linked to the molecular vibration of oxygen, m_N is the one for nitrogen and m_C is the one related to translational and rotational modes. The reason for which the attenuation due to molecular translation and rotation can be considered together is that they vary in the same way with frequency and temperature within the frequency range of interest.

The acoustic absorption due to molecular vibration is dependent on the maximum intensity loss per wavelength and the frequency at which this loss occurs. This frequency is called the *relaxation frequency*. It corresponds to the relaxation time which characterizes the transfer of translational energy to internal vibrational modes, and it depends on the peculiar collisional dynamics that occur in the gas. The relaxation frequency of oxygen is different from that of nitrogen but, for both gases, it is dependent on the amount of water vapor in the atmosphere. Because of the difference between the relaxation frequencies of oxygen and nitrogen, the energy loss due to the relaxation of oxygen and nitrogen molecules is estimated separately and the two components added to obtain the total attenuation due to molecular vibration.

For a given gas the maximum intensity loss per wavelength is dependent on temperature and independent of pressure. ESDU item no. 78002^[29] provides empirical formulas for the estimation of relaxation frequencies and the maximum intensity loss per wavelength. This methodology allows an estimate of the coefficients of the atmospheric absorption effect, but does not take into account any temperature or relative wind gradient.

3.2.5 Evaluation of lateral attenuation effect

In the literature, *lateral attenuation* is defined in a number of different ways and as yet there is no universally accepted definition. In this context, lateral attenuation is defined as the difference between the one-third-octave band and sideline free-field sound pressure levels where the propagation distance r and the source radiation angle θ associated with the two far-field sound pressure levels are the same. It is assumed that there is clear line of sight between the aircraft and the observer. More than a real single effect, lateral attenuation is the sum of all the effects due to non-ideal conditions, the absorption of sound as it propagates over a porous surface, and any source installation effects.

The magnitude of lateral attenuation increases with distance and, at low elevation angles β (see Figure 3.2), increases with decreasing values of β . At larger distances, the values of lateral attenuation tend asymptotically to a value which depends on frequency and elevation angle.

ESDU item no. 82027^[30] provides two sets of lateral attenuation data, one for each of two common configurations of jet-powered civil aircraft:

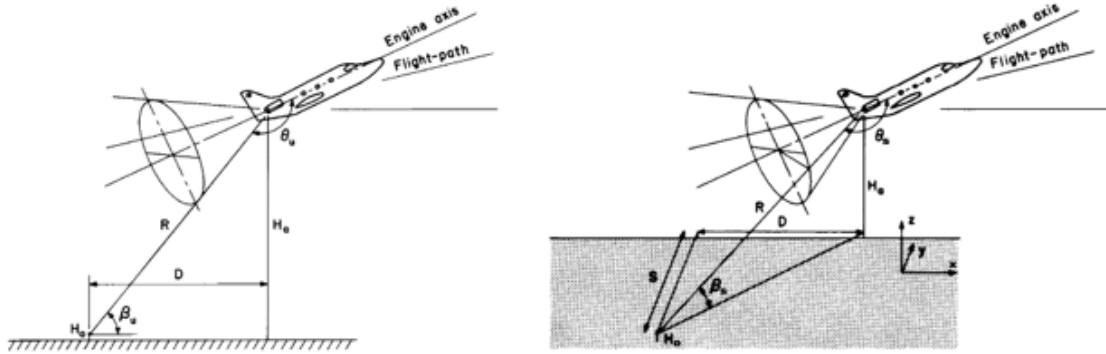


Figure 3.2: Relationship between source and observer (ESDU item no. 82027) [30].

- i. Aircraft with engines mounted below the wing;
- ii. Aircraft with engines mounted in the rear fuselage.

The values of lateral attenuation for each frequency have been found for the given combination of propagation distance r and elevation angle β . A series of graphs for both the aircraft configurations are reported in the ESDU document. By interpolating this database starting from the actual values of r and β , it is possible to obtain the correction of interest.

3.2.6 Evaluation of engine noise

It is necessary to perform a preliminary global computation of the contribution of engine noise to the overall noise level. This is particularly important for predicting acoustic emission of an airplane for those conditions where engine noise provides a major contribution.

At present, ATTILA⁺⁺ has only the capability to accept external input generated by the user to estimate engine noise for a specific flight condition. Different tables of *SPL* must be provided for different engine throttle values and for the two engine ratings that are currently employed by ATTILA⁺⁺ to perform engine noise estimations for ICAO certification:

- **Take-off** (for Flyover and Lateral conditions);
- **Approach** (for Approach conditions).

SPL spectra must be provided, for each engine setting, for different throttle ratios, here referring to the ratio between the actual engine output in terms of thrust and the one that is actually available, for a specific flight condition (Mach number, flight altitude and ISA temperature) and a specific engine setting.

Based on the input data provided through the engine noise dataset, ATTILA⁺⁺ performs an engine noise assessment by employing linear interpolation on the data provided. Additional effects are taken into account in order to have an estimate of the engine free-field noise contribution: a Doppler shift (see section 2.5.3) is applied to the interpolated data in order to consider source motion, and the actual radial distance is also taken into account to simulate the effects of noise spreading (see section 2.5.2) due to propagation.

Finally, it is appropriate to take a quick look at the methodology contained in ESDU item no. 98008^[26] for estimating the noise generated by fans and compressors. Although it is not currently implemented in ATTILA⁺⁺, UNINA's group is currently studying the problem of turbofan noise on the basis of this document. The engine dataset necessary for the analyses performed by ATTILA⁺⁺ is currently calculated by means of a different software which makes use of the ESDU document. Therefore, the results that will be shown in the next chapter also include an engine noise contribution obtained in this way.

The method is based on the one originally derived by Heidmann (1975)^[31]. It considers the noise radiated from the inlet duct and the discharge duct separately. In both cases, there is a broadband noise component and a discrete tone component. In the noise emitted from the fan or compressor inlet duct there is also an additional combination tone, or *buzz-saw* component when the relative tip speed is supersonic.

At each angle, the component spectra are summed on an energy basis. For multi-stage fans, the final spectrum is obtained by summing the sound energy from each stage. For each component, the procedure predicts the spectrum shape, the spectrum level and the free-field directivity. The spectrum shape, which is essentially fixed for each component, is placed within the frequency range according to the value of the blade passing frequency (see equation 2.52). The spectrum levels are predicted from the mass flow rate, the total temperature rise associated with a fan stage, and both the design and operating values of the rotor tip relative inlet Mach number.

Corrections are then applied to these basic spectrum levels on the basis of:

- The presence or absence of inlet guide vanes;
- The rotor-stator spacing;
- Inlet flow distortions which are present for static and low speed ground-roll operations and absent at the higher speeds occurring in flight;
- Tone cut-off where the fundamental tone is suppressed according to a criterion determined by the number of rotor and stator blades and the value of the rotor tip Mach number.

ESDU item no. 98008^[26] has been validated for up to two stages, thus it is not suggested for turbofans with more than two fan or compressor stages. It is assumed that the operating point is near the steady-state operating line and caution must be exercised if the operating point is above the design point. It is also assumed that inlet and discharge ducts do not amplify or attenuate the generated noise. The method predicts free-field *SPL* values in one-third-octave bands from 50 Hz to 10 kHz for a still lossless atmosphere, and these vary with the polar angle θ but not with the azimuthal angle ϕ_f . In general, this method predicts adequately the general properties of far-field noise spectra. The trends exhibited by experimental data are predicted in a satisfactory manner, but the method does not always predict the detailed variations in the spectra from angle to angle. This is true especially for non-typical fan operating conditions.

Specifying in detail the procedures provided by this method is beyond the scope of this chapter, since ATTILA⁺⁺ does not implement it internally. However, it is necessary to specify that the results provided by this ESDU item are highly dependent on the number of *revolutions per minute*, *RPM*. Therefore, knowing the correlation between *RPM* and throttle ratios for different flight conditions is of fundamental importance for a correct estimation of the aircraft noise by ATTILA⁺⁺.

In the end, it is also important to specify that the methodology does not allow to estimate all the acoustic sources of a typical engine (see Figure 2.6), so it is reasonable to assume that the final result constitutes an underestimation of the total noise emitted by an engine.

3.2.7 Noise metrics

ATTILA⁺⁺ (v0.8.1) allows the estimation of aircraft noise levels in terms of the following quantities:

- *SPL* in 24 one-third-octave bands;
- *OASPL*;
- *PNL*;
- *PNLT*;
- *EPNL* (with or without tone correction).

The procedures adopted to estimate *OASPL*, *PNL*, *PNLT* and *EPNL* have already been described in section 2.4. ATTILA⁺⁺ allows the estimation of the *EPNL* with or without the tone correction. For this reason, in the input and output files of ATTILA⁺⁺ (v0.8.1) a distinction is made between the *EPNL_{nT}* (without tone correction), and the *EPNL*, which is the classic metric to which the regulations refer.

3.3 Software architecture of ATTILA⁺⁺

3.3.1 General overview

This section is aimed at providing a brief description of the current state of ATTILA, giving an overview of the software architecture up to now. The updated noise tool is completely written in C⁺⁺ and it has been designed following all the paradigms of object-oriented programming:

- Bottom-up approach;
- Program organized around objects, grouped in classes;
- Focus on data with methods to operate upon object's data;
- Interaction between objects through functions;
- Reusability of design through creation of new classes by adding features to existing classes.

The general architecture of the software is described by Figure 3.3, Figure 3.4 and Figure 3.5. Figure 3.3 provides an overview on the typical workflow of ATTILA⁺⁺. Here, the classes and the set of input and output data have been highlighted, along with their usage during the analysis workflow. Figure 3.4 shows the hierarchy of classes which exists in ATTILA⁺⁺ (v0.8.1).

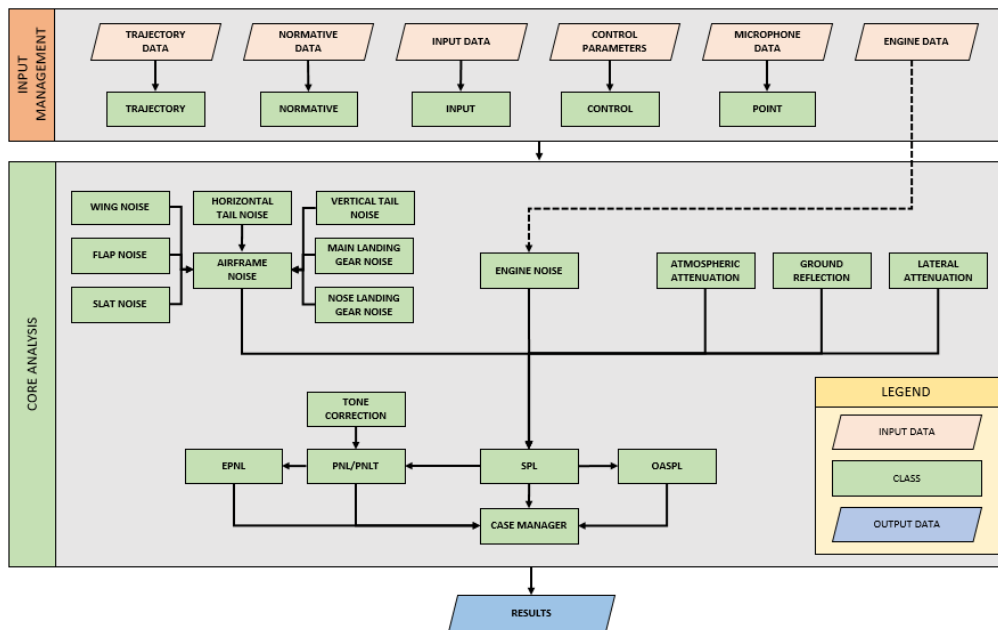


Figure 3.3: Main architecture and typical analysis workflow of ATTILA⁺⁺ (v0.8.1).

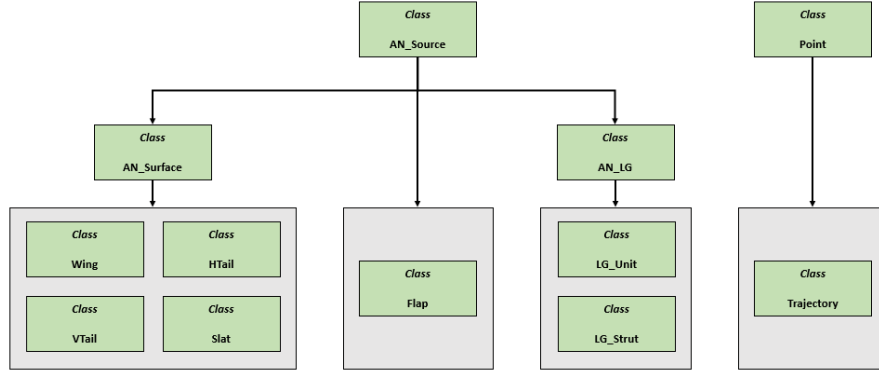


Figure 3.4: Hierarchy of classes and inheritance relationships in ATTILA⁺⁺ (v0.8.1).

All the classes related to single airframe components (lifting surfaces, high-lift devices, etc.) derive from the same super-class, *AN_Source*, from which they inherit methods and attributes. A distinction has been made between classes modeling landing gear components, the one modeling flaps, and those modeling wings and high-lift devices, since the implemented methodologies for the estimation of the mean-square acoustic pressure were quite different. In view of this, classes for landing gear components and classes for lifting surfaces are connected with two different super-classes, *AN_LG* and *AN_Surface* respectively, which in turn inherit methods and attributes from the most generic airframe super-class, *AN_Source*.

Figure 3.5, finally, shows an overview on the utility classes (i.e., classes that do not require to be instantiated and implement methods to be employed across several different classes) that ATTILA⁺⁺ has been provided with. These classes have here been distinguished depending on the phase of the workflow shown in Figure 3.3 in which they are employed the most.

3.3.2 Description of the classes

This paragraph provides a more in-depth description of the system of classes employed by ATTILA⁺⁺. The role of each of the classes shown in Figure 3.3, Figure 3.4 and Figure 3.5 will be described. For each of them, only a brief overview on its role will be provided. A detailed description of the functions implemented in each class goes well beyond the purpose of this discussion.

Input management

The following classes are used by ATTILA⁺⁺ in order to fulfil tasks related to input data management:

- **Input.** It allows the extraction and the management of main input data (e.g., wing span, wing area, number of flap slots, etc.).

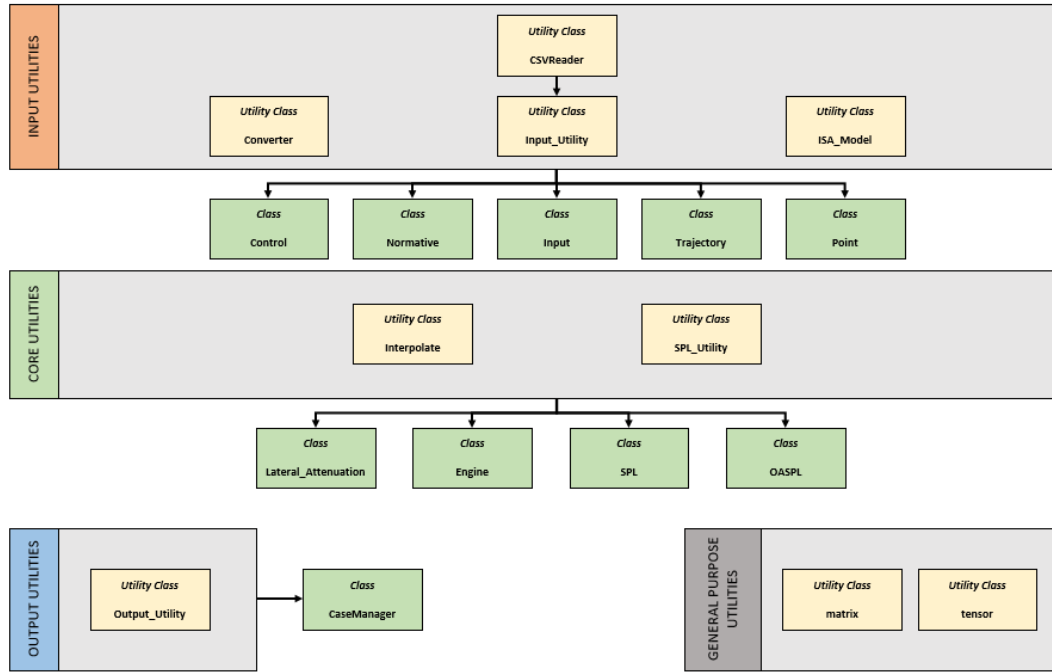


Figure 3.5: Utility classes and their most prominent usage in ATTILA⁺⁺ (v0.8.1).

- ***Point***. It allows the extraction and the management of microphone data. These data include the microphone positions with respect to a global reference frame and atmospheric conditions (air temperature, pressure, density, sound speed, kinematic viscosity, specific heat ratio) at receiver locations. The utility class *ISA_Model* is used in order to estimate these conditions.
- ***Trajectory***. It allows the extraction and the management of trajectory data and inherits microphone-related attributes from class *Point*. Trajectory attributes include aircraft time histories in terms of coordinates X, Y and Z with respect to a global reference frame, flight speed, engine throttle, climb angle, flap deflection angle, eventual slat extension, and eventual landing gear extraction. Atmospheric conditions at source locations are estimated thanks to the methods inherited from class *Point*.
- ***Normative***. It allows the extraction and the management of regulation-related parameters and additional input parameters in general. Currently, it is employed in order to manage the one-third-octave band frequencies and the reference pressure value for airframe noise estimation.
- ***Control***. It allows the extraction and the management of the input parameters related to the control of noise analysis. These parameters include the ones which allow to include/exclude specific calculations from the overall analysis, the ones allowing to include/exclude airframe and engine contributions to the overall noise level, the ones specifying the noise metrics to be employed for the analysis, and the ones defining the verbosity of the output files.

Airframe noise

The following classes are used by ATILA⁺⁺ (v0.8.1) to perform the estimation of the root mean-square acoustic pressure produced by airframe noise sources, according to the methodology proposed by ESDU item no. 90023^[28] and already illustrated to the reader in section 3.2.2:

- ***AN_Source***. The most general class for the estimation of airframe noise. Its methods and attributes are inherited by all the airframe noise classes. Implemented methods include those that allow to estimate the Strouhal number, the non-dimensional acoustic power, and the root mean-square acoustic pressure with no propagation effect taken into account.
- ***AN_Surface***. The most general class for the estimation of noise produced by lifting surfaces. Its methods and attributes are inherited by all the classes related to lift-generating components. Implemented methods include those allowing to estimate the spectrum function, specific constants and characteristic lengths of lift-generating components.
- ***AN_LG***. The most general class for the estimation of noise produced by landing gear components. Its methods and attributes are inherited by the classes modelling noise emissions of landing gear struts and landing gear units. Implemented methods include those allowing to estimate the spectrum function and the characteristic lengths of landing gear components.
- ***Wing***. It allows to estimate the contribution of the wing to the overall airframe noise. Its method *calculate*, by employing the functions inherited from classes *AN_Source* and *AN_Surface*, allows to perform the estimation of the root mean-square acoustic pressure for each required combination of source position, receiver position, and one-third-octave band center frequency.
- ***HTail***. It allows to estimate the contribution of the horizontal tail to the overall airframe noise. Its method *calculate*, by employing the functions inherited from classes *AN_Source* and *AN_Surface*, allows to perform the estimation of the root mean-square acoustic pressure for each required combination of source position, receiver position, and one-third-octave band center frequency.
- ***VTail***. It allows to estimate the contribution of the vertical tail to the overall airframe noise. Its method *calculate*, by employing the functions inherited from classes *AN_Source* and *AN_Surface*, allows to perform the estimation of the root mean-square acoustic pressure for each required combination of source position, receiver position, and one-third-octave band center frequency.
- ***Slat***. It allows to estimate the contribution of the slats to the overall airframe noise. Its method *calculate*, by employing the functions inherited from classes *AN_Source* and *AN_Surface*, allows to perform the estimation of the root

mean-square acoustic pressure for each required combination of source position, receiver position, and one-third-octave band center frequency.

- **Flap.** It allows to estimate the contribution of the flaps to the overall airframe noise. Its method *calculate*, by employing the functions inherited from class *AN_Source*, allows to perform the estimation of the root mean-square acoustic pressure for each required combination of source position, receiver position, and one-third-octave band center frequency.
- **LG_Unit.** It allows to estimate the contribution of a single landing gear unit to the overall airframe noise. Its method *calculate*, by employing the functions inherited from classes *AN_Source* and *AN_LG*, allows to perform the estimation of the root mean-square acoustic pressure for each required combination of source position, receiver position, and one-third-octave band center frequency.
- **LG_Strut.** It allows to estimate the contribution of a single landing gear strut to the overall airframe noise. Its method *calculate*, by employing the functions inherited from classes *AN_Source* and *AN_LG*, allows to perform the estimation of the root mean-square acoustic pressure for each required combination of source position, receiver position, and one-third-octave band center frequency.
- **Airframe.** It manages the evaluation of the overall airframe noise in terms of root mean-square acoustic pressure. The overall airframe noise is estimated by taking directives, in terms of aircraft layout (e.g. number of landing gear units/struts) and contributions to be considered, from the set of input parameters.

Engine noise

The following class is used by ATTILA⁺⁺ (v0.8.1) to provide the engine noise:

- **Engine.** It allows to estimate the total contribution of the engines to the overall aircraft noise. The performed noise estimation, in terms of *SPL* spectra in one-third-octave bands, relies on an externally provided engine data set, which is interpolated/extrapolated in terms of polar emission angle and throttle setting. The *SPL* values provided by its method *calculate* have to be intended for free-field conditions, i.e. they do not take propagation effects into account.

Propagation effects

The following classes are used by ATTILA⁺⁺ (v0.8.1) to perform more accurate noise estimations, by taking into account propagation effects that are not directly considered by the methodologies proposed by ESDU item no. 90023^[28] for airframe noise calculations. The corrections provided by the methods implemented in these classes are also used to better estimate the contribution of engine noise:

- ***Ground_Reflection***. It allows to take into account the effect of ground reflection on the aircraft's noise emissions, according to the methodology proposed by ESDU item no. 94035^[20] already discussed in section 3.2.3. The method *calculate* implemented in this class allows to estimate the increase in *SPL* with respect to the free-field spectra, due to the reflection of sound waves on the ground.
- ***Atmospheric_Attenuation***. It allows to take into account the effects of atmospheric attenuation on the aircraft's noise emissions, according to the methodology described by ESDU item no. 78002^[29] already discussed in section 3.2.4. Its method *calculate* allows to perform the estimation of the reductions in *SPL* (i.e., one value for each source position, receiver position and one-third-octave band center frequency) due to the atmospheric attenuation, that have to be algebraically added to the free-field *SPL*.
- ***Lateral_Attenuation***. It allows to evaluate the effects of lateral attenuation on the overall aircraft's noise emissions, according to the procedure described by ESDU item no. 82027^[30] already discussed in section 3.2.5. The method *calculate* implemented in this class performs the estimation of the reductions in *SPL* (i.e., one value for each combination of source position, receiver location and one-third-octave band center frequency) to be algebraically added to the total free-field *SPL*.

Noise metrics

The following classes are used by ATTILA⁺⁺ to perform the assessment of the environmental noise by means of different metrics:

- ***SPL***. It allows to manage the assessment of aircraft's noise emissions in terms of sound pressure levels. This class supervises the estimation of the overall *SPL* spectra by energetically adding the contributions of airframe, engines, and propagation effects. The effects of ground reflection and atmospheric attenuation are also estimated for each isolated component. Instead, the effect of lateral attenuation is estimated only for the total *SPL* spectra.
- ***OASPL***. It allows to manage the assessment of aircraft's noise emissions in terms of overall sound pressure levels (see section 2.4.1).

- ***Tone_Correction***. It allows to manage the evaluation of the tonal correction, in order to estimate the tone-corrected perceived noise level. The procedure implemented for the calculation of the tone correction factors has been described in section 2.4.4.
- ***PNL***. It allows to manage both the evaluation of perceived noise level (*PNL*) and tone-corrected perceived noise level (*PNLT*). Tone correction is applied by employing the methods provided by class *Tone_Correction*. The procedure adopted for the estimation of *PNL* and *PNLT* is the same as described in sections 2.4.2, 2.4.3 and 2.4.4.
- ***EPNL***. It allows to manage the evaluation of the effective perceived noise level (*EPNL*), with or without the tone correction. The procedure adopted for the estimation of *EPNL* is the one described in section 2.4.5. *PNL* and *PNLT* values employed for the estimation of *EPNL* are provided by the methods implemented in class *PNL*.

Analysis and output management

The following class is used by ATTILA⁺⁺ (v0.8.1) in order to fulfil tasks related to the general management of calculation and generation of output files:

- ***CaseManager***. It allows to manage the effective calculation of all the contributions, the additional effects and the noise metrics required by the user and specified in the input files. Instances of class *CaseManager* are built and initialized by instances of each one of the classes aimed at the input management. The actual operation of reading from the input files is performed by those classes. The directives and the attributes collected by these classes are directly used by *CaseManager* in order to carry out the creation of new instances of classes attending to calculation tasks, such as classes related to airframe noise, classes for the modeling of additional effects, and classes related to the calculation of noise quantities. Dedicated methods of class *CaseManager* also allow to create separate *.txt* files for each performed analysis, following the directives set by the user to establish the verbosity of output files. Class *Output_Utility* is employed by these methods.

Utility classes

The following classes are used by ATTILA⁺⁺ (v0.8.1) to implement general purpose methods used across several different classes, or simply to collect methods implemented in some specific classes:

- ***CSVReader***. Utility class collecting static methods for reading values from files in *.csv* format.

- ***Input_UTILITY***. Utility class collecting static methods supporting file reading operations. It directly employs all the static methods provided by class *CSVReader*.
- ***Converter***. Utility class providing static methods for unit conversions.
- ***ISA_Model***. Utility class providing static methods for the calculation of atmospheric parameters. The formulas employed are those of the *International Standard Atmosphere* (ISA).
- ***Interpolate***. Utility class collecting static methods for linear interpolation. These are mainly employed to carry out tasks related to the calculation of engine noise and to the application of the effects of lateral attenuation.
- ***SPL_UTILITY***. Utility class providing static methods for *SPL* manipulation. It also contains methods for the estimation of the effects of spherical spreading and Doppler shift, described in sections 2.5.2 and 2.5.3.
- ***Output_UTILITY***. Utility class providing static methods for exporting results to output files.

3.3.3 Technical and user interfaces

In order to directly interface ATTILA⁺⁺ with the NPSS environment, a dedicated method has been added to the classes which provide for the estimation of *SPL* and *EPNL*. This method requires all the data necessary to carry out the whole calculation, i.e., the method must be provided with all the same input values also required from a stand-alone user by means of input files.

Users can set, for each calculation condition, both the trajectory of the airplane and the positions of the receivers. Moreover, a fourth calculation case has been included, allowing to define from the beginning a new calculation condition, in addition to the three envisaged by the regulations and already available in the MATLAB version of ATTILA. A larger customization is now allowed to the user in terms of output values to be produced and to be printed for each calculation condition. It is now possible to select which noise metrics should be employed for the noise estimation. Users can select the level of detail of the output files, deciding whether to add or not information regarding time histories of noise parameters related to the trajectory, titles, and single contributions to the overall aircraft noise. The software allows to manage a high number of input parameters, even those that are usually deemed constant, such as gas properties or the ones directly provided by regulations. Embedded or internally estimated values are employed in case they are not directly provided by the user.

Input files

This sub-section provides an overview on the input files managed by the tool. For each file a detailed description of the input parameters has been provided:

- i. **Input data.** File *Input* allows to manage input data related to aircraft type, characteristics and dimensions of airframe components, and some additional parameters mostly related to the application of the effects of ground reflection. All the managed input parameters have been listed in Table 3.1.
- ii. **Normative parameters.** File *Normative* allows to manage input data related to regulations and additional input parameters in general. All the managed input parameters have been listed in Table 3.2.
- iii. **Control parameters.** File *ControlParameters* allows to manage input data related to analysis directives (e.g., which analyses should be performed, which aircraft components should be considered, which noise metrics should be employed) and to the verbosity of output files. All the managed input parameters have been listed in Table 3.3.
- iv. **Trajectory data.** *Trajectory* files allow to manage input data related to aircraft trajectory and, in case, atmospheric conditions at source locations. All the managed parameters have been listed in Table 3.4. Different files should be provided for each different analysis to be performed:
 - *Approach*;
 - *Flyover*;
 - *Lateral*;
 - *User Defined*.
- v. **Receivers data.** *Receivers* files allow to manage input data related to receiver positions and, in case, atmospheric conditions at receiver locations. All the managed parameters have been listed in Table 3.5. Different files should be provided for each different analysis to be performed:
 - *Approach*;
 - *Flyover*;
 - *Lateral*;
 - *User Defined*.

Table 3.1: Set of input parameters for file *Input.csv* (ATTILA⁺⁺ v0.8.1).

Variable	Description	Additional Notes
NAME	Project name.	
WAT	Aircraft type index.	0 – Transport airplane; 1 – Glider.
WWT	Wing type index.	1 – Conventional wing; 2 – Delta wing.
SW	Wing surface.	
BW	Wing span.	
SH	Horizontal tail surface.	
BH	Horizontal tail span.	
SV	Vertical tail surface.	
BV	Vertical tail span.	
SF	Overall flap surface.	
BF	Overall flap span.	
N_SLOT	Number of flap slots.	
N_MLG	Number of main landing gear units.	
N_WHEEL_MLG	Number of wheels on main landing gear units.	
D_MLG	Diameter of undeformed tyre of main landing gear wheels.	
S_MLG	Length of uncompressed main landing gear struts.	
N_WHEEL_NLG	Number of wheels on nose landing gear units.	

Continued on next page

Table 3.1 – *Continued from previous page*

Variable	Description	Additional Notes
D_NLG	Diameter of undeformed tyre of nose landing gear wheels.	
S_NLG	Length of uncompressed nose landing gear struts.	
N_ENG	Number of engines.	
POS_ENG	Engine position index.	0 – Rear-mounted; 1 – Under-wing-mounted.
TYPE_GROUND	Ground type.	1 – Snow; 2 – Grass; 3 – Sand; 4 – Limestone; 5 – Wet; 6 – Tarmac.
TYPE_TURB	Air turbulence.	1 – Perfectly still; 2 – Normally still; 3 – Moderately still; 4 – Turbulent.

Table 3.2: Set of input parameters for file *Normative.csv* (ATTILA⁺⁺ v0.8.1).

Variable	Description	Additional Notes
F	Array of one-third-octave band frequencies.	If not provided, center frequencies from 50 Hz to 10000 Hz are used.
P_REF	Reference pressure.	Default value is $2 \cdot 10^{-5}$ Pa.

Table 3.3: Set of input parameters for file *ControlParameters.csv* (ATTILA⁺⁺ v0.8.1).

Variable	Description	Additional Notes
U	Unit reference system.	1 – SI units; 2 – Imperial units.
ENGINE_FILE	File containing the engine dataset.	
ICAPP	Run case Approach.	0 – Not required; 1 – Required.
ICLAT	Run case Lateral.	0 – Not required; 1 – Required.
ICFLY	Run case Flyover.	0 – Not required; 1 – Required.
ICUD	Run case User-Defined.	0 – Not required; 1 – Required.
UD_T_FILE	File containing the definition of the User-Defined trajectory.	
APPROACH_T_FILE	File containing the definition of the Approach trajectory.	
FLYOVER_T_FILE	File containing the definition of the Flyover trajectory.	
LATERAL_T_FILE	File containing the definition of the Lateral trajectory.	
UD_R_FILE	File containing the definition of the User-Defined receivers.	
APPROACH_R_FILE	File containing the definition of the Approach receivers.	
FLYOVER_R_FILE	File containing the definition of the Flyover receivers.	
LATERAL_R_FILE	File containing the definition of the Lateral receivers.	
IA1	Include the contribution of the wing.	0 – Exclude; 1 – Include.

Continued on next page

Table 3.3 – Continued from previous page

Variable	Description	Additional Notes
IA2	Include the contribution of the horizontal tail.	0 – Exclude; 1 – Include.
IA3	Include the contribution of the vertical tail.	0 – Exclude; 1 – Include.
IA4	Include the contribution of the leading edge slats.	0 – Exclude; 1 – Include.
IA5	Include the contribution of the flaps.	0 – Exclude; 1 – Include.
IA6	Include the contribution of the main landing gear.	0 – Exclude; 1 – Include.
IA7	Include the contribution of the nose landing gear.	0 – Exclude; 1 – Include.
IAIR	Include the contribution of the airframe.	0 – Exclude; 1 – Include.
IENG	Include the contribution of the engines.	0 – Exclude; 1 – Include.
IATM	Include the effect of atmospheric attenuation.	0 – Exclude; 1 – Include.
IREFL	Include the effect of ground reflection.	0 – Exclude; 1 – Include.
ILAT	Include the effect of lateral attenuation.	0 – Exclude; 1 – Include.
ISPL	Calculate the <i>SPL</i> .	0 – Not required; 1 – Required.
IOASPL	Calculate the <i>OASPL</i> .	0 – Not required; 1 – Required.
IPNL	Calculate the <i>PNL</i> .	0 – Not required; 1 – Required.
IPNLT	Calculate the <i>PNLT</i> .	0 – Not required; 1 – Required.

Continued on next page

Table 3.3 – *Continued from previous page*

Variable	Description	Additional Notes
IEPNL_NT	Calculate the $EPNL_nT$.	0 – Not required; 1 – Required.
IEPNL	Calculate the $EPNL$.	0 – Not required; 1 – Required.
IOCSV	Generate output files in <i>.csv</i> format.	0 – Not required; 1 – Required.
IOMAX	Print the most critical results (in terms of maximum $EPNL$) in a separate file.	0 – Not required; 1 – Required.
IOMAP	Generate $EPNL_MAP$ files.	0 – Not required; 1 – Required.
IOEW	Print results for all involved receiver locations.	0 – Not required; 1 – Required.
IOALL	Print all the information of interest.	0 – Not required; 1 – Required.
IOSEP	Print frames.	0 – Not required; 1 – Required.
IOTIT	Print titles.	0 – Not required; 1 – Required.
IOTIME	Print arrays containing the reference times.	0 – Not required; 1 – Required.
IOPART	Print all the contributions and the additional effects.	0 – Not required; 1 – Required.
IOTR	Print trajectory details.	0 – Not required; 1 – Required.
IOMIC	Print receiver details.	0 – Not required; 1 – Required.
IOTC	Print tone correction results.	0 – Not required; 1 – Required.
IOA1	Print the contribution of the wing.	0 – Not required; 1 – Required.

Continued on next page

Table 3.3 – *Continued from previous page*

Variable	Description	Additional Notes
IOA2	Print the contribution of the horizontal tail.	0 – Not required; 1 – Required.
IOA3	Print the contribution of the vertical tail.	0 – Not required; 1 – Required.
IOA4	Print the contribution of the leading edge slats.	0 – Not required; 1 – Required.
IOA5	Print the contribution of the flaps.	0 – Not required; 1 – Required.
IOA6	Print the contribution of the main landing gear.	0 – Not required; 1 – Required.
IOA7	Print the contribution of the nose landing gear.	0 – Not required; 1 – Required.
IOAIR	Print the contribution of the airframe.	0 – Not required; 1 – Required.
IOENG	Print the contribution of the engines.	0 – Not required; 1 – Required.
IOATM	Print the contribution of the atmospheric attenuation.	0 – Not required; 1 – Required.
IOREFL	Print the contribution of the ground reflection.	0 – Not required; 1 – Required.
IOLAT	Print the contribution of the lateral attenuation.	0 – Not required; 1 – Required.
PREC	Number of significant digits to be printed after comma.	Default value is 2.
WIDTH	Number of characters to be used as field width for values.	Default value is 10.
WIDTH_TITLE	Number of characters to be used as field width for titles.	Default value is 16.
FILLER	Separator character.	Default delimiter is comma.

Table 3.4: Set of input parameters for *Trajectory.csv* files (ATTILA⁺⁺ v0.8.1).

Variable	Description	Additional Notes
NAME	Name of the trajectory.	
LINEAR	Use a linear trajectory extrapolated from the first coordinates given.	0 – Not required; 1 – Required.
N_LIN	Number of positions to be extrapolated.	
DELTA_LIN	Time interval between two consecutive extrapolated source positions.	
X	X-coordinate of the aircraft.	At least one value must be provided.
Y	Y-coordinate of the aircraft.	At least one value must be provided.
Z	Z-coordinate of the aircraft.	At least one value must be provided.
V	Flight speed.	At least one value must be provided.
THROTTLE_RATE	Throttle valve opening ratio.	At least one value must be provided.
CLIMB_ANGLE	Climb angle.	At least one value must be provided.
FLAP_DEFL	Flap deflection angle.	At least one value must be provided.
SLAT_ON	Extend slats.	0 – Not extended; 1 – Extended. At least one value must be provided.

Continued on next page

Table 3.4 – *Continued from previous page*

Variable	Description	Additional Notes
MLG_ON	Extract main landing gear.	0 – Retracted; 1 – Extracted. At least one value must be provided.
NLG_ON	Extract nose landing gear.	0 – Retracted; 1 – Extracted. At least one value must be provided.
T	Air temperature at source location.	Internally estimated if not provided.
P	Ambient pressure at source location.	Internally estimated if not provided.
RHO	Ambient density at source location.	Internally estimated if not provided.
NU	Kinematic viscosity of air at source location.	Internally estimated if not provided.
GAMMA	Specific heat ratio of air at source location.	Internally estimated if not provided.
C	Speed of sound at source location.	Internally estimated if not provided.
M	Flight Mach number.	Internally estimated if not provided.

Table 3.5: Set of input parameters for *Receivers.csv* files (ATTILA⁺⁺ v0.8.1).

Variable	Description	Additional Notes
NAME	Name of the receivers.	
LINEAR	Use a linear array of receivers extrapolated from the first coordinates given.	0 – Not required; 1 – Required.
N_LIN	Number of positions to be extrapolated.	
DELTA_LIN	Distance between two consecutive extrapolated receiver positions.	
X	X-coordinate of the receivers.	At least one value must be provided.
Y	Y-coordinate of the receivers.	At least one value must be provided.
Z	Z-coordinate of the receivers.	At least one value must be provided.
T	Air temperature at receiver locations.	Internally estimated if not provided.
P	Ambient pressure at receiver locations.	Internally estimated if not provided.
RHO	Ambient density at receiver locations.	Internally estimated if not provided.
NU	Kinematic viscosity of air at receiver locations.	Internally estimated if not provided.
GAMMA	Specific heat ratio of air at receiver locations.	Internally estimated if not provided.
C	Ambient speed of sound at receiver locations.	Internally estimated if not provided.
REL_HUM	Relative humidity at receiver locations (%).	

Output files

Several output files can be produced on request by users for each analysis scenario (Approach, Flyover, Lateral, User-Defined). These files are stored in a folder named *RESULTS*:

- **<CaseName>**. File containing aircraft noise emission expressed in each available metric (*SPL*, *OASPL*, *PNL*, *PNLT*, *EPNL_{nT}*, *EPNL*) or in a subset of them, according to user's requests. The results reported in this file always refer to the microphone which recorded the highest *EPNL* value, and cover every provided position of the aircraft along the trajectory. When requested, isolated contributions to the overall result (including propagation effects) are included in the file. Output values can also be separated by commas. Filename corresponds to the considered analysis scenario (e.g., *FLYOVER.txt*).
- **EPNL_MAP**. File containing the *EPNL* values recorded by all microphones, together with their coordinates in the global reference frame.
- **<CaseName>_<index>**. Additional files which can be produced on request, for each analysis scenario, and for each microphone involved in the simulation. The file structure is the same as described for file *<CaseName>*. These files are stored in a sub-folder named *ALL MICROPHONES*. Their filenames are made up of the case name followed by an index which enumerates the receivers (e.g., *FLYOVER_1.txt*).

Figure 3.6 shows how output files are stored by ATTILA⁺⁺ (v0.8.1), while Figure 3.7, Figure 3.8 and Figure 3.9 exhibit how much the appearance of output files is affected by the different settings given in file *ControlParameters.csv*. Finally, Figure 3.10 shows the structure of file *EPNL_MAP*.

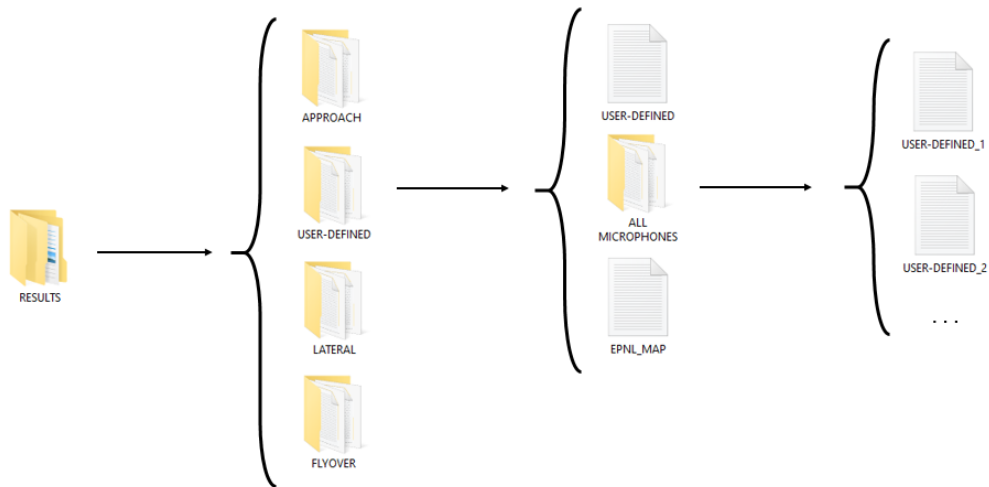


Figure 3.6: Arrangement of output files (ATTILA⁺⁺ v0.8.1).

TOTAL AIRCRAFT (WITH ATMOSPHERIC ATTENUATION, GROUND REFLECTION AND LATERAL ATTENUATION) -----									
Time	0.00	0.50	1.00	1.50	2.00	2.50	3.00	3.50	4.00
Frequency	SPL								

50 Hz	48.71	48.98	49.26	49.54	49.82	50.11	50.41	50.70	51.00
63 Hz	50.17	50.43	50.69	50.96	51.23	51.50	51.77	52.04	52.32
80 Hz	50.88	51.11	51.33	51.56	51.78	52.01	52.23	52.44	52.65
100 Hz	51.58	51.76	51.93	52.10	52.27	52.42	52.56	52.69	52.80
125 Hz	52.38	52.47	52.54	52.59	52.63	52.63	52.61	52.56	52.46
160 Hz	46.51	46.40	46.27	46.12	45.95	45.78	45.64	45.57	45.63
200 Hz	44.34	44.76	45.30	45.95	46.71	47.56	48.50	49.49	50.53
250 Hz	50.47	51.21	51.98	52.75	53.55	54.35	55.16	55.97	56.77
315 Hz	53.62	54.20	54.79	55.37	55.95	56.52	57.08	57.62	58.15
400 Hz	54.26	54.62	54.95	55.27	55.55	55.79	56.00	56.15	56.24
500 Hz	52.23	52.24	52.20	52.10	51.95	51.75	51.52	51.30	51.16
630 Hz	47.61	47.92	48.42	49.08	49.90	50.81	51.78	52.76	53.70
800 Hz	50.44	51.03	51.56	51.99	52.34	52.58	52.69	52.68	52.54
1000 Hz	48.19	48.09	48.03	48.10	48.40	48.98	49.79	50.74	51.69
1250 Hz	46.92	47.60	48.14	48.50	48.68	48.71	48.66	48.70	48.99
1600 Hz	42.97	43.71	44.47	45.15	45.67	46.02	46.29	46.59	47.01
2000 Hz	39.12	39.68	40.25	40.77	41.22	41.69	42.28	42.99	43.67
2500 Hz	33.00	33.61	34.09	34.51	35.09	35.94	36.88	37.55	37.88
3150 Hz	22.73	23.41	24.32	25.33	26.19	26.87	27.65	28.61	29.48
4000 Hz	6.80	7.91	9.07	10.24	11.38	12.56	13.73	14.80	16.03
5000 Hz	-15.98	-14.33	-12.71	-11.10	-9.43	-7.81	-6.19	-4.54	-2.91
6300 Hz	-51.58	-49.18	-46.78	-44.39	-41.99	-39.59	-37.20	-34.81	-32.43
8000 Hz	-107.73	-104.10	-100.46	-96.83	-93.20	-89.58	-85.97	-82.36	-78.76
10000 Hz	-186.15	-180.75	-175.36	-169.99	-164.60	-159.25	-153.90	-148.56	-143.25

OASPL	62.50	62.83	63.16	63.49	63.84	64.18	64.54	64.92	65.31
PNL	66.37	66.77	67.21	67.60	67.97	68.33	68.69	69.04	69.44
PNLT	67.06	67.78	68.32	68.73	69.03	69.12	69.27	69.30	69.67
(Tone Corr.)	0.70	1.01	1.11	1.13	1.06	0.79	0.59	0.26	0.23
EPNLnT	80.55								
EPNL	81.22								

Figure 3.7: Main output file with essential information (ATTILA⁺⁺ v0.8.1).

MICROPHONE POSITIONS -----									
X	6500.00								
Y	0.00								
Z	1.20								
Temperature	288.14								
Pressure	101310.59								
Density	1.22								
Sound Speed	340.32								
Kin. Viscosity	1.5e-005								
Heat Ratio	1.40								

FLYOVER TRAJECTORY -----									
Time	0.00	0.50	1.00	1.50	2.00	2.50	3.00	3.50	4.00
X	5033.10	5071.10	5109.10	5147.10	5185.20	5223.20	5261.20	5299.30	5337.30
Y	0.00	0.00	0.00	0.00	0.00	0.00	0.00	0.00	0.00
Z	441.08	443.18	445.29	447.39	449.49	451.59	453.70	455.80	457.89
Flight Speed	76.10	76.10	76.10	76.10	76.10	76.10	76.10	76.10	76.10
Throttle Rate	0.48	0.48	0.48	0.48	0.48	0.48	0.48	0.48	0.48
Climb Angle	7.87	7.87	7.87	7.87	7.87	7.88	7.88	7.88	7.89
Temperature	285.28	285.27	285.26	285.24	285.23	285.21	285.20	285.19	285.17
Pressure	96138.05	96113.83	96089.62	96065.43	96041.25	96017.09	95992.93	95968.78	95944.66
Density	1.17	1.17	1.17	1.17	1.17	1.17	1.17	1.17	1.17
Sound Speed	338.62	338.62	338.61	338.60	338.59	338.58	338.58	338.57	338.56
Kin. Viscosity	0.00	0.00	0.00	0.00	0.00	0.00	0.00	0.00	0.00
Mach Number	0.22	0.22	0.22	0.22	0.22	0.22	0.22	0.22	0.22
Time Rec.	4.52	4.92	5.31	5.71	6.10	6.50	6.90	7.30	7.69
Distance	1531.43	1495.70	1460.07	1424.58	1389.12	1353.91	1318.85	1283.88	1249.18
Theta	24.56	25.06	25.58	26.12	26.70	27.31	27.95	28.62	29.33
Phi	0.00	0.00	0.00	0.00	0.00	0.00	0.00	0.00	0.00
Beta	90.00	90.00	90.00	90.00	90.00	90.00	90.00	90.00	90.00

Figure 3.8: Additional information on microphones and trajectory (ATTILA⁺⁺ v0.8.1).

WING (WITH ATMOSPHERIC ATTENUATION AND GROUND REFLECTION) =====										
OASPL	46.59	47.06	47.53	48.01	48.50	48.99	49.50	50.02	50.56	
PNLT	51.34	51.41	52.08	52.67	53.14	53.50	53.20	53.72	54.51	
EPNL	68.22									
=====										
ENGINE GROUP (WITH ATMOSPHERIC ATTENUATION AND GROUND REFLECTION) =====										
OASPL	60.69	61.03	61.37	61.73	62.08	62.45	62.83	63.23	63.65	
PNLT	65.17	65.92	66.45	66.86	67.18	67.24	67.58	67.95	68.42	
EPNL	80.10									
=====										
TOTAL AIRCRAFT (WITH ATMOSPHERIC ATTENUATION, GROUND REFLECTION AND LATERAL ATTENUATION) =====										
OASPL	62.50	62.83	63.16	63.49	63.84	64.18	64.54	64.92	65.31	
PNLT	67.06	67.78	68.32	68.73	69.03	69.12	69.27	69.30	69.67	
EPNL	81.22									
=====										

Figure 3.9: Example of main output file with minimum verbosity (ATTILA⁺⁺ v0.8.1).

EPNL FOOTPRINT =====										
X	0.00	0.00	0.00	0.00	0.00	2000.00	2000.00	2000.00	2000.00	2000.00
Y	-500.00	-250.00	0.00	250.00	500.00	-500.00	-250.00	0.00	250.00	500.00
Z	1.20	1.20	1.20	1.20	1.20	1.20	1.20	1.20	1.20	1.20
EPNL	80.73	92.66	125.47	92.66	80.73	85.70	92.87	99.91	92.87	85.70
=====										

Figure 3.10: Example of file *EPNL_MAP* (ATTILA⁺⁺ v0.8.1).

3.4 Functional innovations of ATTILA⁺⁺

3.4.1 Applied improvements

ATTILA⁺⁺ (v0.8.1) has already achieved the fulfillment of more than half of the requirements reported in section 3.1.3. The main goal concerns the capability of ATTILA⁺⁺ to manage a multitude of receivers for each calculation session. The user can define the position of each microphone, specifying its X, Y and Z coordinates. In the MATLAB version, the positions of the microphones were fixed in accordance with the directives of the certification authorities reported in section 2.6.5. Furthermore, it is now possible for the source to describe arbitrary trajectories, which means that trajectories involving three dimensions are now allowed. These two innovations have made it possible to give the software the ability to calculate the noise level (in terms of *EPNL*) in a grid of points, thus obtaining the aircraft's acoustic footprint.

Several conceptual errors and inaccuracies have been found in the MATLAB version of ATTILA, and corrected in ATTILA⁺⁺. The interventions aimed at correcting the main existing inaccuracies are here briefly summarized:

- The flap deflection angles in take-off and landing conditions were reversed before the calculation phase. It means that the input value corresponding to the flap deflection under approach conditions was used in the take-off phases (i.e. for the analysis of cases Flyover and Lateral), and vice versa.
- The contribution of slats to the total noise was taken into account twice.
- The contribution of ground reflection was always subtracted from the free-field solution. This means that the sign of ground reflection correction was not taken into account. Furthermore, as explained in section 2.5.5, this contribution should be subtracted only if the intent is to transform a measured quantity into a free-field solution. Since ATTILA⁺⁺ aims to provide a prediction of the value that will be measured during a certification test, the contribution must be added algebraically to the *SPL* estimated by the other modules.
- Rough assumptions were made about the atmospheric properties of the air. Now they are recalculated at each point on the basis of the ISA model, or given by the user as additional input.
- Before linearly interpolating to obtain the engine noise, the *SPL* values were converted into effective pressures. Interpolating from the latter gave different results, less reliable and less sensitive to variations in throttle.
- The formula used for the calculation of the *EPNL* has been slightly modified in order to make it equal to definition 2.38. Previously, the integral was divided by the observation time instead of the reference time of 10 seconds.

- Negative *SPL* values were sometimes canceled, with compromising effects on the tone correction procedure. In fact, it was not excluded that the tonal correction procedure could lead to the identification of tones even at very low *SPL* values. It has been agreed that this circumstance can never coincide with real situations, since tonal peaks with such a low associated energy level would not be perceivable by a human ear. Moreover, even in the absence of distinct acoustic sources there is always a background noise that raises the pressure level. Therefore, the tonal correction procedure has been slightly modified in order to ignore tones with an amplitude lower than 30 dB, threshold which is roughly representative of the minimum level of background noise that exists during an experimental test.
- The horizontal distance between source and receiver, used for calculating the ground reflection effect according to ESDU item no. 94035 ^[20], was erroneously not considered in absolute value. Furthermore, now it has been completely replaced by the distance of the receiver from the vertical plane containing the aircraft, in order to be more general and valid for all trajectories.
- In some circumstances, flap contribution was incorrectly set to zero because of a manipulation of the formula for the directivity index (see section 3.2.2).
- In accordance with the requirements established and reported in section 3.1.3, the software had to become able to work on arbitrary flight paths, as well as arbitrary receiver locations. This led to the need to modify the formulas used for the calculation of the polar emission angle, θ , and of the azimuthal angle, ϕ_f (see Figure 3.1). Previously, θ was calculated as:

$$\theta = \arccos\left(\frac{\Delta x}{r}\right) + \alpha \quad (3.7)$$

And ϕ_f was calculated as:

$$\phi_f = \arcsin\left(\frac{|\Delta y|}{\sqrt{\Delta y^2 + \Delta z^2}}\right) \quad (3.8)$$

Where α is the climb angle and Δx , Δy and Δz represent the distances of the source from the receiver (positive if the coordinate of the source is greater). These formulas are valid only if one considers a trajectory and a microphone both contained by the same single vertical plane. Starting from geometric considerations (see Figure 3.11) it is possible to demonstrate the following relationships, valid in the most general case:



Figure 3.11: Airplane-microphone geometric configuration in the most general case.

$$\begin{cases} \bar{A} = \frac{|\Delta y - \Delta x \tan \Delta|}{\sqrt{1 + \tan^2 \Delta}} & \Delta \neq \pm \frac{\pi}{2} \\ \bar{A} = |\Delta x| & \Delta = \pm \frac{\pi}{2} \end{cases} \quad (3.9)$$

$$\begin{cases} \bar{B} = \left| \Delta z \cos \alpha - \frac{\Delta x + \Delta y \tan \Delta}{\cos \Delta (1 + \tan^2 \Delta)} \sin \alpha \right| & \Delta \neq \pm \frac{\pi}{2} \\ \bar{B} = |\Delta z \cos \alpha \mp \Delta y \sin \alpha| & \Delta = \pm \frac{\pi}{2} \end{cases} \quad (3.10)$$

Where \bar{A} represents the distance of the receiver from the vertical plane containing the straight line tangent to the trajectory of the aircraft, and \bar{B} represents the distance between the trajectory and the orthogonal projection of the microphone on the aforementioned plane. In equations 3.9 and 3.10, Δ is the angle between the vertical plane tangent to the trajectory and the reference plane XZ. Finally, let us define:

$$\bar{C} = \sqrt{\bar{A}^2 + \bar{B}^2} \quad (3.11)$$

Axes X, Y, and Z are automatically determined on the basis of the first two positions occupied by the aircraft. For subsequent positions the angle Δ is calculated by using the 2-argument arctangent function:

$$\Delta = \arctan 2(y_{s,i+1} - y_{s,i}, x_{s,i+1} - x_{s,i}) \quad (3.12)$$

Where x_s and y_s represent the coordinates of the aircraft and the subscripts i and $i+1$ refer to two consecutive instants of time. In conclusion, it is possible to calculate θ in one of the following ways:

$$\theta = \arcsin\left(\frac{\bar{C}}{r}\right) \quad (3.13)$$

$$\theta = \pi - \arcsin\left(\frac{\bar{C}}{r}\right) \quad (3.14)$$

Where r is the distance between source and receiver. Equation 3.13 is valid if the microphone is in the fore arc, and equation 3.14 if it is in the aft arc. Similarly:

$$\phi_f = \arcsin\left(\frac{\bar{A}}{\bar{C}}\right) \quad (3.15)$$

These improvements made it possible to generalize the calculation to any source-receiver configuration, as well as to make the definition of the global reference system better manageable, avoiding sign errors that previously could have occurred. A formal demonstration of the above formulas, studied by the author of this thesis, goes far beyond the purpose of this dissertation.

3.4.2 Future developments

In compliance with the specifications provided by the Topic Leader, the following additions and upgrades have already been scheduled for the future, with regards to those objectives that still need to be fulfilled (see section 3.1.3):

- Work will be done in order to allow the software to accept additional external data containing the contribution of one or more noise sources already estimated by different tools.
- Work will be done in order to include additional noise metrics (e.g. *Sound exposure level, SEL*) and enrich the output content of ATTILA⁺⁺.

- The software will prospectively exit clearly on errors, reporting events, exceptions, and warnings in a log file. Part of this work is currently being performed by UNINA, by catching possibly mistaken values at input level. In a second phase, UNINA is going to be supported in this activity by LeadTech, speeding up the whole process, also thanks to LeadTech's experience on this type of task.
- A suitable solution allowing to include the evaluation of noise shielding effect (see section 2.5.2) by adapting the methodology illustrated by ESDU item no. 79011 ^[32] is currently under study. This strategy has already been discussed and agreed with the Topic Leader. The software architecture already allows to easily include supplementary modules for the estimation of additional effects, so most of the work will be focused on the tailoring of the methodology mentioned above.
- Lastly, there is the intention to add a module for the calculation of propeller noise based on the theoretical model contained in ESDU item no. 95029 ^[33]. The addition of a module dedicated to the estimation of noise emitted by propellers requires some thoughts. The methodology employed for the estimation of airframe noise, in fact, supposes that the aircraft analyzed is equipped with turbojet or turbofan engines ^[28]. The same happens with the methodology for the estimation of lateral attenuation, which also has been developed starting from empirical data for turbojet and turbofan aircraft. Thus, in order to allow ATTILA⁺⁺ to correctly estimate noise levels for a propeller-driven aircraft, a different approach for the estimation of airframe noise and lateral attenuation effects should be considered. Such an approach would be an addition to the one already available, if it specializes for turboprop aircraft, or would totally replace the one currently employed, in case it is a general-purpose methodology which can be applied for both jet and propeller-driven airplanes. In any case, the addition of a module for the estimation of propeller noise should be probably considered at a later stage.

All the functional improvements of the software will be accompanied by a series of technical improvements, in order to achieve all the targets of ADORNO.

4

Aircraft Noise Analysis

4.1 Test case specification

4.1.1 Introduction

In Chapter 2 the problem of aircraft noise has been described and, more generally, the foundations for the understanding of acoustic phenomena have been laid. In Chapter 3, a software for estimating the aircraft's noise emissions has been introduced. This last chapter aims to present the results of the analysis carried out on a specific regional aircraft by means of ATTILA⁺⁺.

The test case will first be introduced and described in detail. Following, the output results will be reported and discussed, comparing the expected *EPNL* values with those actually measured and made available by the official EASA Type Certificate^[34]. In conclusion, the attention will be focused on the results of a sensitivity analysis carried out on the airframe noise and on the total noise produced by the aircraft when some significant design parameters change. This analysis constitutes the first fundamental step towards the application of a multi-disciplinary design optimization (MDO) for aircraft configuration which also integrates tools for noise assessment.

4.1.2 Test case: the Airbus A220-300

The experimental validation of ATTILA⁺⁺ has already been scheduled within the framework of the ADORNO project, but at the moment there is no official data available to testify to its reliability. Nonetheless, it is already possible to give an idea of the effectiveness, the reliability, and the prospective of future developments of ATTILA⁺⁺ by defining a test case based on a real commercial aircraft. The choice fell on the **Airbus A220-300** (Figure 4.1).



Figure 4.1: Airbus A220-300 (ex Bombardier CS300). Credits: Rami Khanna-Prade ^[35].

The Airbus A220 ^[36] (Figure 4.2) is a family of narrow-body, twin-engine, medium-range jet airliners. It was designed by Bombardier Aerospace and originally marketed as the Bombardier CSeries. Bombardier sold the CSeries airliner program to Airbus and it is now marketed by Airbus Canada Limited Partnership, a joint venture between Airbus and the Quebec government's investment arm *Investissement Québec*. The airliner is optimized for the 100-150 seat market segment, and includes the A220-100 and A220-300 models.

The 130-to-160-seat A220-300 (ex CS300) first flew on 27 February 2015, received an initial type certification on 11 July 2016, and entered service on 14 December 2016. The aircraft contains 70 % advanced materials comprising 46 % composite materials and 24 % aluminium–lithium. Bombardier claimed an overall 15 % lower seat-mile cost, 20 % lower fuel burn and a CO₂ emissions advantage, a 25 % reduction in maintenance costs, and a four-fold reduction in the noise footprint compared to existing production aircraft ^[37]. Moreover, the engine and the wings would save up to 20 % fuel compared to the Airbus A320neo and the Boeing 737 Next Generation ^[36].

The Airbus A220-300 is equipped with two PW1524G ^[38] high-bypass geared turbofan engines, belonging to the Pratt & Whitney's PW1000G family. They use an advanced gear system allowing the fan to operate at a speed different from that of the low-pressure compressor and turbine. MTU Aero Engines is a revenue and risk sharing partner on the PW1000G with a program share of 17 % in the PW1524G. The company is responsible for the first four stages of the high-pressure compressor and the high-speed low-pressure turbine. MTU also provides brush seals and nickel integrated blade rotors (IBR) for the rear stages of the high-pressure compressor ^[39].



Figure 4.2: Airbus A220-100 and Airbus A220-300 illustration with front, side and top views, wearing the Bombardier livery [36].

One of the main reasons why the choice fell on the A220-300 is connected to the acoustic emissions of the engine, which are significantly lower than those of aircraft of the same category. This will assist in the development of more accurate techniques for the prediction of engine noise. More in general, the alleged reduced noise footprint of the aircraft makes it of particular interest from the point of view of noise emissions and the study of factors that determined its optimization. In fact, understanding the primary sources responsible for noise represents the first step towards the development of methodologies for the analysis of noise emissions that can be included in the early stages of the aircraft design cycle.

4.1.3 Noise levels certified by EASA

The Type Certificate Data Sheet for Noise (TCDSN) published by EASA [34] allows us to have real data on which to make some initial considerations about the likelihood of the results provided by ATTILA⁺⁺. The results of certification tests conducted in Approach, Flyover and Lateral conditions are listed in Table 4.1. The conditions under which the certification tests were performed have already been described in section 2.6.5. It is important to keep in mind that the values measured during any experimental test are always subject to variability, mainly in relation to the experimental setup and the environmental circumstances.

Although it is true that the values in Table 4.1 are a good starting point to be able to calibrate the software, they do not necessarily indicate the exact level of pressure perceivable around the runway. Among the main causes of discrepancy, there could be the ground effect already analyzed in section 2.5.5 and the fact that

Table 4.1: Noise levels of the A220-300 certified by EASA (TCDS for Noise) ^[34].

Approach [EPNdB]	Flyover [EPNdB]	Lateral [EPNdB]
92.4	81.2	87.8

real one-third-octave filters used for measurements never correspond to the case of ideal filters. However, ATTILA⁺⁺ aims to partially emulate the aforementioned causes of error (see section 3.2.3), to get values as close as possible to those that can realistically come out of an experimental test.

4.1.4 Input data

In this paragraph the main geometric characteristics of the aircraft will be described, since they represent the main starting point for the acoustic estimates that can be produced using ATTILA⁺⁺. The way in which input data are provided to the software has already been extensively explored in Chapter 3.

Main Data

With reference to the input variables listed in Table 3.1, Table 4.2 shows the values referring to the real dimensions of the A220-300. Table 4.3 shows the additional input data necessary for the evaluation of the ground reflection effect. The values were obtained from online sources ^[36] ^[37] or digitizing scale figures of the aircraft. The chosen one-third-octave bands coincide with the default values, i.e. the bands from 17th to 40th shown in Table 2.1. The reference pressure is $p_{Ref} = 2 \cdot 10^{-5}$ Pa.

Table 4.2: Geometric input data for ATTILA⁺⁺ v0.8.1 (see also Table 3.1).

Variable	Description	Value
NAME	Project name.	A220-300
WAT	Aircraft type index.	0
WWT	Wing type index.	1
SW	Wing surface (S_w), in m ² .	112.30
BW	Wing span (b_w), in m.	35.10
SH	Horizontal tail surface (S_h), in m ² .	28.01
BH	Horizontal tail span (b_h), in m.	11.94

Continued on next page

Table 4.2 – Continued from previous page

Variable	Description	Value
SV	Vertical tail surface (S_v), in m^2 .	22.81
BV	Vertical tail span (b_v), in m.	6.14
SF	Overall flap surface (S_f), in m^2 .	25.46
BF	Overall flap span (b_f), in m.	10.53
N_SLOT	Number of flap slots (N_{slot}).	1
N_MLG	Number of main landing gear units (N_{MLG}).	2
N_WHEEL_MLG	Number of wheels on main landing gear units ($N_{Wheel,MLG}$).	2
D_MLG	Diameter of undeformed tyre of main landing gear wheels (d_{MLG}), in m.	1.06
S_MLG	Length of uncompressed main landing gear struts (s_{MLG}), in m.	1.50
N_WHEEL_NLG	Number of wheels on nose landing gear units ($N_{Wheel,NLG}$).	2
D_NLG	Diameter of undeformed tyre of nose landing gear wheels (d_{NLG}), in m.	1.06
S_NLG	Length of uncompressed nose landing gear struts (s_{NLG}), in m.	1.50
N_ENG	Number of engines (N_{Eng}).	2
POS_ENG	Engine position index.	1

Table 4.3: Ground input parameters for ATTILA⁺⁺ v0.8.1 (see also Table 3.1).

Variable	Description	Value
TYPE_GROUND	Ground type.	2
TYPE_TURB	Air turbulence.	4

Control Data

For the sake of brevity, not all input data relating to the control file (Table 3.3) will be reported. Table 4.4 lists only the main variables useful for customizing the calculation according to the need to simulate certification tests. *ICAPP*, *ICFLY* and *ICLAT* (all set to 1) indicate that the analysis will be carried out in all three certification points. In the case of Lateral, the measurement must take place in a certain number of points arranged along the sideline (at a distance of 450 m from the runway). *IOMAX* = 1 causes the software to automatically identify the receiver where the maximum value of *EPNL* has been registered.

Table 4.4: Control parameters for ATTILA⁺⁺ v0.8.1 (see also Table 3.3).

Variable	Description	Value
U	Unit reference system.	1
ICAPP	Run case Approach.	1
ICLAT	Run case Lateral.	1
ICFLY	Run case Flyover.	1
IA1	Include the contribution of the wing.	1
IA2	Include the contribution of the horizontal tail.	1
IA3	Include the contribution of the vertical tail.	1
IA4	Include the contribution of the leading edge slats.	1
IA5	Include the contribution of the flaps.	1
IA6	Include the contribution of the main landing gear.	1
IA7	Include the contribution of the nose landing gear.	1
IAIR	Include the contribution of the airframe.	1
IENG	Include the contribution of the engines.	1
IATM	Include the effect of atmospheric attenuation.	1
IREFL	Include the effect of ground reflection.	1

Continued on next page

Table 4.4 – Continued from previous page

Variable	Description	Value
ILAT	Include the effect of lateral attenuation.	1
IOASPL	Calculate the <i>OASPL</i> .	1
IEPNL	Calculate the <i>EPNL</i> .	1
IOMAX	Print the most critical results (in terms of maximum <i>EPNL</i>) in a separate file.	1
IOALL	Print all the information of interest.	1
PREC	Number of significant digits to be printed after comma.	2

Definition of receivers

Three different calculation conditions have been set up, one for each of the test cases described in section 2.6.5. Table 4.5 shows the coordinates of the microphones used for the analysis.

The chosen reference system is such that the runway is parallel to the X-axis and starts at $X = 0$ m. Note that for case Lateral the calculation was repeated in 81 equally spaced (50 m) microphones all arranged at 450 m lateral distance from the runway. This was done simply by inserting the first coordinate ($X = 0$) in the appropriate file (see Table 3.5), and then specifying $N_LIN = 81$ and $DELTA_LIN = 50$. For each of the test conditions, the relative humidity of the air was set equal to $RH = 70$ % ($REL_HUM = 70$). All other atmospheric characteristics have been calculated internally.

Table 4.5: Receiver positions for ATTILA⁺⁺ v0.8.1 (see also Table 3.5).

Case	X [m]	Y [m]	Z [m]
Approach	−2000	0	1.2
Flyover	6500	0	1.2
Lateral	81 points evenly spaced from 0 to 4000	450	1.2

Definition of trajectories

For case Approach, the trajectory is calculated in such a way that the touchdown occurs at the beginning of the runway (located at $X = 0$) maintaining a constant speed and a constant descent angle equal to -3° . In the cases of Flyover and Lateral, the same trajectory referring to the take-off phase and subsequent first and second climb segments is used.

Table 4.6 summarizes the content of the file defining the approach trajectory, with reference to the template of Table 3.4. Since $LINEAR = 1$, a straight path is automatically generated by the software starting from the specified coordinates. The speed, the throttle ratio, the flap deflection and the angle of descent remain constant throughout the phase, as well as the landing gears remain constantly extracted and the slat constantly extended.

Table 4.6: Approach trajectory for ATTILA⁺⁺ v0.8.1 (see also Table 3.4).

Variable	Description	Value
NAME	Name of the trajectory.	APPROACH
LINEAR	Use a linear trajectory extrapolated from the first coordinates given.	1
N_LIN	Number of positions to extrapolate.	100
DELTA_LIN	Time interval between two consecutive extrapolated source positions.	0.5
X	X-coordinate of the aircraft, in m.	-3200
Y	Y-coordinate of the aircraft, in m.	0
Z	Z-coordinate of the aircraft, in m.	167.705
V	Flight speed, in m s^{-1} .	70.21
THROTTLE_RATE	Throttle valve opening ratio.	0.1
CLIMB_ANGLE	Climb angle (α), in $^\circ$.	-3
FLAP_DEFL	Flap deflection angle (δ_f), in $^\circ$.	40
SLAT_ON	Extend slats.	1
MLG_ON	Extract main landing gear.	1
NLG_ON	Extract nose landing gear.	1

The points occupied by the source are calculated every 0.5 seconds, consistently with the speed provided ($DELTA_LIN = 0.5$). The atmospheric parameters and the Mach number are calculated internally. ATTILA⁺⁺ recognizes when the alleged point occupied by the aircraft falls below the ground level, and in that case it truncates the trajectory before this happens. For this reason, although $N_LIN = 100$ points have been requested, only 92 points will actually describe the trajectory. Figure 4.3 shows the trajectory obtained from the data of Table 4.6.

Take-off trajectory is the product of the aircraft's performance analysis by JPAD^[10]. Therefore, it has been given as input in the form of a list of coordinates and consecutive configurations over time (at regular intervals of 0.5 seconds). For the sake of brevity this list will not be reported, but in any case the trajectory is shown in Figure 4.4. The thrust cutback point near $X = 3400$ m is clearly visible. Here, engine thrust is reduced from full throttle to around 48 %. It also constitutes the transition between the first climb segment and the second climb segment, where the landing gears and the slats are retracted. The flap deflection is constantly equal to 15° during the whole maneuver.

Engine noise data set

As previously discussed in section 3.2.6, the beta version of ATTILA⁺⁺ has not the ability to estimate the engine noise internally. The engine dataset, in terms of one-third-octave band sound pressure levels, has been given as additional input. It was obtained by means of an external code that implements the theory contained in the ESDU item no. 98008^[26]. The engine characteristics required to perform this calculation were partly found on the internet, partly obtained through analyses carried out with GasTurb 13^[40]. Data coming from the latter, however, were subject to important errors due to the lack of knowledge of UNINA's research group about the real technical characteristics of the PW1524G.

For the moment, the engine data have been slightly calibrated in order to obtain overall noise values similar to those reported by EASA (see Table 4.1). This is justified by stressing that the main purpose of this discussion is not to demonstrate the ability of the software to perfectly replicate the real noise levels produced by the aircraft. The objective is rather to study the influence of the main airframe components on noise, starting from realistic values of total acoustic emission.

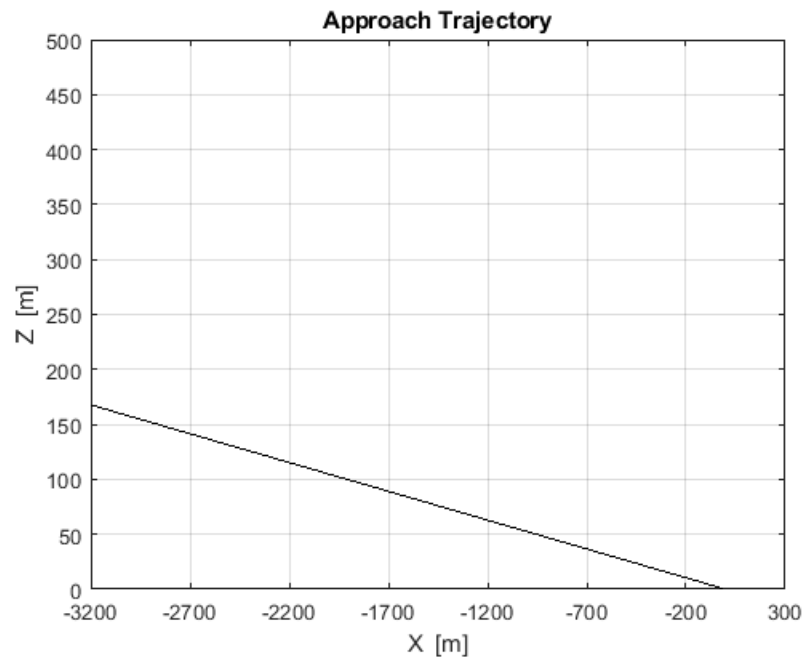


Figure 4.3: Approach trajectory of the Airbus A220-300 (92 points).

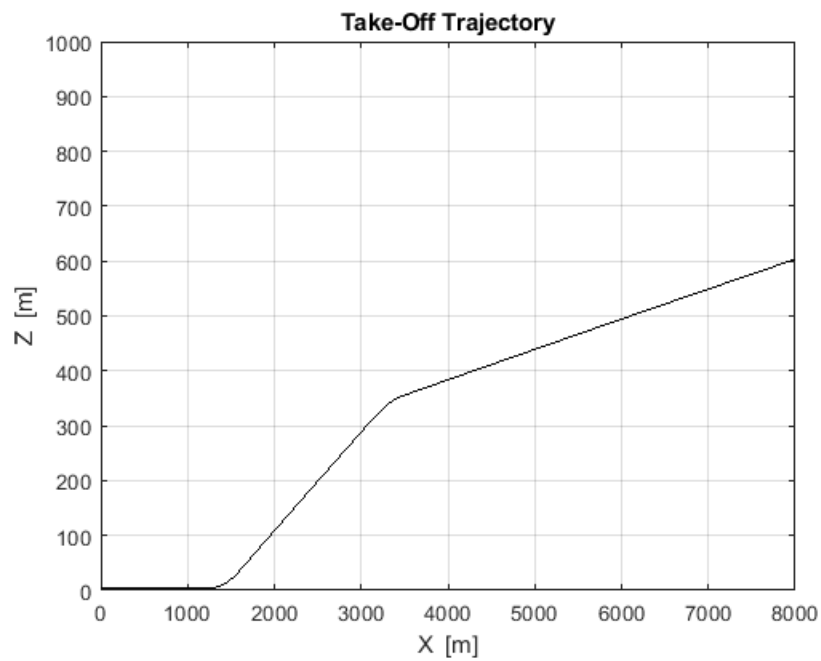


Figure 4.4: Take-off trajectory of the Airbus A220-300 (246 points).

4.2 Estimation of noise levels

4.2.1 Introduction

Based on the input data listed in the previous section, three different analyses were carried out with ATTILA⁺⁺. They refer to the conditions of Approach, Flyover and Lateral regulated by the ICAO, and they will be identified with these names for the rest of this discussion.

In sections 4.1.3 and 4.1.4 the reasons why ATTILA⁺⁺ cannot claim to produce estimates that perfectly coincide with reality have already been explained. The main cause is the current poor reliability of the engine noise spectra. In the next section a sensitivity analysis of airframe noise will be carried out in order to identify the design parameters with the greatest influence on the overall acoustic emission of a turbofan aircraft. Each parameter of interest will be increased or decreased by a certain percentage, and the variations in *EPNL* and *OASPL*_{Max} will also be expressed in percentage terms. However, the logarithmic scale on which all the acoustic quantities are expressed determines that there are strong disparities between the percentage variation in the contribution of *EPNL* due to the airframe alone, and the *EPNL* of the total aircraft (i.e. including also the engine). In take-off conditions, a 1 % change in the airframe *EPNL* involves a change between 0.2 % and 0.06 % in the overall *EPNL*.

For a better reading of the results that will be presented, and waiting for future versions of the software able to better estimate the engine noise, it was decided to calibrate the engine dataset in order to obtain that the total emissions coincide with the official values of Table 4.1. In this way it is possible to have a perception of the real relative impact of each design parameter aimed at best meeting the aircraft's airworthiness requirements. The contributions of ground reflection, atmospheric attenuation and lateral attenuation were considered in each of the three cases under analysis.

4.2.2 Aircraft noise prediction in Approach conditions

Figure 4.5 refers to the Approach trajectory assigned by Table 4.6 and also shown in Figure 4.3. It shows the values of the overall sound pressure level measured by the microphone every considered instant of time (i.e. every 0.5 seconds). The reception times shown on the abscissa axis differ from the emission times because of the delay due to the limited speed of sound. Table 4.7 shows the overall *EPNL* values in Approach compared with those reported by the EASA Type Certificate Data Sheet ^[34]. The values reported by EASA specify the measured *EPNL* up to the first decimal digit, therefore further digits after the comma calculated by the software would not be relevant. The two values, when rounded to the first decimal digit, are identical.

Table 4.7: Approach EPNL of the A220-300 estimated by ATTILA⁺⁺ v0.8.1 compared with the one certified by EASA (see Table 4.1).

ATTILA ⁺⁺ [EPNdB]	EASA [EPNdB]	Difference [%]
92.4	92.4	0.0

Table 4.8 lists the *EPNL* values produced by each isolated source. The total airframe contribution refers to the sum of the effects of all previous components. The contributions of the airframe and the engine group together give rise to the overall noise level. All values are corrected from propagation phenomena and ground reflection effect. It is evident that the contribution of airframe noise is not negligible compared to that of the engine, but rather almost comparable. This is due to the fact that, during the landing phase, the landing gears and the deflection of flaps make the airframe noise particularly significant. At the same time, the minimum throttle ratio mitigates the noise generated by the propulsion system. This combination of circumstances makes the case of Approach the one most significantly affected by aerodynamic noise, and also the best choice for carrying out the parametric analysis that will be presented in the next section.

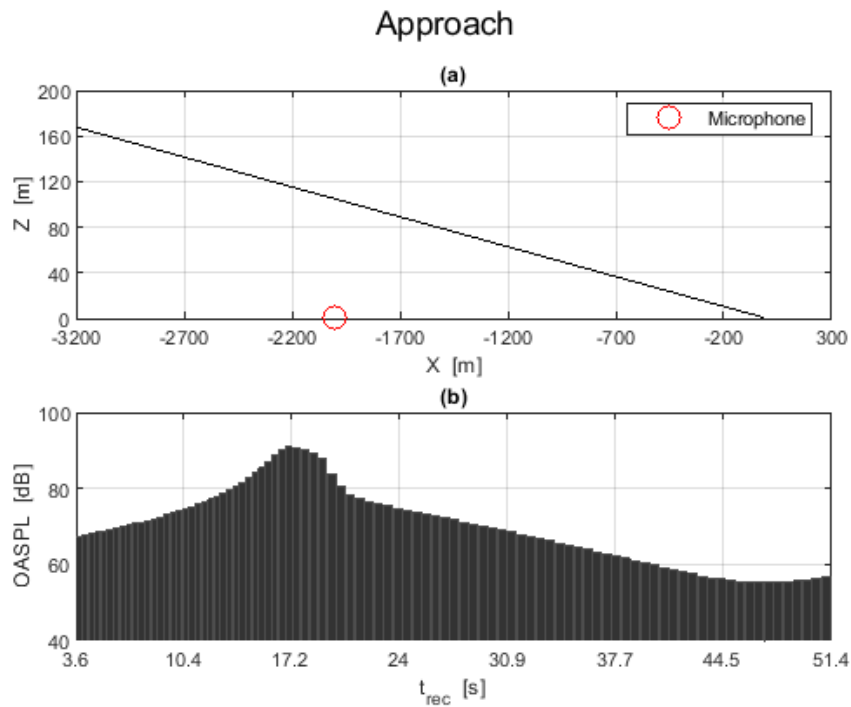


Figure 4.5: (a) Approach trajectory and microphone position; (b) *OASPL* values recorded by the Approach microphone. [ATTILA⁺⁺ v0.8.1]

Table 4.8: Individual effective perceived noise levels produced by the A220-300 in Approach conditions. The effects of ground reflection and atmospheric attenuation are included. [ATTILA⁺⁺ v0.8.1]

Source	EPNL [EPNdB]
Wing	77.4
Horizontal Tail	71.0
Vertical Tail	$-\infty$
Flaps	85.7
Slats	79.9
Main Landing Gear	78.9
Nose Landing Gear	75.8
Airframe (Total)	88.4
Engine Group (Total)	89.8
Aircraft (Total)	92.4

Note that the software establishes that the vertical tail does not generate any contribution when the microphone is in the same vertical plane that also contains the aircraft trajectory. If the noise contribution connected to the propulsion system were eliminated, 88.4 dB connected to aerodynamic phenomena would still be measured. Once again it is possible to conclude that all efforts made to limit airframe noise are rewarded especially during this phase.

Finally, Table 4.9 refers to the maximum overall sound pressure levels measured by the microphone during the maneuver, for each acoustic source. These values are all recorded by the microphone after about 16.5 seconds. The single contributions of *OASPL* have been added together as indicated by equation 2.25.

Table 4.9: Individual maximum overall sound pressure levels produced by the A220-300 in Approach conditions. The effects of ground reflection and atmospheric attenuation are included. [ATTILA⁺⁺ v0.8.1]

Source	OASPL _{Max} [dB]
Wing	77.2
Horizontal Tail	71.2
Vertical Tail	$-\infty$
Flaps	84.5
Slats	76.1
Main Landing Gear	79.2
Nose Landing Gear	76.2
Airframe (Total)	86.5
Engine Group (Total)	88.9
Aircraft (Total)	90.9

4.2.3 Aircraft noise prediction in Lateral conditions

With reference to the take-off trajectory also shown in Figure 4.4, it has been assumed that the beginning of the Lateral phase coincides with the beginning of the ground run phase, and the end occurs when the first climb segment ends. The landing gears remain extracted and the slats remain extended throughout the considered period. During the Lateral certification test, an array of microphones is placed parallel to the runway at a distance of 450 m. The reference microphone is the one that has recorded the maximum *EPNL* value. The calculation was therefore repeated in 81 different points (see Table 4.5), and the maximum point was identified at 2500 m from the beginning of the runway. Figure 4.6 shows the values of the overall sound pressure level measured by the reference microphone every considered instant of time (i.e. every 0.5 seconds).

Table 4.10: Lateral EPNL of the A220-300 estimated by ATTILA⁺⁺ v0.8.1 compared with the one certified by EASA (see Table 4.1).

ATTILA ⁺⁺ [EPNdB]	EASA [EPNdB]	Difference [%]
87.8	87.8	0.0

Table 4.10 shows the overall *EPNL* values in Lateral conditions compared with those reported by the EASA Type Certificate Data Sheet ^[34]. When rounded to the first decimal digit, they are identical. Mainly due to the reduced deflection of the flaps (only 15°), the contribution of airframe noise is negligible compared to that of the engine noise. Furthermore, the latter is particularly high since the throttle ratio is maximum (100 %) during the ground run phase. Even if the contribution of airframe noise were canceled, the overall effective perceived noise level would be reduced by only 0.3 dB. However, the *EPNL* recorded in the case of Approach (see Table 4.8) is higher than that measured in the take-off phase, despite the fact that the main noise source (the engine) radiates less acoustic power. The reason is mainly connected to the shorter distances from the microphone and, more generally, to the different source-receiver geometric configuration. This does not make Lateral conditions preferable for the sensitivity study that is intended to be carried out below.

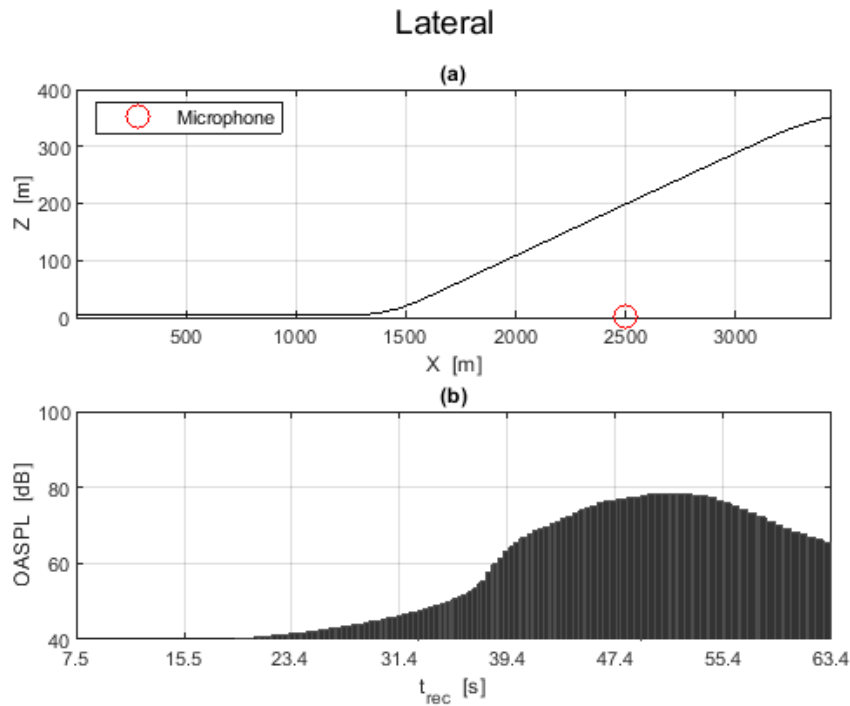


Figure 4.6: (a) Take-off trajectory and Lateral microphone position (found 2500 m from the starting point); (b) *OASPL* values recorded by the Lateral microphone. [ATTILA⁺⁺ v0.8.1]

Table 4.11: Individual effective perceived noise levels produced by the A220-300 in Lateral conditions. The effects of ground reflection and atmospheric attenuation are included. [ATTILA⁺⁺ v0.8.1]

Source	EPNL [EPNdB]
Wing	60.2
Horizontal Tail	52.5
Vertical Tail	56.6
Flaps	61.4
Slats	62.0
Main Landing Gear	73.3
Nose Landing Gear	70.1
Airframe (Total)	76.1
Engine Group (Total)	87.5
Aircraft (No lateral attenuation)	89.2
Aircraft (With lateral attenuation)	87.8

Table 4.11 lists the *EPNL* values produced by each isolated source. The total airframe contribution refers to the sum of the effects of all previous components. The contributions of the airframe and the engine group together give rise to the overall noise level. All values are corrected from propagation phenomena and ground reflection effect.

Finally, Table 4.12 refers to the maximum overall sound pressure levels measured by the microphone during the maneuver, for each acoustic source. These values are all recorded by the microphone after about 46.0 seconds.

Table 4.12: Individual maximum overall sound pressure levels produced by the A220-300 in Lateral conditions. The effects of ground reflection and atmospheric attenuation are included. [ATTILA⁺⁺ v0.8.1]

Source	OASPL _{Max} [dB]
Wing	55.3
Horizontal Tail	49.6
Vertical Tail	55.3
Flaps	59.5
Slats	54.3
Main Landing Gear	71.7
Nose Landing Gear	68.7
Airframe (Total)	73.6
Engine Group (Total)	76.6
Aircraft (No lateral attenuation)	79.2
Aircraft (With lateral attenuation)	78.4

4.2.4 Aircraft noise prediction in Flyover conditions

With reference to the take-off trajectory also shown in Figure 4.4, it has been assumed that the beginning of the Flyover phase coincides with the beginning of the second climb segment. The landing gears are retracted as well as the slats. Figure 4.7 shows the values of the overall sound pressure level measured by the reference microphone every considered instant of time (i.e. every 0.5 seconds).

Table 4.13 shows the overall *EPNL* values in Flyover compared with those reported in the EASA Type Certificate Data Sheet ^[34]. The two values, when rounded to the first decimal digit, are identical.

Table 4.13: Flyover EPNL of the A220-300 estimated by ATTILA⁺⁺ v0.8.1 compared with the one certified by EASA (see Table 4.1).

ATTILA ⁺⁺ [EPNdB]	EASA [EPNdB]	Difference [%]
81.2	81.2	0.0

Mainly due to the reduced deflection of flaps (only 15°), the contribution of airframe noise is negligible compared to that of the engine noise. Moreover, the landing gears and the slats are retracted during the second climb segment. However the throttle ratio is reduced (48 %) compared to the early stages of the take-off phase, but remains higher than in Approach. These characteristics imply that, even if the contribution of airframe noise were canceled, the overall effective perceived noise level would be reduced by only 1.1 dB. As already highlighted in the previous paragraph, the *EPNL* recorded in Approach (see Table 4.8) is higher than the one measured in this phase, despite the main noise source (the engines) radiating less acoustic power. The reason is mainly connected to the shorter distances from the microphone and, more in general, to the different source-receiver geometric configuration. In conclusion, Approach is to be preferred to Flyover for the sensitivity analysis carried out in the next section.

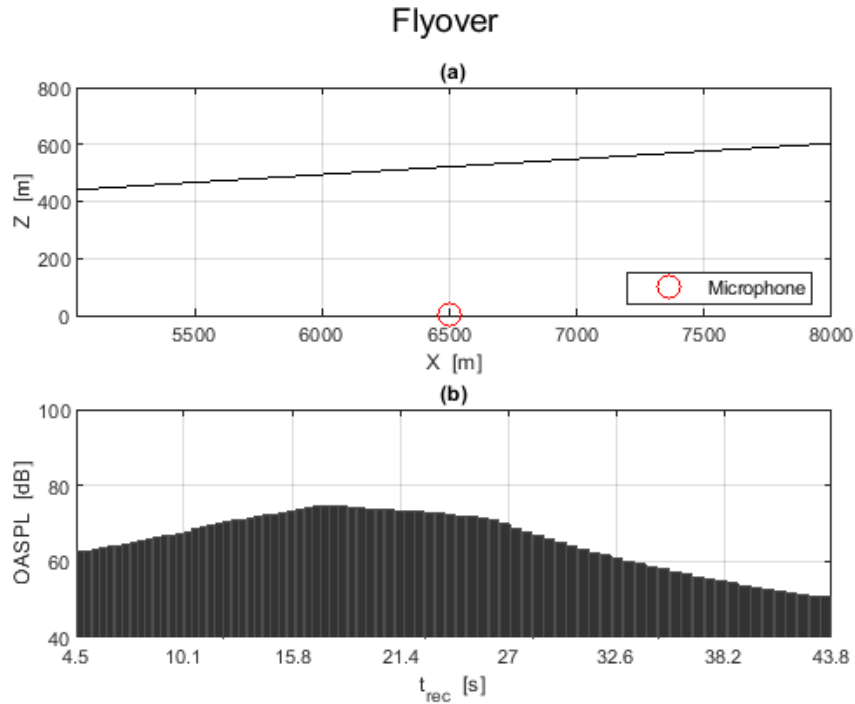
**Figure 4.7:** (a) Take-off trajectory and Flyover microphone position; (b) *OASPL* values recorded by the Flyover microphone. [ATTILA⁺⁺ v0.8.1]

Table 4.14 lists the *EPNL* values produced by each isolated source. The total airframe contribution refers to the sum of the effects of all previous components. The contributions of the airframe and the engine group together give rise to the overall noise level. All values are corrected from propagation phenomena and the ground reflection effect.

Note that the software provides that the vertical tail does not generate any contribution when the microphone is in the same vertical plane that also contains the aircraft trajectory. Furthermore, as mentioned above, the contributions of landing gears and slats are also absent.

Finally, Table 4.15 refers to the maximum overall sound pressure levels measured by the microphone during the maneuver, for each acoustic source. These values are all recorded by the microphone after about 17.5 seconds.

Table 4.14: Individual effective perceived noise levels produced by the A220-300 in Flyover conditions. The effects of ground reflection and atmospheric attenuation are included. [ATTILA⁺⁺ v0.8.1]

Source	EPNL [EPNdB]
Wing	68.2
Horizontal Tail	61.7
Vertical Tail	$-\infty$
Flaps	69.5
Slats	69.2
Main Landing Gear	$-\infty$
Nose Landing Gear	$-\infty$
Airframe (Total)	74.2
Engine Group (Total)	80.1
Aircraft (Total)	81.2

Table 4.15: Individual maximum overall sound pressure levels produced by the A220-300 in Flyover conditions. The effects of ground reflection and atmospheric attenuation are included. [ATTILA⁺⁺ v0.8.1]

Source	OASPL _{Max} [dB]
Wing	63.9
Horizontal Tail	58.1
Vertical Tail	$-\infty$
Flaps	65.6
Slats	61.6
Main Landing Gear	$-\infty$
Nose Landing Gear	$-\infty$
Airframe (Total)	68.5
Engine Group (Total)	73.6
Aircraft (Total)	74.8

4.3 Sensitivity analysis of airframe noise

4.3.1 Overview

Multi-disciplinary design optimization (MDO) is a field of research that applies numerical optimization methods to solve design problems incorporating a number of disciplines. Each MDO process has an *objective function* at its base, representing cost, performance, or other design property to be optimized. The *objective* is a numeric value that must be maximized or minimized. Many times it is convenient to weigh various objectives and sum them to form a single reference objective.

Integrating a noise estimate into the MDO process is one of the main purposes of the ADORNO project. For each aircraft design parameter (geometric parameters, propulsion parameters, etc.) it is possible to search, within established limits, for the value that optimizes the objective. Even a minimal variation of certain parameters can have significant consequences on aerodynamics, structural properties and performances. A different environmental impact can also result from these changes, but often it is not measured by the chosen objective function.

On the other hand, it may happen that large variations of certain other parameters do not generate any relevant change in the objective function. If this independence has been previously proven, then it may be legitimate to exclude these parameters from the MDO chain. This can be advantageous to reduce the numerical effort and to aim for faster and less sophisticated analyses.

Understanding which parameters are most responsible for the generation of aircraft noise is therefore the first step towards the integration of acoustics among the disciplines involved in the optimization process. The main objective of this paragraph, and of the entire dissertation, is to perform a *parametric* (or *sensitivity*) analysis on the basis of the test case already presented above in this chapter.

The results relating to the case of Approach will be the main reference (see Table 4.8 and Table 4.9), and one parameter will be changed at a time while the remaining ones will be kept constant. Not all parameters were taken into consideration, but only those that were considered to have a significant effect in terms of percentage changes in the final results, or those that would allow reflections consequent to the analysis of results. Here they are:

- i. Wing surface area;
- ii. Overall flap surface area;
- iii. Overall flap span;
- iv. Number of flap slots;

- v. Flap deflection angle;
- vi. Tyre diameter of main landing gear wheels;
- vii. Number of wheels on main landing gear units;
- viii. Angle of descent.

For each imposed change, the percentage variations in *EPNL* and *OASPL* values measured over time will be evaluated. It will be done in terms of total noise emitted, as well as of airframe noise and of the noise generated by the single isolated component under analysis.

4.3.2 Effects of wing surface

The wing surface area is the first parameter object of this analysis. Keeping all the other input data unchanged, its value has been increased and decreased by 10 % and 20 %. Figure 4.8 shows the *OASPL* values that would be recorded by the reference microphone in presence of only the wing, for different values of wing surface. Although the variation is minimal, it is still clearly visible and allows to conclude that an increase in wing surface is responsible for an increase in the noise emitted. The change in total airframe noise is shown in Figure 4.9, which makes it clear that the effect on airframe noise is negligible. Consequently, the effect on total noise can also be ignored (see Figure 4.10).

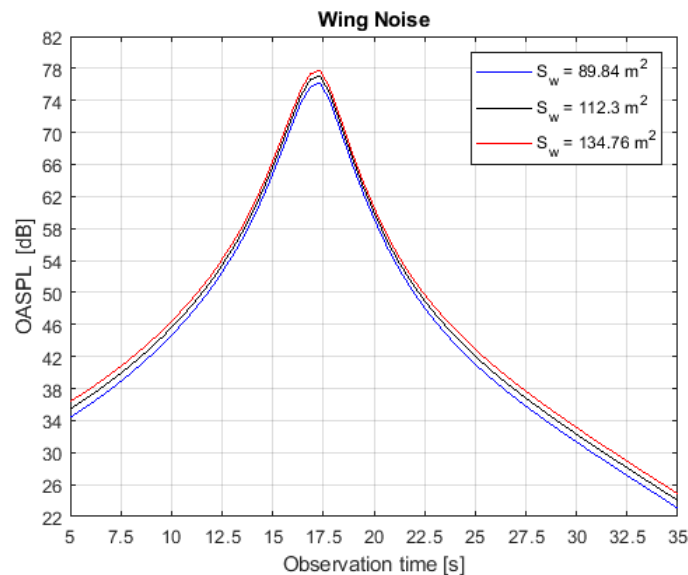


Figure 4.8: *OASPL* produced by the isolated wing in Approach: **(blue)** $S_w = 89.84 \text{ m}^2$ ($- 20 \%$); **(black)** $S_w = 112.30 \text{ m}^2$ (starting value); **(red)** $S_w = 134.76 \text{ m}^2$ ($+ 20 \%$). [ATTILA⁺⁺ v0.8.1]

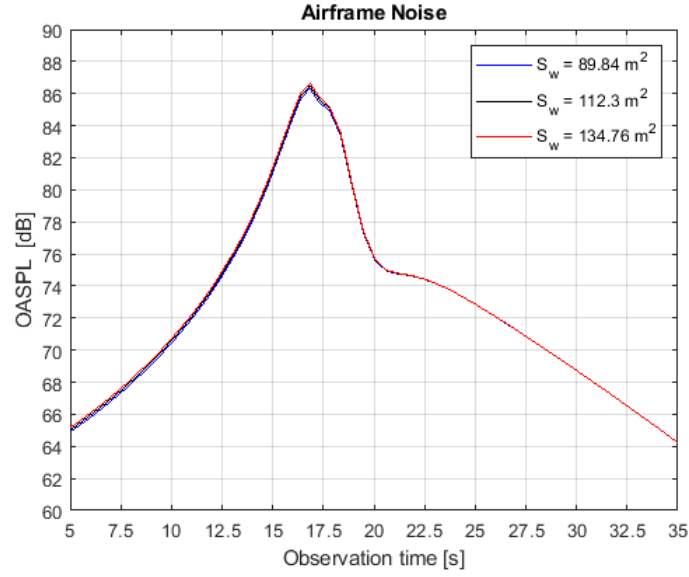


Figure 4.9: Airframe *OASPL* in Approach: **(blue)** $S_w = 89.84 \text{ m}^2$ (-20%); **(black)** $S_w = 112.30 \text{ m}^2$ (starting value); **(red)** $S_w = 134.76 \text{ m}^2$ ($+20\%$). [ATTILA⁺⁺ v0.8.1]

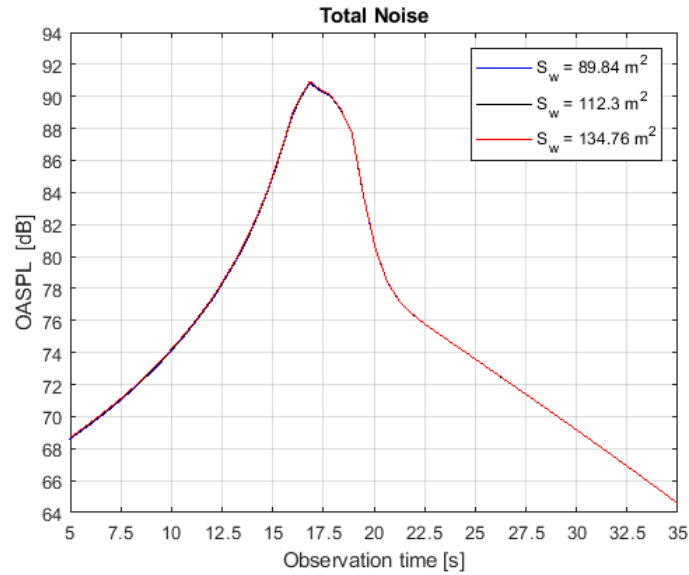


Figure 4.10: Total *OASPL* in Approach: **(blue)** $S_w = 89.84 \text{ m}^2$ (-20%); **(black)** $S_w = 112.30 \text{ m}^2$ (starting value); **(red)** $S_w = 134.76 \text{ m}^2$ ($+20\%$). [ATTILA⁺⁺ v0.8.1]

The maximum calculated values of *OASPL* are also reported in Table 4.16, and Table 4.17 reports all the *EPNL* values of interest. Note that a 20 % increase in the wing surface area causes a 0.40 % change in the *EPNL* produced by the isolated wing, but only a 0.03 % change in measurable noise. This is strongly connected to the logarithmic nature of acoustic quantities, and once again underlines the importance of reporting the percentage differences in terms of total noise in order to perceive their real importance. Figure 4.11 and Figure 4.12, respectively, graphically display the same values listed in Table 4.16 and Table 4.17.

It is possible to assert that direct variations of the wing surface area do not constitute an effective method of noise reduction. This same conclusion is valid for the wing span. Percentage variations of the latter, according to the method proposed by the ESDU item no. 90023^[28], have effects of equal intensity, with the only difference that an increase in the wing span causes a reduction in the overall noise. Analogous analyses could be carried out on the tailplane, leading to similar results by virtue of the similar role it plays in the generation of total noise (see Table 4.8).

However, it is possible to significantly reduce the noise produced by aerodynamic surfaces by intervening differently. Airframe noise from slats, leading edge flaps, and clean aerodynamic surfaces has been shown to be trailing edge noise caused by the turbulent boundary layer (Fink, 1977)^[22]. One concept for decreasing trailing edge noise is the use of sawtooth trailing edges to take advantage of the edge sweepback effect, as demonstrated by Howe (1991)^[41] and Chong (2015)^[42].

In conclusion, in the design process of the aircraft configuration, it is legitimate to attribute a minimum weight to the direct effect that clean aerodynamic surfaces have on the acoustic emissions of an aircraft. This does not mean that changing the dimensions of lifting surfaces does not play an important role in this regard. As is well known, the aircraft design process is very complex and highly iterative, so other important changes may result from a small initial modification, with consequences on performances and environmental impact.

Table 4.16: Changes in $OASPL_{Max}$ for different values of wing surface area, with reference to the isolated wing, the airframe and the complete aircraft. The original input data ($S_w = 112.3 \text{ m}^2$) is used as reference value. [ATTILA⁺⁺ v0.8.1]

Isolated Wing				
$S_w \text{ [m}^2\text{]}$	% of Change	$OASPL_{Max} \text{ [dB]}$	Diff. [dB]	% of Change
89.84	− 20.0	76.26	− 0.89	− 1.154
101.07	− 10.0	76.73	− 0.42	− 0.544
112.30	+ 0.0	77.15	+ 0.00	+ 0.000
123.53	+ 10.0	77.52	+ 0.37	+ 0.480
134.76	+ 20.0	77.85	+ 0.70	+ 0.907
Airframe				
$S_w \text{ [m}^2\text{]}$	% of Change	$OASPL_{Max} \text{ [dB]}$	Diff. [dB]	% of Change
89.84	− 20.0	86.32	− 0.17	− 0.197
101.07	− 10.0	86.41	− 0.08	− 0.093
112.30	+ 0.0	86.49	+ 0.00	+ 0.000
123.53	+ 10.0	86.57	+ 0.08	+ 0.093
134.76	+ 20.0	86.64	+ 0.09	+ 0.173
Complete Aircraft				
$S_w \text{ [m}^2\text{]}$	% of Change	$OASPL_{Max} \text{ [dB]}$	Diff. [dB]	% of Change
89.84	− 20.0	90.83	− 0.06	− 0.066
101.07	− 10.0	90.87	− 0.02	− 0.022
112.30	+ 0.0	90.89	+ 0.00	+ 0.000
123.53	+ 10.0	90.92	+ 0.03	+ 0.033
134.76	+ 20.0	90.95	+ 0.06	+ 0.066

Table 4.17: Changes in *EPNL* for different values of wing surface area, with reference to the isolated wing, the airframe and the complete aircraft. The original input data ($S_w = 112.3 \text{ m}^2$) is used as reference value. [ATTILA⁺⁺ v0.8.1]

Isolated Wing				
$S_w \text{ [m}^2\text{]}$	% of Change	EPNL [dB]	Diff. [dB]	% of Change
89.84	− 20.0	76.97	− 0.41	− 0.530
101.07	− 10.0	77.19	− 0.19	− 0.246
112.30	+ 0.0	77.38	+ 0.00	+ 0.000
123.53	+ 10.0	77.55	+ 0.17	+ 0.220
134.76	+ 20.0	77.69	+ 0.31	+ 0.401
Airframe				
$S_w \text{ [m}^2\text{]}$	% of Change	EPNL [dB]	Diff. [dB]	% of Change
89.84	− 20.0	88.34	− 0.05	− 0.057
101.07	− 10.0	88.37	− 0.02	− 0.023
112.30	+ 0.0	88.39	+ 0.00	+ 0.000
123.53	+ 10.0	88.41	+ 0.02	+ 0.023
134.76	+ 20.0	88.43	+ 0.04	+ 0.045
Complete Aircraft				
$S_w \text{ [m}^2\text{]}$	% of Change	EPNL [dB]	Diff. [dB]	% of Change
89.84	− 20.0	92.37	− 0.03	− 0.033
101.07	− 10.0	92.39	− 0.01	− 0.011
112.30	+ 0.0	92.40	+ 0.00	+ 0.000
123.53	+ 10.0	92.42	+ 0.02	+ 0.022
134.76	+ 20.0	92.43	+ 0.03	+ 0.033

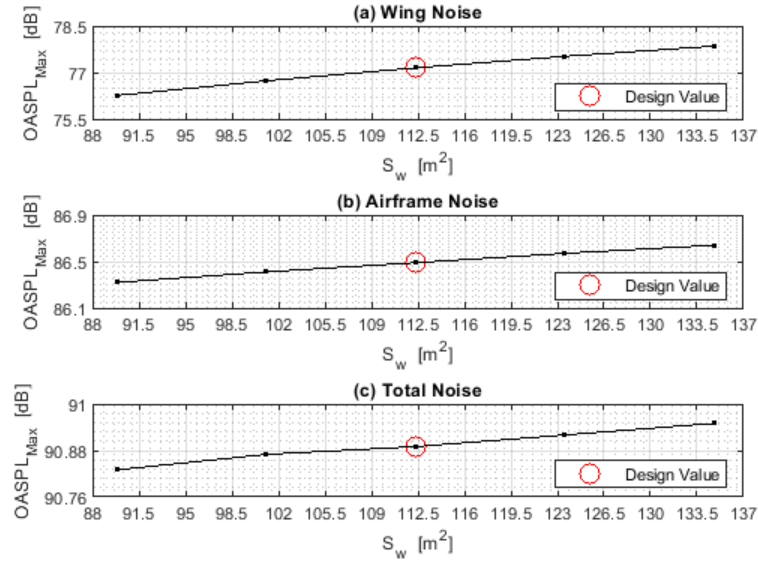


Figure 4.11: Changes in $OASPL_{Max}$ for different values of wing surface area (the red circle marks the starting value): (a) variation in noise produced by the isolated wing; (b) variation in total airframe noise; (c) variation in total aircraft noise. [ATTILA⁺⁺ v0.8.1]

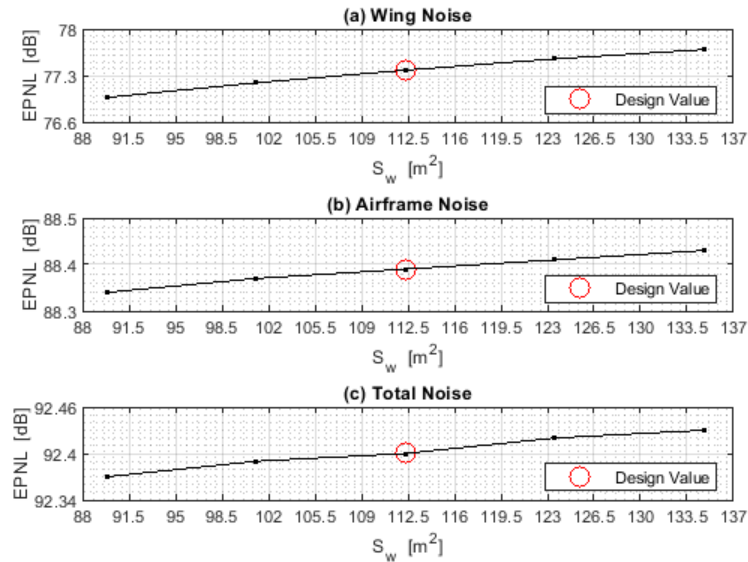


Figure 4.12: Changes in $EPNL$ for different values of wing surface area (the red circle marks the starting value): (a) variation in noise produced by the isolated wing; (b) variation in total airframe noise; (c) variation in total aircraft noise. [ATTILA⁺⁺ v0.8.1]

4.3.3 Effects of flap surface

A reduction in the noise associated with flaps seems to be the most promising way to achieve a significant reduction in airframe noise. In fact, the results of Table 4.8 show that flaps are the most important of all aerodynamic noise sources. A first attempt can be made by changing the value of the flap surface area.

Keeping all the other input data unchanged, the value of the overall flap area has been increased and decreased by 10 % and 20 %. Figure 4.13 shows the *OASPL* values that would be recorded by the reference microphone in presence of only the flap, for different values of flap surface area. Although the variation is minimal, it is still clearly visible and allows to conclude that an increase in flap surface is responsible for an increase in the noise emitted. The change in total airframe noise is shown in Figure 4.14, which makes it clear that the effect on airframe noise is negligible. Consequently, the effect on total noise can also be ignored (see Figure 4.15). The maximum calculated values of *OASPL* are also reported in Table 4.18 and Figure 4.16. Table 4.19 and Figure 4.17 report all the *EPNL* values of interest. Note that a 20 % increase in the flap surface area causes a 0.47 % change in the *EPNL* produced by the isolated flap, but less than a 0.1 % change in measurable noise. The effect is therefore small and negligible, although slightly higher than that of the wing surface analyzed in section 4.3.2. In conclusion, as already established with regard to the wing surface, it is possible to attribute little relevance also to the direct acoustic effects of small changes in the flap surface area.

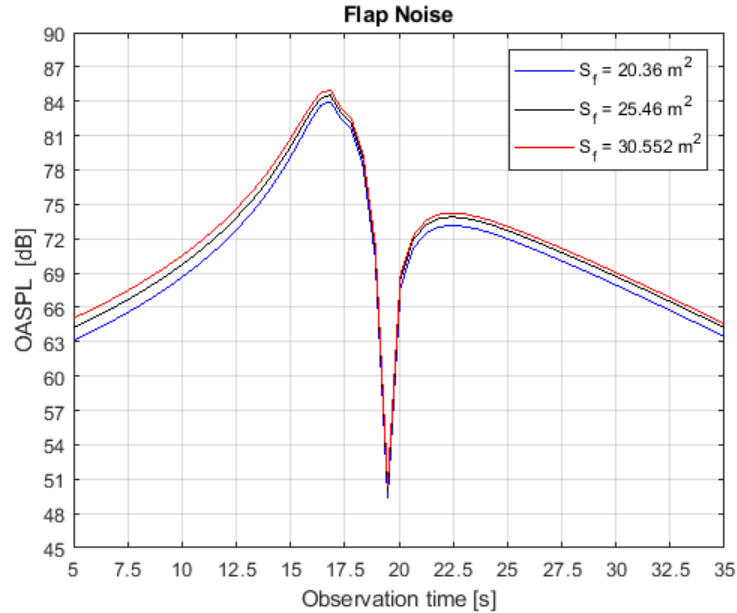


Figure 4.13: *OASPL* produced by the isolated flap in Approach: (blue) $S_f = 20.36 \text{ m}^2$ (− 20 %); (black) $S_f = 25.46 \text{ m}^2$ (starting value); (red) $S_f = 30.55 \text{ m}^2$ (+ 20 %). [ATTILA⁺⁺ v0.8.1]

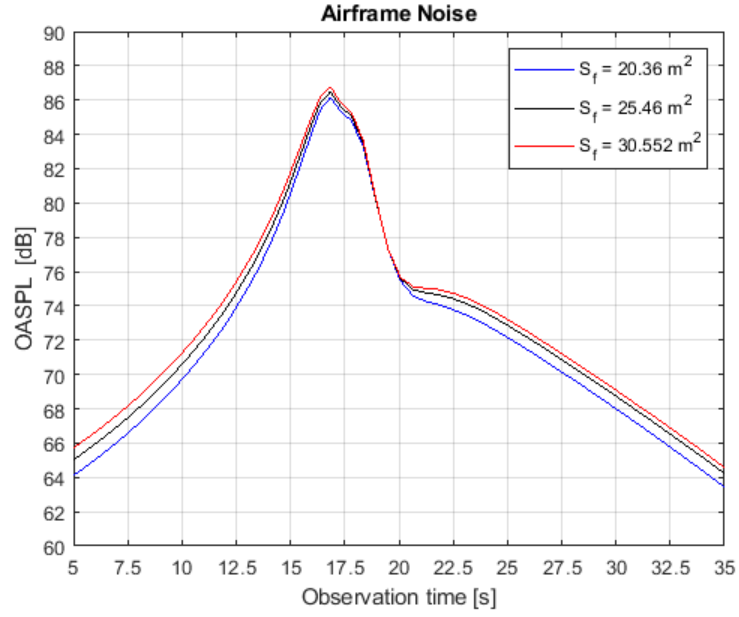


Figure 4.14: Airframe *OASPL* in Approach: (blue) $S_f = 20.36 \text{ m}^2$ (− 20 %); (black) $S_f = 25.46 \text{ m}^2$ (starting value); (red) $S_f = 30.55 \text{ m}^2$ (+ 20 %). [ATTILA⁺⁺ v0.8.1]

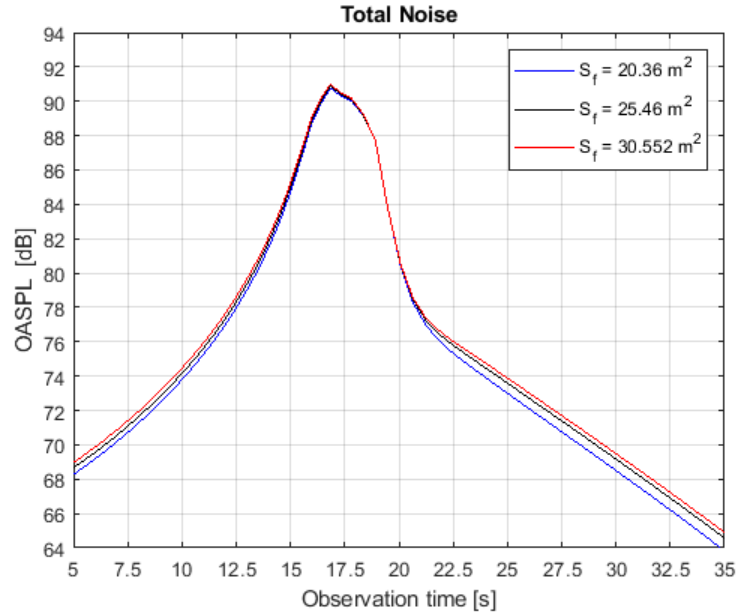


Figure 4.15: Total *OASPL* in Approach: (blue) $S_f = 20.36 \text{ m}^2$ (− 20 %); (black) $S_f = 25.46 \text{ m}^2$ (starting value); (red) $S_f = 30.55 \text{ m}^2$ (+ 20 %). [ATTILA⁺⁺ v0.8.1]

Table 4.18: Changes in $OASPL_{Max}$ for different values of flap surface area, with reference to the isolated flap, the airframe and the complete aircraft. The original input data ($S_f = 25.46 \text{ m}^2$) is used as reference value. [ATTILA⁺⁺ v0.8.1]

Isolated Flap				
$S_f \text{ [m}^2\text{]}$	% of Change	$OASPL_{Max} \text{ [dB]}$	Diff. [dB]	% of Change
20.36	− 20.0	83.99	− 0.54	− 0.639
22.91	− 10.0	84.27	− 0.26	− 0.308
25.46	+ 0.0	84.53	+ 0.00	+ 0.000
28.01	+ 10.0	84.77	+ 0.24	+ 0.284
30.55	+ 20.0	84.98	+ 0.45	+ 0.532
Airframe				
$S_f \text{ [m}^2\text{]}$	% of Change	$OASPL_{Max} \text{ [dB]}$	Diff. [dB]	% of Change
20.36	− 20.0	86.15	− 0.34	− 0.393
22.91	− 10.0	86.32	− 0.17	− 0.197
25.46	+ 0.0	86.49	+ 0.00	+ 0.000
28.01	+ 10.0	86.64	+ 0.15	+ 0.173
30.55	+ 20.0	86.78	+ 0.29	+ 0.335
Complete Aircraft				
$S_f \text{ [m}^2\text{]}$	% of Change	$OASPL_{Max} \text{ [dB]}$	Diff. [dB]	% of Change
20.36	− 20.0	90.77	− 0.12	− 0.132
22.91	− 10.0	90.84	− 0.05	− 0.055
25.46	+ 0.0	90.89	+ 0.00	+ 0.000
28.01	+ 10.0	90.95	+ 0.06	+ 0.066
30.55	+ 20.0	91.00	+ 0.11	+ 0.121

Table 4.19: Changes in *EPNL* for different values of flap surface area, with reference to the isolated flap, the airframe and the complete aircraft. The original input data ($S_f = 25.46 \text{ m}^2$) is used as reference value. [ATTILA⁺⁺ v0.8.1]

Isolated Flap				
$S_f \text{ [m}^2\text{]}$	% of Change	EPNL [dB]	Diff. [dB]	% of Change
20.36	− 20.0	85.20	− 0.49	− 0.572
22.91	− 10.0	85.46	− 0.23	− 0.268
25.46	+ 0.0	85.69	+ 0.00	+ 0.000
28.01	+ 10.0	85.90	+ 0.21	+ 0.245
30.55	+ 20.0	86.09	+ 0.40	+ 0.467
Airframe				
$S_f \text{ [m}^2\text{]}$	% of Change	EPNL [dB]	Diff. [dB]	% of Change
20.36	− 20.0	88.11	− 0.28	− 0.317
22.91	− 10.0	88.26	− 0.13	− 0.147
25.46	+ 0.0	88.39	+ 0.00	+ 0.000
28.01	+ 10.0	88.52	+ 0.13	+ 0.147
30.55	+ 20.0	88.62	+ 0.23	+ 0.260
Complete Aircraft				
$S_f \text{ [m}^2\text{]}$	% of Change	EPNL [dB]	Diff. [dB]	% of Change
20.36	− 20.0	92.29	− 0.11	− 0.119
22.91	− 10.0	92.35	− 0.05	− 0.054
25.46	+ 0.0	92.40	+ 0.00	+ 0.000
28.01	+ 10.0	92.45	+ 0.05	+ 0.054
30.55	+ 20.0	92.49	+ 0.09	+ 0.097

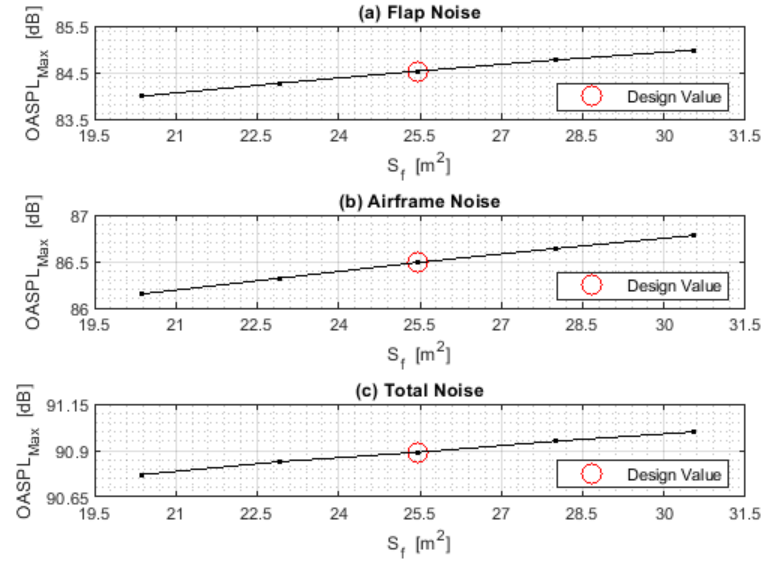


Figure 4.16: Changes in $OASPL_{Max}$ for different values of flap surface area (the red circle marks the starting value): (a) variation in noise produced by the isolated flap; (b) variation in total airframe noise; (c) variation in total aircraft noise. [ATTILA⁺⁺ v0.8.1]

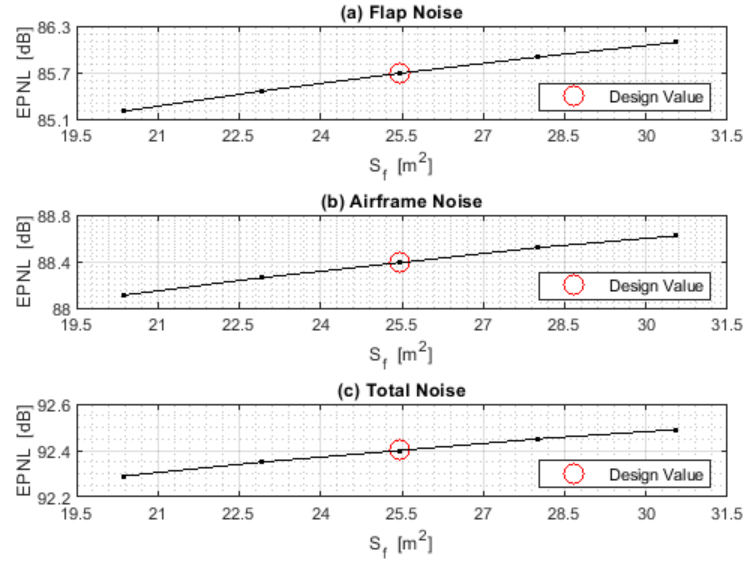


Figure 4.17: Changes in $EPNL$ for different values of flap surface area (the red circle marks the starting value): (a) variation in noise produced by the isolated flap; (b) variation in total airframe noise; (c) variation in total aircraft noise. [ATTILA⁺⁺ v0.8.1]

The distinguishing trend of the *OASPL* due to flaps over time is strictly connected to the way directivity was modeled as a function of azimuthal angle and emission angle (M.R. Fink, 1977) ^[22]. In particular, a minimum noise level is expected right after the aircraft has passed over the microphone, at the exact moment when the straight line connecting the microphone with the acoustic center of the aircraft is parallel to flap chord (i.e. when the tangent of the azimuthal angle and the tangent of the flap deflection angle have the same absolute value but different signs).

4.3.4 Effects of flap span

The next results to be presented are still related to the contribution of flaps. This time, variations of 10 % and 20 % were imposed on the overall span of the flaps. Figure 4.18 shows the *OASPL* values that would be recorded by the reference microphone in presence of only the flap, for different values of flap span. It can be seen that for low values of the Strouhal number (i.e. at low frequencies) an increase in flap span causes a reduction in the noise level, while the opposite occurs for high values of the Strouhal number (i.e. at high frequencies). Overall, an increase in flap span results in a slight and negligible increase in the total noise emitted. Changes in airframe and total noise are shown in Figure 4.19 and Figure 4.20. The maximum calculated values of *OASPL* are also reported in Table 4.20 and Figure 4.21. Table 4.21 and Figure 4.22 report all the *EPNL* values of interest. The percentage changes in noise are almost the same as in the case of the overall flap surface area. The effect is therefore small and negligible, although slightly higher than that of the wing surface analyzed in section 4.3.2.

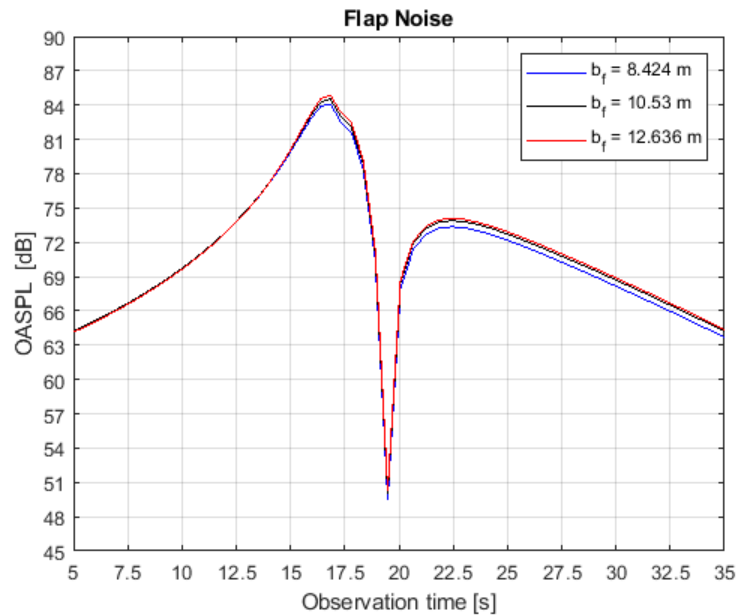


Figure 4.18: *OASPL* produced by the isolated flap in Approach: **(blue)** $b_f = 8.42$ m ($- 20$ %); **(black)** $b_f = 10.53$ m (starting value); **(red)** $b_f = 12.64$ m ($+ 20$ %). [ATTILA⁺⁺ v0.8.1]

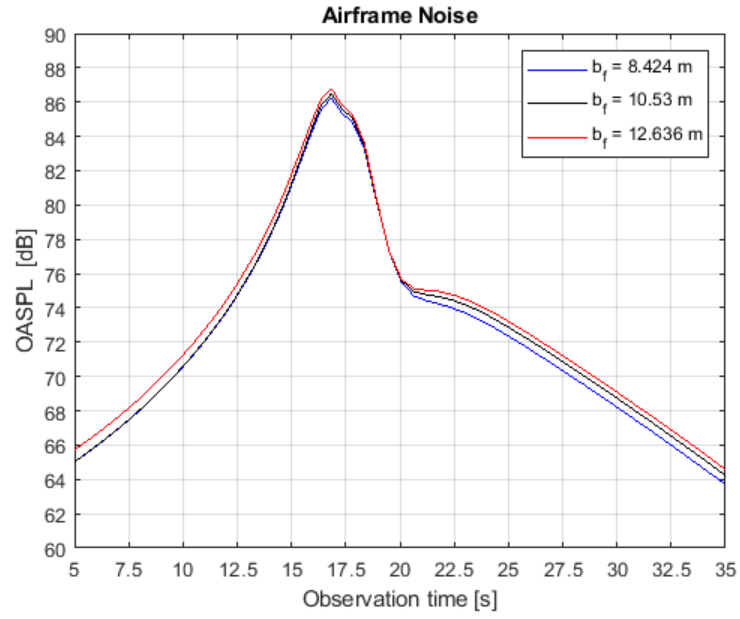


Figure 4.19: Airframe *OASPL* values in Approach: (blue) $b_f = 8.42$ m (-20%); (black) $b_f = 10.53$ m (starting value); (red) $b_f = 12.64$ m ($+20\%$). [ATTILA⁺⁺ v0.8.1]

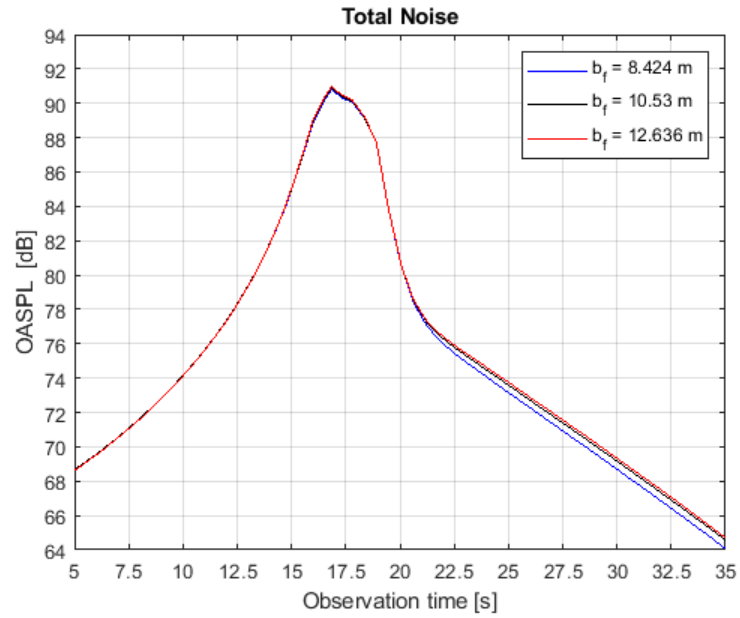


Figure 4.20: Total *OASPL* values in Approach: (blue) $b_f = 8.42$ m (-20%); (black) $b_f = 10.53$ m (starting value); (red) $b_f = 12.64$ m ($+20\%$). [ATTILA⁺⁺ v0.8.1]

Table 4.20: Changes in $OASPL_{Max}$ for different values of flap span, with reference to the isolated flap, the airframe and the complete aircraft. The original input data ($b_f = 10.53$ m) is used as reference value. [ATTILA⁺⁺ v0.8.1]

Isolated Flap				
b_f [m]	% of Change	$OASPL_{Max}$ [dB]	Diff. [dB]	% of Change
8.42	− 20.0	84.11	− 0.42	− 0.497
9.48	− 10.0	84.33	− 0.20	− 0.237
10.53	+ 0.0	84.53	+ 0.00	+ 0.000
11.58	+ 10.0	84.71	+ 0.18	+ 0.213
12.64	+ 20.0	84.88	+ 0.35	+ 0.414
Airframe				
b_f [m]	% of Change	$OASPL_{Max}$ [dB]	Diff. [dB]	% of Change
8.42	− 20.0	86.23	− 0.26	− 0.301
9.48	− 10.0	86.36	− 0.13	− 0.150
10.53	+ 0.0	86.49	+ 0.00	+ 0.000
11.58	+ 10.0	86.71	+ 0.22	+ 0.254
12.64	+ 20.0	86.78	+ 0.29	+ 0.335
Complete Aircraft				
b_f [m]	% of Change	$OASPL_{Max}$ [dB]	Diff. [dB]	% of Change
8.42	− 20.0	90.80	− 0.09	− 0.099
9.48	− 10.0	90.85	− 0.04	− 0.044
10.53	+ 0.0	90.89	+ 0.00	+ 0.000
11.58	+ 10.0	90.94	+ 0.05	+ 0.055
12.64	+ 20.0	90.98	+ 0.09	+ 0.099

Table 4.21: Changes in *EPNL* for different values of flap span, with reference to the isolated flap, the airframe and the complete aircraft. The original input data ($b_f = 10.53$ m) is used as reference value. [ATTILA⁺⁺ v0.8.1]

Isolated Flap				
b_f [m]	% of Change	EPNL [dB]	Diff. [dB]	% of Change
8.42	− 20.0	85.17	− 0.52	− 0.607
9.48	− 10.0	85.45	− 0.24	− 0.280
10.53	+ 0.0	85.69	+ 0.00	+ 0.000
11.58	+ 10.0	85.91	+ 0.22	+ 0.257
12.64	+ 20.0	86.10	+ 0.41	+ 0.478
Airframe				
b_f [m]	% of Change	EPNL [dB]	Diff. [dB]	% of Change
8.42	− 20.0	88.11	− 0.28	− 0.317
9.48	− 10.0	88.26	− 0.13	− 0.147
10.53	+ 0.0	88.39	+ 0.00	+ 0.000
11.58	+ 10.0	88.51	+ 0.12	+ 0.136
12.64	+ 20.0	88.62	+ 0.23	+ 0.260
Complete Aircraft				
b_f [m]	% of Change	EPNL [dB]	Diff. [dB]	% of Change
8.42	− 20.0	92.29	− 0.11	− 0.119
9.48	− 10.0	92.35	− 0.05	− 0.054
10.53	+ 0.0	92.40	+ 0.00	+ 0.000
11.58	+ 10.0	92.45	+ 0.05	+ 0.054
12.64	+ 20.0	92.50	+ 0.10	+ 0.108

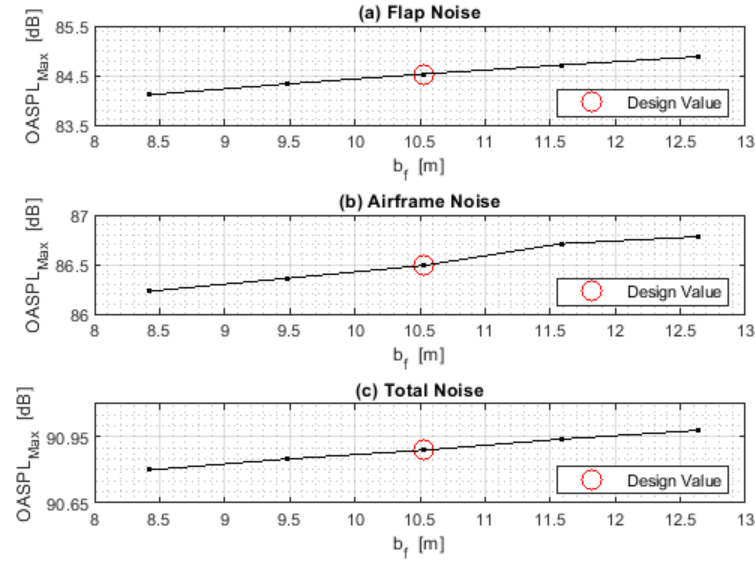


Figure 4.21: Changes in $OASPL_{Max}$ for different values of flap span (the red circle marks the starting value): (a) variation in noise produced by the isolated flap; (b) variation in total airframe noise; (c) variation in total aircraft noise. [ATTILA⁺⁺ v0.8.1]

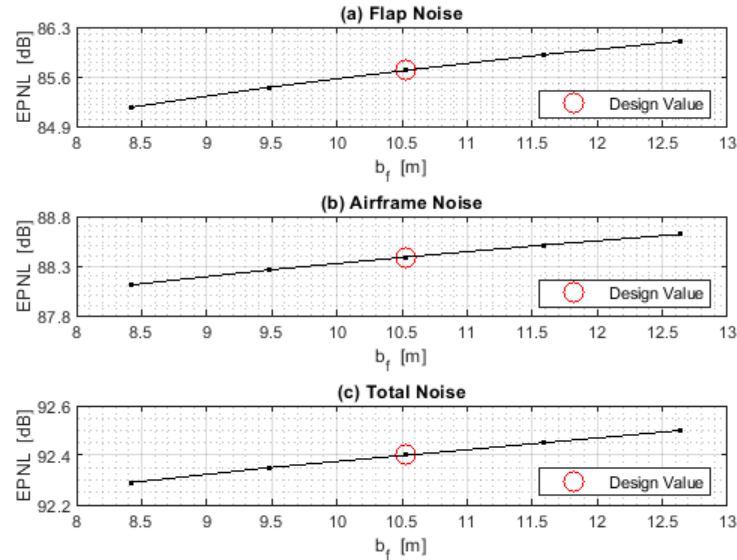


Figure 4.22: Changes in $EPNL$ for different values of flap span (the red circle marks the starting value): (a) variation in noise produced by the isolated flap; (b) variation in total airframe noise; (c) variation in total aircraft noise. [ATTILA⁺⁺ v0.8.1]

4.3.5 Effects of flap slots

According to the theoretical model used by ATTILA⁺⁺, the number of flap slots also plays a role in the evaluation of the directivity index and of the acoustic power radiated by flaps. The model does not identify any difference between single-slotted and double-slotted flaps, nevertheless it attributes to triple-slotted flaps the role of more powerful and more directional acoustic sources.

Single-slotted, double-slotted and triple-slotted flaps are compared here in terms of noise emissions. Figure 4.23 shows the *OASPL* values that would be recorded by the reference microphone in presence of only the flap, for different numbers of slots. The change in total airframe noise is shown in Figure 4.24, and the change in total aircraft noise is shown in Figure 4.25. The maximum calculated values of *OASPL* are also reported in Table 4.22. Table 4.23 reports all the *EPNL* values of interest. Figure 4.26 and Figure 4.27, respectively, graphically display the same values listed in Table 4.22 and Table 4.23.

It is remarkable that the *EPNL* in Approach increases by 1.66 EPNdB (+ 1.8 %) when changing from a single-slotted or double-slotted configuration to triple-slotted flaps. A variation of over 1 dB makes the number of flaps a potential parameter of interest for the optimization processes that take into account noise emissions.

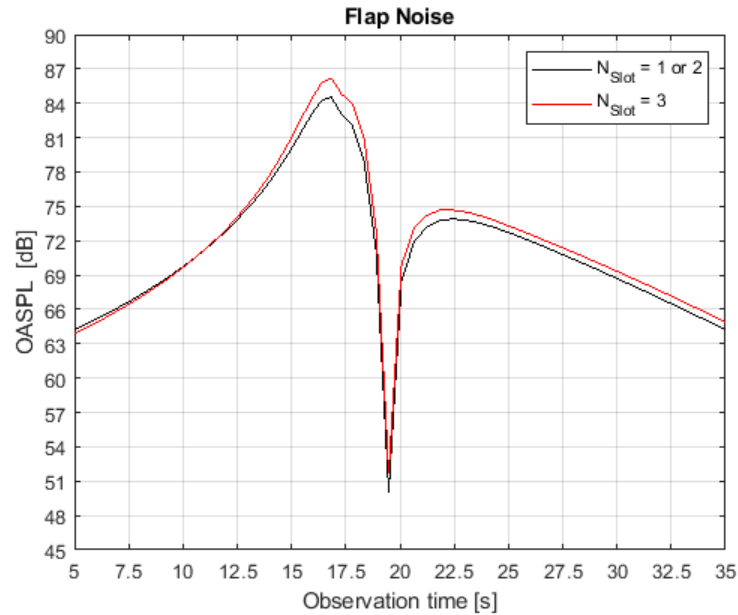


Figure 4.23: *OASPL* produced by the isolated flap in Approach: **(black)** single-slotted and double-slotted flap; **(red)** triple-slotted flap. [ATTILA⁺⁺ v0.8.1]

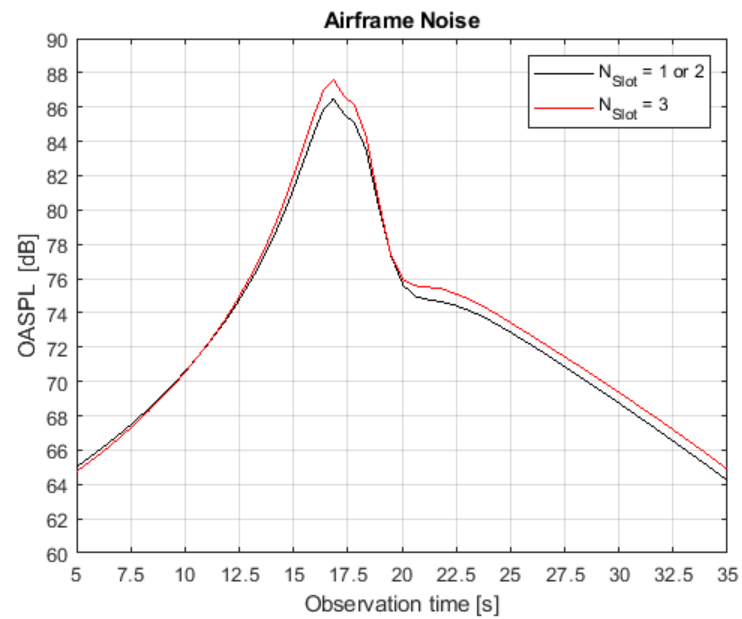


Figure 4.24: Airframe *OASPL* in Approach: **(black)** single-slotted and double-slotted flap; **(red)** triple-slotted flap. [ATTILA⁺⁺ v0.8.1]

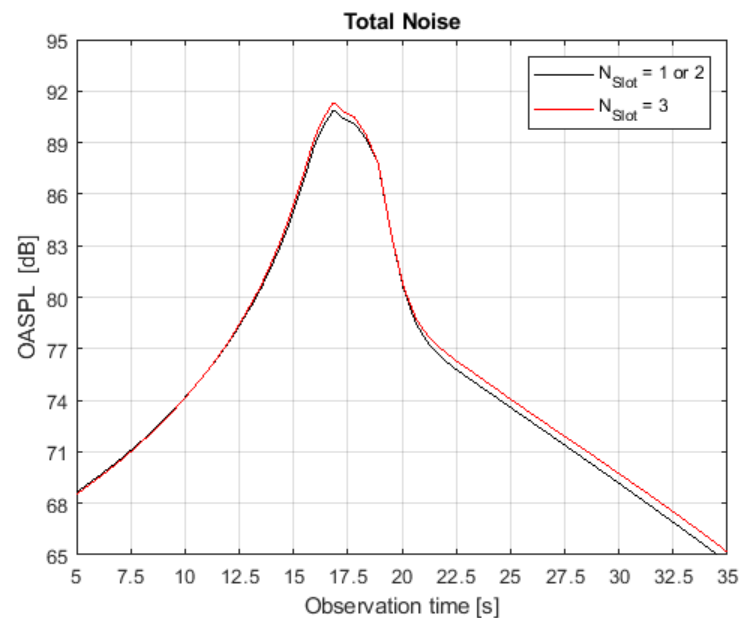


Figure 4.25: Total *OASPL* in Approach: **(black)** single-slotted and double-slotted flap; **(red)** triple-slotted flap. [ATTILA⁺⁺ v0.8.1]

Table 4.22: Changes in $OASPL_{Max}$ for different numbers of flap slots, with reference to the isolated flap, the airframe and the complete aircraft. The original input data ($N_{Slot} = 1$) is used as reference value. [ATTILA⁺⁺ v0.8.1]

Isolated Flap				
N_{Slot}	% of Change	$OASPL_{Max}$ [dB]	Diff. [dB]	% of Change
1, 2	+ 0.0	84.53	+ 0.00	+ 0.000
3	+ 200.0	86.19	+ 1.66	+ 1.964
Airframe				
N_{Slot}	% of Change	$OASPL_{Max}$ [dB]	Diff. [dB]	% of Change
1, 2	+ 0.0	86.49	+ 0.00	+ 0.000
3	+ 200.0	87.62	+ 1.13	+ 1.307
Complete Aircraft				
N_{Slot}	% of Change	$OASPL_{Max}$ [dB]	Diff. [dB]	% of Change
1, 2	+ 0.0	90.89	+ 0.00	+ 0.000
3	+ 200.0	91.34	+ 0.45	+ 0.495

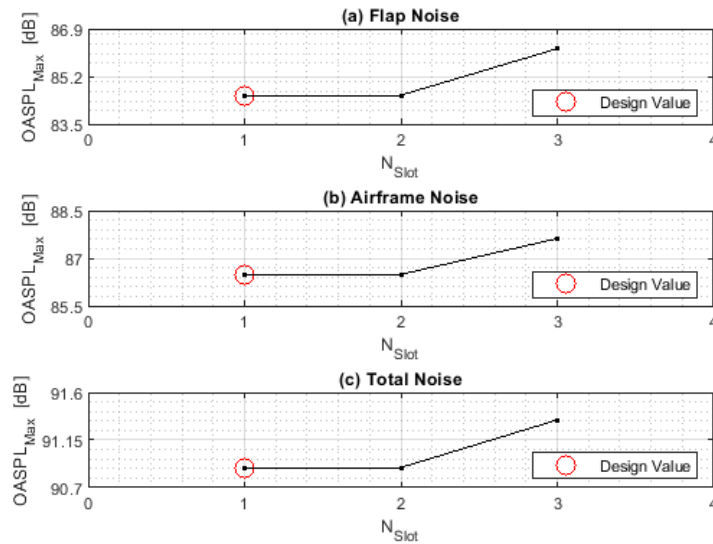


Figure 4.26: Changes in $OASPL_{Max}$ for different numbers of flap slots (the red circle marks the starting value): (a) variation in noise produced by the isolated flap; (b) variation in total airframe noise; (c) variation in total aircraft noise. [ATTILA⁺⁺ v0.8.1]

Table 4.23: Changes in *EPNL* for different numbers of flap slots, with reference to the isolated flap, the airframe and the complete aircraft. The original input data ($N_{Slot} = 1$) is used as reference value. [ATTILA⁺⁺ v0.8.1]

Isolated Flap				
N_{Slot}	% of Change	EPNL [dB]	Diff. [dB]	% of Change
1, 2	+ 0.0	85.69	+ 0.00	+ 0.000
3	+ 200.0	90.19	+ 4.50	+ 5.252
Airframe				
N_{Slot}	% of Change	EPNL [dB]	Diff. [dB]	% of Change
1, 2	+ 0.0	88.39	+ 0.00	+ 0.000
3	+ 200.0	91.55	+ 3.16	+ 3.575
Complete Aircraft				
N_{Slot}	% of Change	EPNL [dB]	Diff. [dB]	% of Change
1, 2	+ 0.0	92.40	+ 0.00	+ 0.000
3	+ 200.0	94.06	+ 1.66	+ 1.797

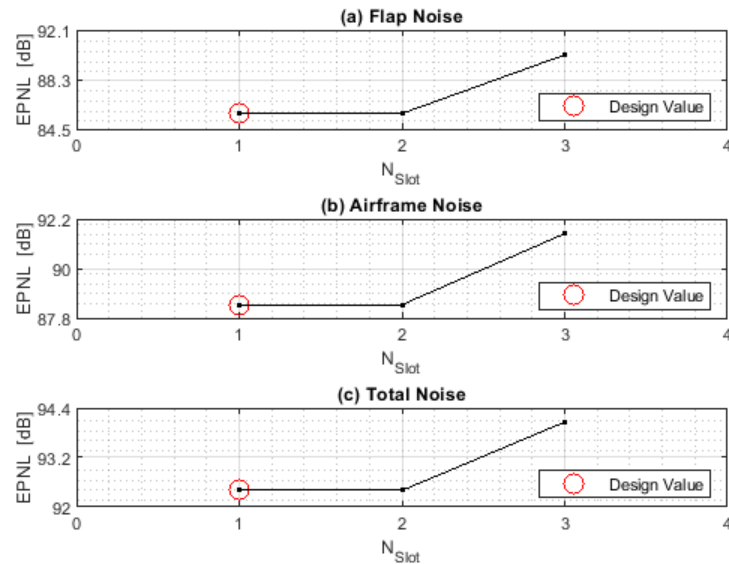


Figure 4.27: Changes in *EPNL* for different numbers of flap slots (the red circle marks the starting value): (a) variation in noise produced by the isolated flap; (b) variation in total airframe noise; (c) variation in total aircraft noise. [ATTILA⁺⁺ v0.8.1]

4.3.6 Effects of flap deflection

The deflection angle of flaps has been varied, considering the values of 20° , 30° and 50° in addition to the original data (40°). Figure 4.28 shows the *OASPL* values that would be recorded by the reference microphone in presence of only the flap, for different values of flap angle. Changes in airframe and total noise are shown in Figure 4.29 and Figure 4.30. The maximum calculated values of *OASPL* are also reported in Table 4.24 and Figure 4.31. Table 4.25 and Figure 4.32 report all the *EPNL* values of interest.

The peculiar trend of the *OASPL* over time connected to flaps has already been discussed in section 4.3.3, where it has been pointed out that a condition of minimum perceived noise occurs when the tangent of the elevation angle coincides with that of the flap angle. Figure 4.28 confirms what has been said, since it clearly shows that the minimum occurs later when the flap angle decreases (i.e. it occurs at higher elevation angles). A similar argument can be done also for the instant of time when the maximum value of *OASPL* is recorded.

A reduction of 10° in flap angle causes a reduction of 1.63 dB (-1.90%) in the *EPNL* caused by flaps, and a reduction of 0.31 dB (-0.34%) in the total *EPNL*. This quantity is sufficient to consider the flap deflection angle (in landing conditions) a parameter of interest if the aim is to optimize the acoustic emissions of an aircraft.

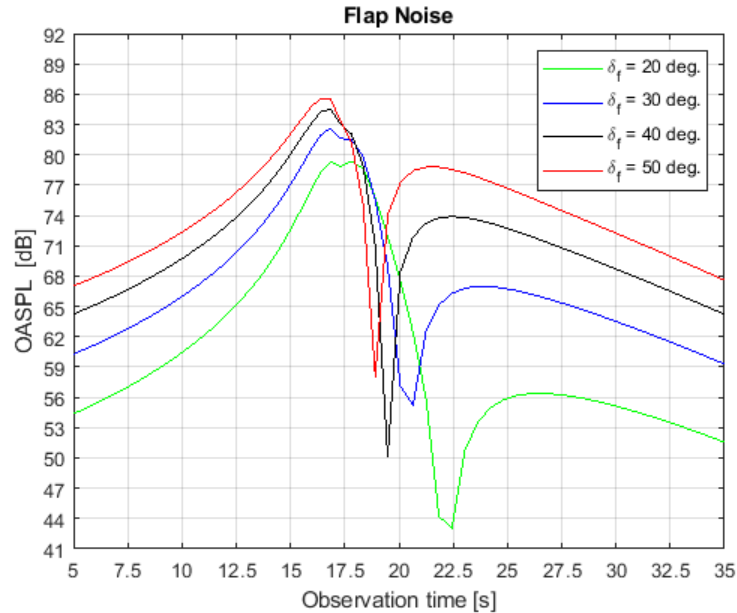


Figure 4.28: *OASPL* produced by the isolated flap in Approach: (green) $\delta_f = 20.0^\circ$ (-50%); (blue) $\delta_f = 30.0^\circ$ (-25%); (black) $\delta_f = 40.0^\circ$ (starting value); (red) $\delta_f = 50.0^\circ$ ($+25\%$). [ATTILA⁺⁺ v0.8.1]

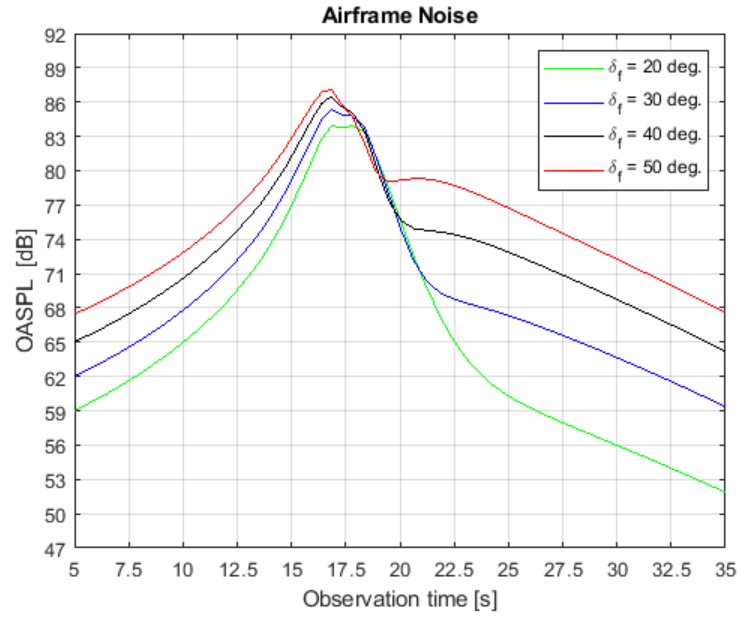


Figure 4.29: Airframe *OASPL* values in Approach: **(green)** $\delta_f = 20.0^\circ$ (-50%); **(blue)** $\delta_f = 30.0^\circ$ (-25%); **(black)** $\delta_f = 40.0^\circ$ (starting value); **(red)** $\delta_f = 50.0^\circ$ ($+25\%$). [ATTILA⁺⁺ v0.8.1]

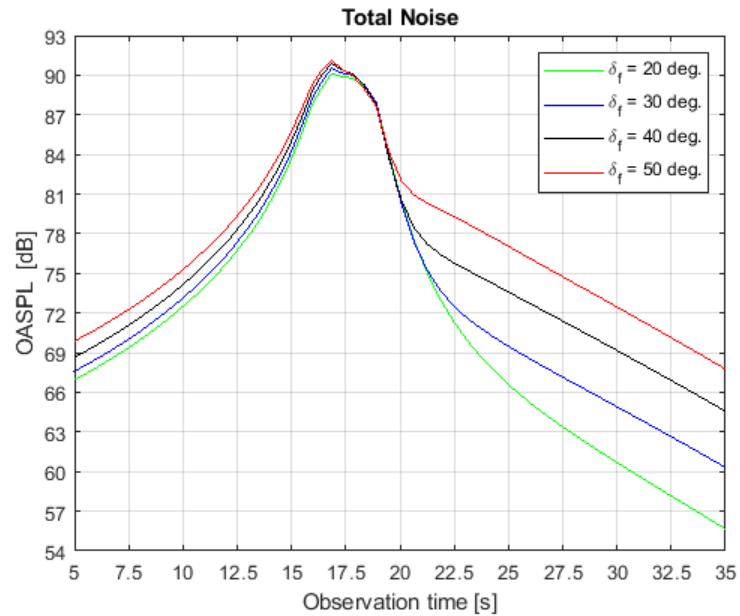


Figure 4.30: Total *OASPL* values in Approach: **(green)** $\delta_f = 20.0^\circ$ (-50%); **(blue)** $\delta_f = 30.0^\circ$ (-25%); **(black)** $\delta_f = 40.0^\circ$ (starting value); **(red)** $\delta_f = 50.0^\circ$ ($+25\%$). [ATTILA⁺⁺ v0.8.1]

Table 4.24: Changes in $OASPL_{Max}$ for different values of flap deflection angle, with reference to the isolated flap, the airframe and the complete aircraft. The original input data ($\delta_f = 40.0^\circ$) is used as reference value. [ATTILA⁺⁺ v0.8.1]

Isolated Flap				
δ_f [°]	% of Change	OASPL _{Max} [dB]	Diff. [dB]	% of Change
20.0	− 50.0	79.35	− 5.18	− 6.128
30.0	− 25.0	82.62	− 1.91	− 2.260
40.0	+ 0.0	84.53	+ 0.00	+ 0.000
50.0	+ 25.0	85.61	+ 1.08	+ 1.278
Airframe				
δ_f [°]	% of Change	OASPL _{Max} [dB]	Diff. [dB]	% of Change
20.0	− 50.0	83.92	− 2.57	− 2.971
30.0	− 25.0	85.37	− 1.12	− 1.295
40.0	+ 0.0	86.49	+ 0.00	+ 0.000
50.0	+ 25.0	87.13	+ 0.64	+ 0.740
Complete Aircraft				
δ_f [°]	% of Change	OASPL _{Max} [dB]	Diff. [dB]	% of Change
20.0	− 50.0	90.13	− 0.76	− 0.836
30.0	− 25.0	90.52	− 0.37	− 0.407
40.0	+ 0.0	90.89	+ 0.00	+ 0.000
50.0	+ 25.0	91.14	+ 0.25	+ 0.275

Table 4.25: Changes in *EPNL* for different values of flap deflection angle, with reference to the isolated flap, the airframe and the complete aircraft. The original input data ($\delta_f = 40.0^\circ$) is used as reference value. [ATTILA⁺⁺ v0.8.1]

Isolated Flap				
δ_f [°]	% of Change	EPNL [dB]	Diff. [dB]	% of Change
20.0	− 50.0	81.26	− 4.43	− 5.170
30.0	− 25.0	84.06	− 1.63	− 1.902
40.0	+ 0.0	85.69	+ 0.00	+ 0.000
50.0	+ 25.0	86.94	+ 1.25	+ 1.459
Airframe				
δ_f [°]	% of Change	EPNL [dB]	Diff. [dB]	% of Change
20.0	− 50.0	86.60	− 1.79	− 2.025
30.0	− 25.0	87.60	− 0.79	− 0.894
40.0	+ 0.0	88.39	+ 0.00	+ 0.000
50.0	+ 25.0	89.27	+ 0.88	+ 0.995
Complete Aircraft				
δ_f [°]	% of Change	EPNL [dB]	Diff. [dB]	% of Change
20.0	− 50.0	91.73	− 0.67	− 0.725
30.0	− 25.0	92.09	− 0.31	− 0.336
40.0	+ 0.0	92.40	+ 0.00	+ 0.000
50.0	+ 25.0	92.76	+ 0.36	+ 0.390

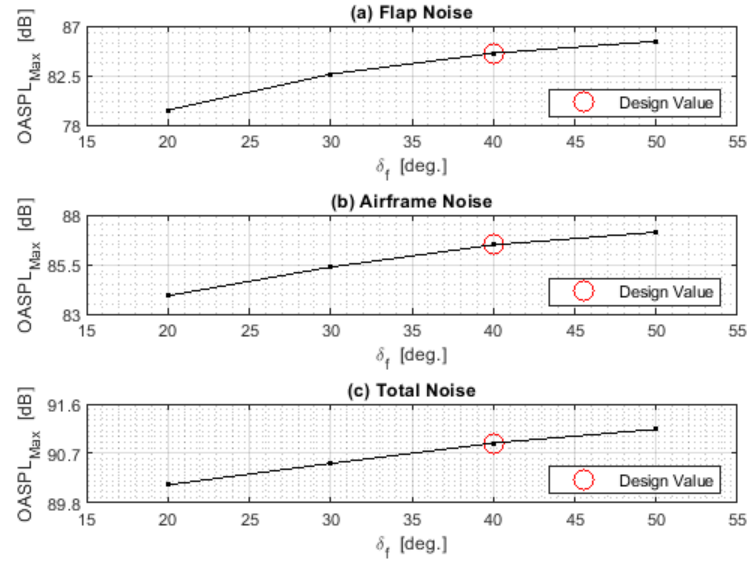


Figure 4.31: Changes in $OASPL_{Max}$ for different values of flap angle (the red circle marks the starting value): (a) variation in noise produced by the isolated flap; (b) variation in total airframe noise; (c) variation in total aircraft noise. [ATTILA⁺⁺ v0.8.1]

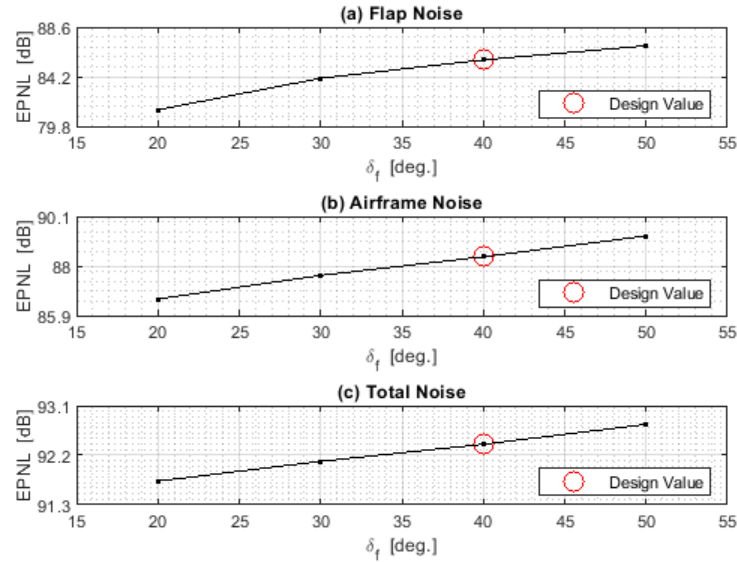


Figure 4.32: Changes in $EPNL$ for different values of flap angle (the red circle marks the starting value): (a) variation in noise produced by the isolated flap; (b) variation in total airframe noise; (c) variation in total aircraft noise. [ATTILA⁺⁺ v0.8.1]

4.3.7 Effects of wheel diameter

As is evident from Table 4.8, landing gears are the second most important source of aerodynamic noise in Approach. In this paragraph we will study the effects of 25 % and a 50 % variations in the diameter of main landing gear wheels, and in the next paragraph the direct consequences of a change in the number of wheels will be discussed. In the first instance, in fact, it seems useful to try to find out if it may be convenient (in terms of noise) to prefer a large number of small wheels rather than a smaller number of wheels with a larger diameter.

Figure 4.33 shows the *OASPL* values that would be recorded by the reference microphone in presence of only the main landing gear, for different values of wheel diameter. Changes in airframe and total noise are shown in Figure 4.34 and Figure 4.35. The maximum calculated values of *OASPL* are also reported in Table 4.26 and Figure 4.36. Table 4.27 and Figure 4.37 report all the *EPNL* values of interest. Note from Figure 4.34 that the noise drop at $t = 19.5$ s connected to the flaps is felt more by the total airframe noise when the contribution of main landing gear decreases.

A 50 % reduction in wheel diameter causes a reduction of 4.56 dB (− 5.78 %) in the *EPNL* related to the isolated source, and a reduction of 0.24 dB (− 0.26 %) in the total *EPNL*. This quantity is sufficient to consider also the diameter of main wheels a significant cause of noise.

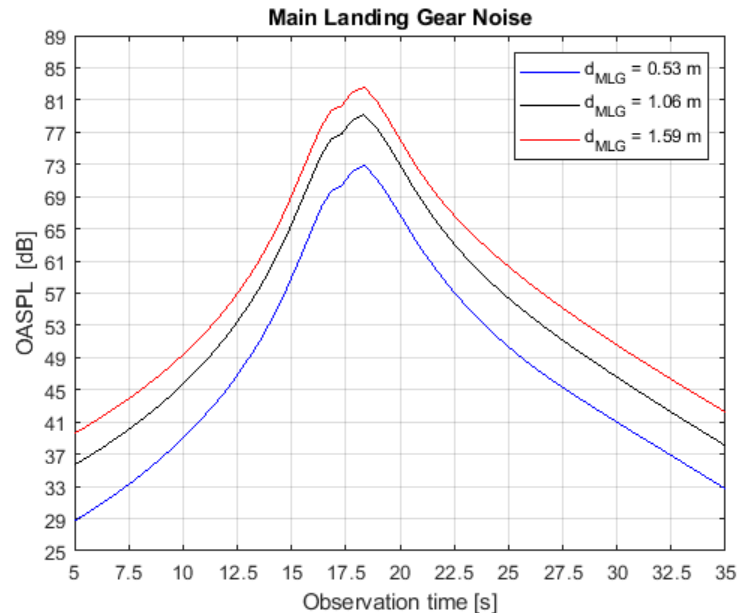


Figure 4.33: *OASPL* produced by the isolated main landing gear in Approach: (blue) $d_{MLG} = 0.53$ m (− 50 %); (black) $d_{MLG} = 1.06$ m (starting value); (red) $d_{MLG} = 1.59$ m (+ 50 %). [ATTILA⁺⁺ v0.8.1]

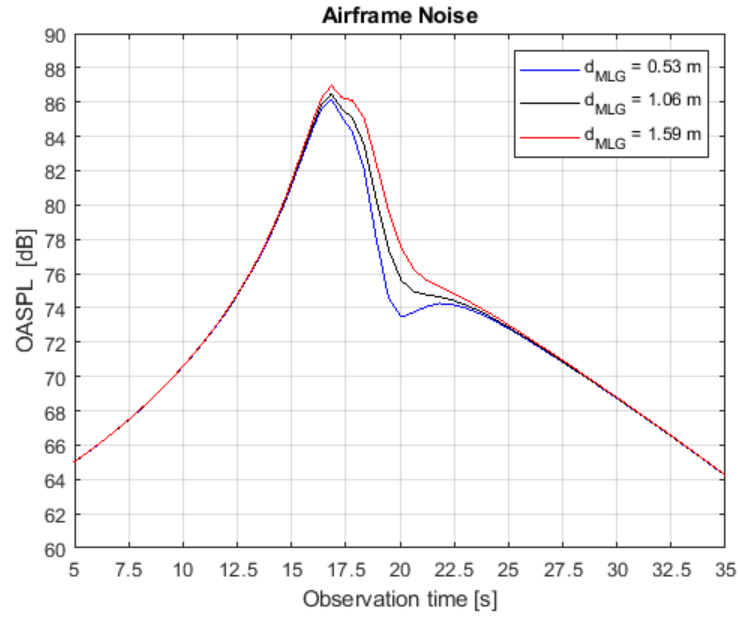


Figure 4.34: Airframe *OASPL* in Approach: (blue) $d_{MLG} = 0.53$ m (-50%); (black) $d_{MLG} = 1.06$ m (starting value); (red) $d_{MLG} = 1.59$ m ($+50\%$). [ATTILA⁺⁺ v0.8.1]

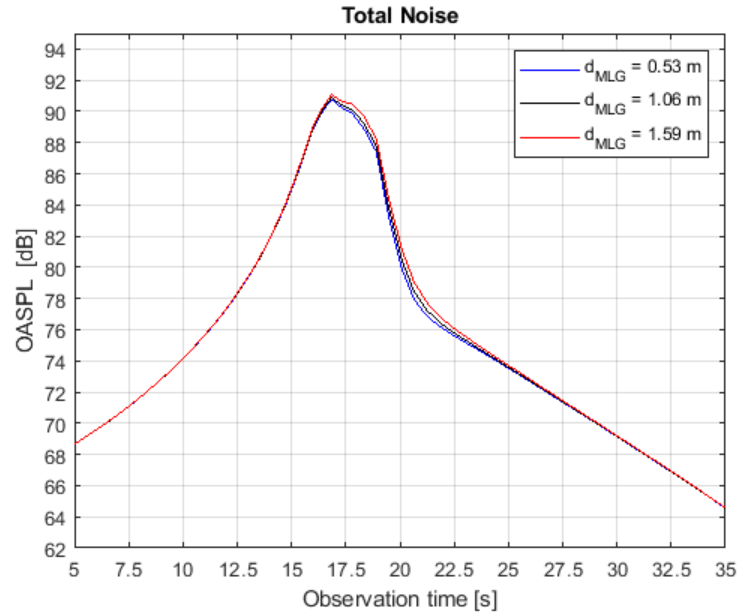


Figure 4.35: Total *OASPL* in Approach: (blue) $d_{MLG} = 0.53$ m (-50%); (black) $d_{MLG} = 1.06$ m (starting value); (red) $d_{MLG} = 1.59$ m ($+50\%$). [ATTILA⁺⁺ v0.8.1]

Table 4.26: Changes in $OASPL_{Max}$ for different values of wheel diameter, with reference to the isolated main landing gear, the airframe and the complete aircraft. The original input data ($d_{MLG} = 1.06$ m) is used as reference value. [ATTILA⁺⁺ v0.8.1]

Isolated Main Landing Gear				
d_{MLG} [m]	% of Change	$OASPL_{Max}$ [dB]	Diff. [dB]	% of Change
0.53	− 50.0	72.87	− 6.31	− 7.969
0.80	− 25.0	76.61	− 2.57	− 3.246
1.06	+ 0.0	79.18	+ 0.00	+ 0.000
1.33	+ 25.0	81.09	+ 1.91	+ 2.412
1.59	+ 50.0	82.58	+ 3.40	+ 4.294
Airframe				
d_{MLG} [m]	% of Change	$OASPL_{Max}$ [dB]	Diff. [dB]	% of Change
0.53	− 50.0	86.17	− 0.32	− 0.370
0.80	− 25.0	86.30	− 0.19	− 0.220
1.06	+ 0.0	86.49	+ 0.00	+ 0.000
1.33	+ 25.0	86.71	+ 0.22	+ 0.254
1.59	+ 50.0	86.97	+ 0.48	+ 0.555
Complete Aircraft				
d_{MLG} [m]	% of Change	$OASPL_{Max}$ [dB]	Diff. [dB]	% of Change
0.53	− 50.0	90.78	− 0.11	− 0.121
0.80	− 25.0	90.83	− 0.06	− 0.066
1.06	+ 0.0	90.89	+ 0.00	+ 0.000
1.33	+ 25.0	90.98	+ 0.09	+ 0.099
1.59	+ 50.0	91.08	+ 0.19	+ 0.209

Table 4.27: Changes in *EPNL* for different values of wheel diameter, with reference to the isolated main landing gear, the airframe and the complete aircraft. The original input data ($d_{MLG} = 1.06$ m) is used as reference value. [ATTILA⁺⁺ v0.8.1]

Isolated Main Landing Gear				
d_{MLG} [m]	% of Change	EPNL [dB]	Diff. [dB]	% of Change
0.53	− 50.0	74.33	− 4.56	− 5.780
0.80	− 25.0	77.03	− 1.86	− 2.358
1.06	+ 0.0	78.89	+ 0.00	+ 0.000
1.33	+ 25.0	80.10	+ 1.21	+ 1.534
1.59	+ 50.0	81.01	+ 2.12	+ 2.687
Airframe				
d_{MLG} [m]	% of Change	EPNL [dB]	Diff. [dB]	% of Change
0.53	− 50.0	88.11	− 0.28	− 0.317
0.80	− 25.0	88.24	− 0.15	− 0.170
1.06	+ 0.0	88.39	+ 0.00	+ 0.000
1.33	+ 25.0	88.55	+ 0.16	+ 0.181
1.59	+ 50.0	88.74	+ 0.35	+ 0.396
Complete Aircraft				
d_{MLG} [m]	% of Change	EPNL [dB]	Diff. [dB]	% of Change
0.53	− 50.0	92.16	− 0.24	− 0.260
0.80	− 25.0	92.22	− 0.18	− 0.195
1.06	+ 0.0	92.40	+ 0.00	+ 0.000
1.33	+ 25.0	92.49	+ 0.09	+ 0.097
1.59	+ 50.0	92.58	+ 0.18	+ 0.195

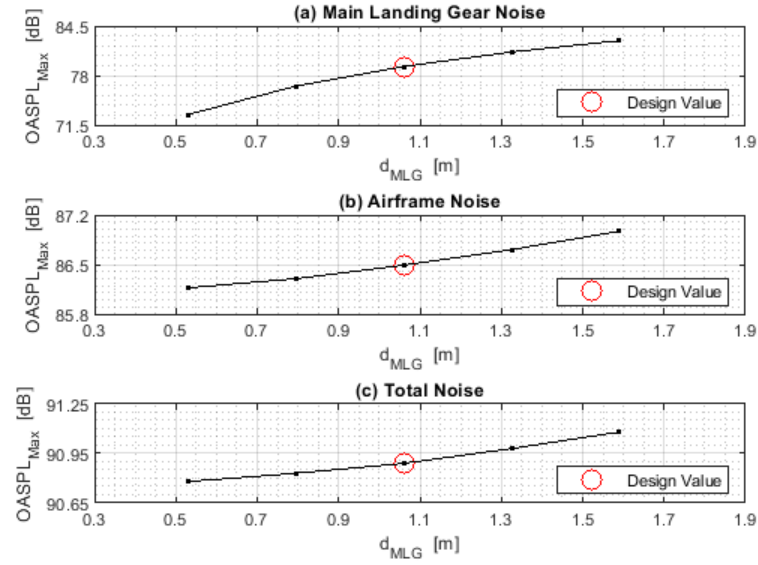


Figure 4.36: Changes in $OASPL_{Max}$ for different values of wheel diameter (the red circle marks the starting value): (a) variation in noise produced by the isolated main landing gear; (b) variation in total airframe noise; (c) variation in total aircraft noise. [ATTILA⁺⁺ v0.8.1]

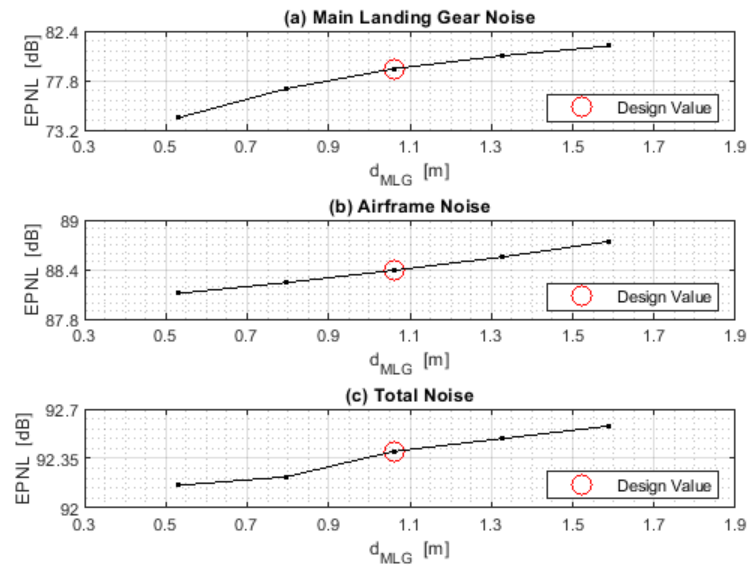


Figure 4.37: Changes in $EPNL$ for different values of wheel diameter (the red circle marks the starting value): (a) variation in noise produced by the isolated main landing gear; (b) variation in total airframe noise; (c) variation in total aircraft noise. [ATTILA⁺⁺ v0.8.1]

4.3.8 Effects of the number of main wheels

As anticipated above, this paragraph has the purpose of presenting the results of the analysis carried out by changing the number of main wheels. The parameter $N_{Wheel,MLG}$ to which we refer below does not represent the number of total wheels, but rather those mounted on a single main landing gear unit. This means that $N_{Wheel,MLG}$ is equal to half of the total wheels belonging to the complete undercarriage.

Figure 4.38 shows the *OASPL* values that would be recorded by the reference microphone in presence of only the main landing gear, for different numbers of wheels. Changes in airframe and total noise are shown in Figure 4.39 and Figure 4.40. The maximum calculated values of *OASPL* are also reported in Table 4.28 and Figure 4.41. Table 4.29 and Figure 4.42 report all the *EPNL* values of interest.

A doubling in the number of wheels causes an increase of 5.47 dB (+ 6.93 %) in the *EPNL* related to the isolated source, and an increase of 0.49 dB (+ 0.53 %) in the total *EPNL*. This means that a doubling in the number of wheels involves an increase in noise equal to twice the reduction caused by halving the diameter (see Table 4.27). By launching ATTILA⁺⁺ again with $N_{Wheel,MLG} = 4$ and $d_{MLG} = 0.53$ m (half of the original value), a slight increase in noise equal to 0.04 dB is obtained. In conclusion, it would not seem possible to derive any direct advantage (in terms of noise emissions) from preferring a greater number of wheels.

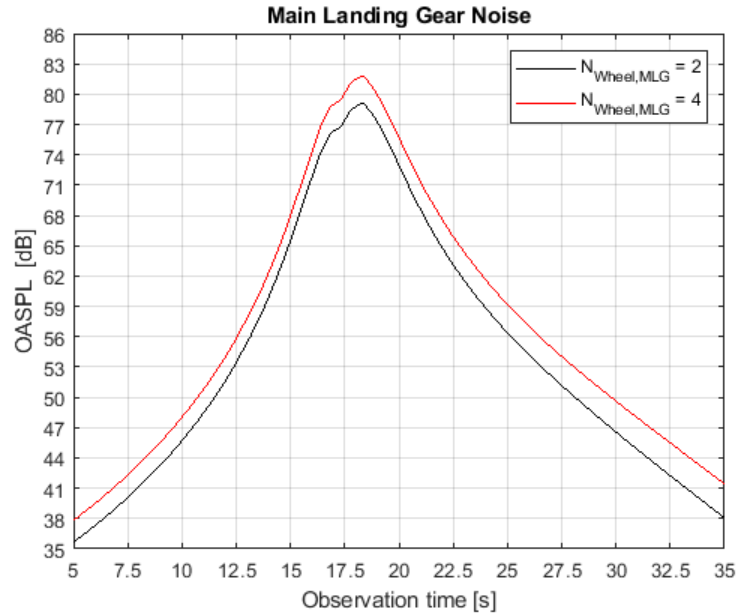


Figure 4.38: *OASPL* produced by the isolated main landing gear in Approach: (black) $N_{Wheel,MLG} = 2$ (starting value); (red) $N_{Wheel,MLG} = 4$. [ATTILA⁺⁺ v0.8.1]

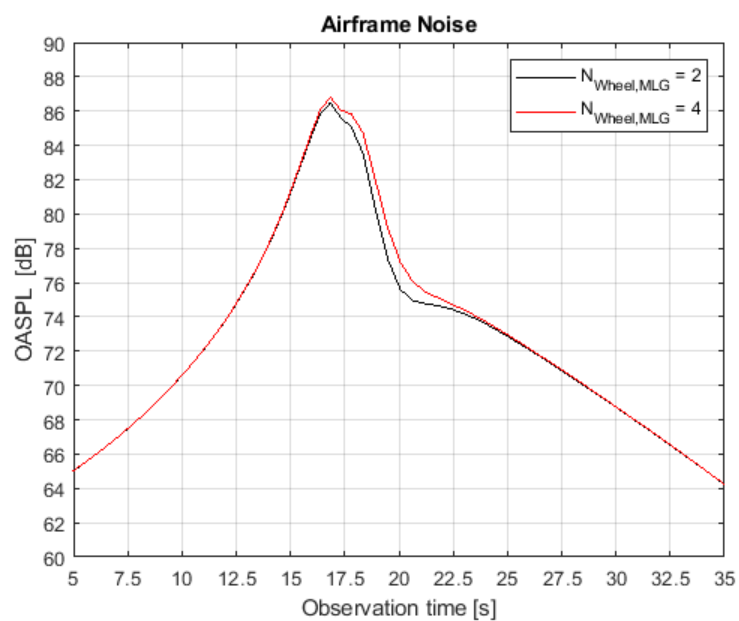


Figure 4.39: Airframe *OASPL* in Approach: **(black)** $N_{Wheel,MLG} = 2$ (starting value); **(red)** $N_{Wheel,MLG} = 4$. [ATTILA⁺⁺ v0.8.1]

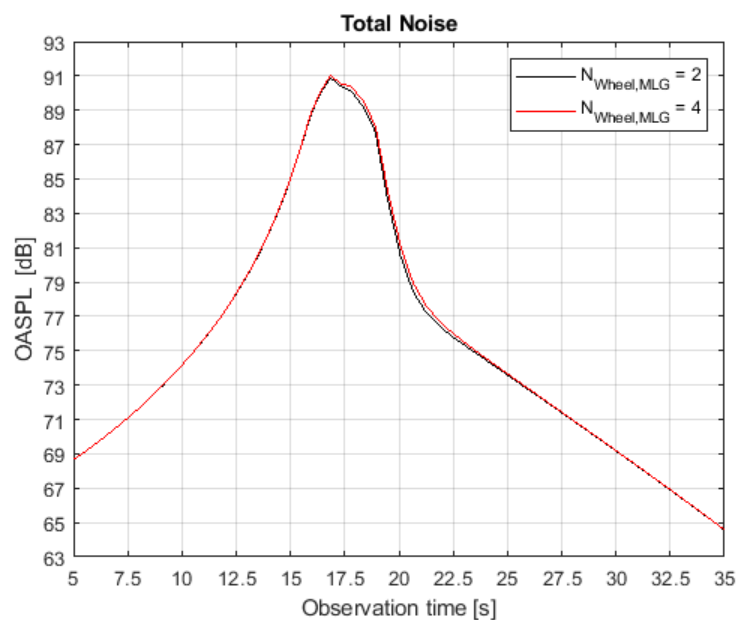


Figure 4.40: Total *OASPL* in Approach: **(black)** $N_{Wheel,MLG} = 2$ (starting value); **(red)** $N_{Wheel,MLG} = 4$. [ATTILA⁺⁺ v0.8.1]

Table 4.28: Changes in $OASPL_{Max}$ for different numbers of main landing gear wheels, with reference to the isolated main landing gear, the airframe and the complete aircraft. The original input data ($N_{Wheel,MLG} = 2$) is used as reference value. [ATTILA⁺⁺ v0.8.1]

Isolated Main Landing Gear				
$N_{Wheel,MLG}$	% of Change	$OASPL_{Max}$ [dB]	Diff. [dB]	% of Change
2	+ 0.0	79.18	+ 0.00	+ 0.000
4	+ 200.0	81.88	+ 2.70	+ 3.410
Airframe				
$N_{Wheel,MLG}$	% of Change	$OASPL_{Max}$ [dB]	Diff. [dB]	% of Change
2	+ 0.0	86.49	+ 0.00	+ 0.000
4	+ 200.0	86.81	+ 0.32	+ 0.370
Complete Aircraft				
$N_{Wheel,MLG}$	% of Change	$OASPL_{Max}$ [dB]	Diff. [dB]	% of Change
2	+ 0.0	90.89	+ 0.00	+ 0.000
4	+ 200.0	91.02	+ 0.13	+ 0.143

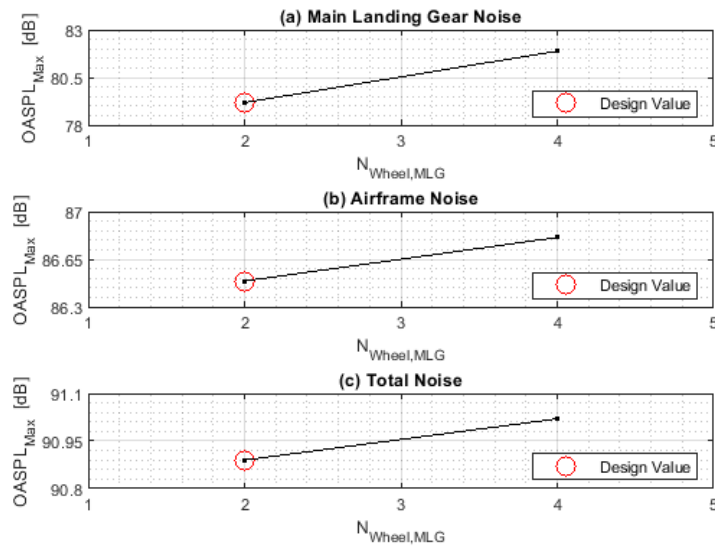


Figure 4.41: Changes in $OASPL_{Max}$ for different numbers of main landing gear wheels (the red circle marks the starting value): (a) variation in noise produced by the isolated main landing gear; (b) variation in total airframe noise; (c) variation in total aircraft noise. [ATTILA⁺⁺ v0.8.1]

Table 4.29: Changes in *EPNL* for different numbers of main landing gear wheels, with reference to the isolated main landing gear, the airframe and the complete aircraft. The original input data ($N_{Wheel,MLG} = 2$) is used as reference value. [ATTILA⁺⁺ v0.8.1]

Isolated Main Landing Gear				
$N_{Wheel,MLG}$	% of Change	EPNL [dB]	Diff. [dB]	% of Change
2	+ 0.0	78.89	+ 0.00	+ 0.000
4	+ 200.0	84.36	+ 5.47	+ 6.934
Airframe				
$N_{Wheel,MLG}$	% of Change	EPNL [dB]	Diff. [dB]	% of Change
2	+ 0.0	88.39	+ 0.00	+ 0.000
4	+ 200.0	89.66	+ 1.27	+ 1.437
Complete Aircraft				
$N_{Wheel,MLG}$	% of Change	EPNL [dB]	Diff. [dB]	% of Change
2	+ 0.0	92.40	+ 0.00	+ 0.000
4	+ 200.0	92.89	+ 0.49	+ 0.530

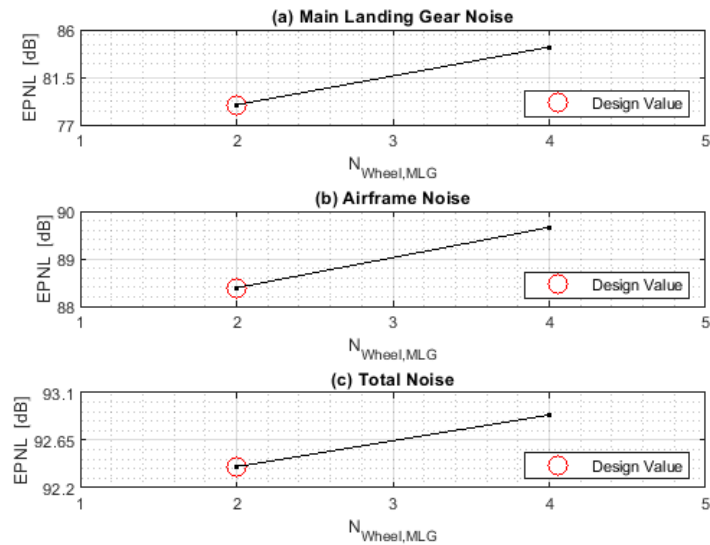


Figure 4.42: Changes in *EPNL* for different numbers of main landing gear wheels (the red circle marks the starting value): (a) variation in noise produced by the isolated main landing gear; (b) variation in total airframe noise; (c) variation in total aircraft noise. [ATTILA⁺⁺ v0.8.1]

4.3.9 Effects of the angle of descent

In this section we have considered the effects of the parameters that most influence noise in Approach conditions. It has been seen that in no case the reductions in total *EPNL* obtained by reducing the aerodynamic noise are comparable to those connected to the engine. Investing efforts in reducing engine noise remains the best way to make the acoustic footprint smaller, both on take-off and on landing. However, important milestones can be achieved by working on the overall aircraft configuration. For example, it is known that modifications of wing surface involve changes in aircraft stability, with the consequent need to modify also the tailplane. More generally, the value assumed by each design parameter is a constraint for the remaining ones, so it is possible to think of looking for the best combination of all of them that also optimizes noise emissions.

The aircraft trajectory, in this sense, plays a fundamental role. Both on take-off and on landing, it is the result of all the aerodynamic and propulsive characteristics of the aircraft, and can determine significant differences in the distance from the microphone. Due to the spreading effect, the *SPL* values decrease by about 6 dB for each doubling in the distance.

Therefore, in this last paragraph the attention will not be focused on the airframe noise, but rather to the effect of the angle of descent on the noise produced during landing. As seen in section 2.6.5, the legislation imposes a -3° path for testing in Approach conditions. However, the value of the angle of descent will be modified in order to stress the crucial importance of the trajectory (in any flight phase) on the noise perceived at ground level.

Trajectories shown in Figure 4.43 correspond to angles of -5° , -4° , -3° and -2° . Figure 4.44 shows the *OASPL* values that would be recorded by the reference microphone for different angles of descent. The maximum calculated values of *OASPL* and the values of *EPNL* are reported in Table 4.30 and Table 4.31. Figure 4.45 also shows all the values of interest.

Note in Figure 4.44 that although higher trajectories cause lower average *OASPL* values, they make higher levels more durable, which means that the reduction in *EPNL* is mitigated. Nevertheless, an increase of just 1° in the angle of descent causes a reduction in *EPNL* equal to -1.58 dB (-1.71%). This is truly remarkable, considering that, before now, an effect of this magnitude could be obtained only by changing the type of flaps (i.e. the number of slots). In conclusion, it is advisable to carefully evaluate the performances from the earliest aircraft design stages, avoiding that not optimal trajectories (especially at take-off) cause dramatic increases in noise emissions.

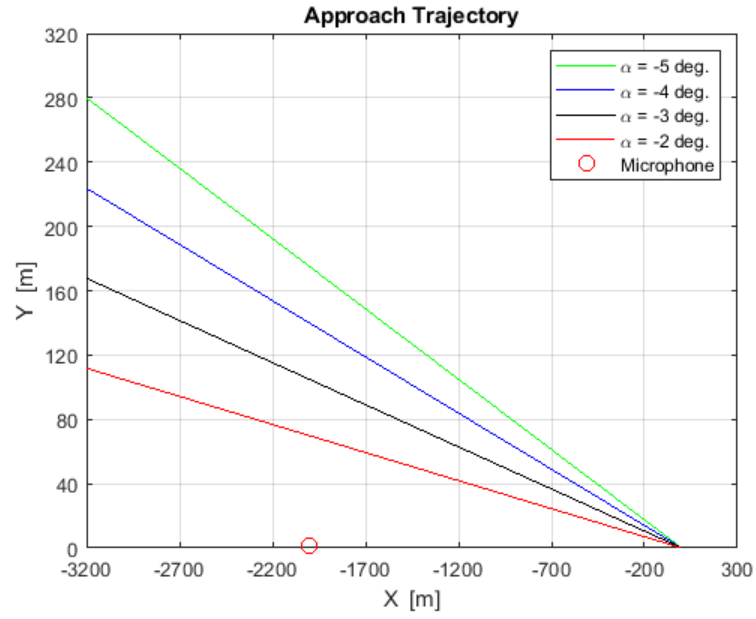


Figure 4.43: Different Approach trajectories: (green) $\alpha = -5^\circ$; (blue) $\alpha = -4^\circ$; (black) $\alpha = -3^\circ$ (starting value); (red) $\alpha = -2^\circ$. [ATTILA⁺⁺ v0.8.1]

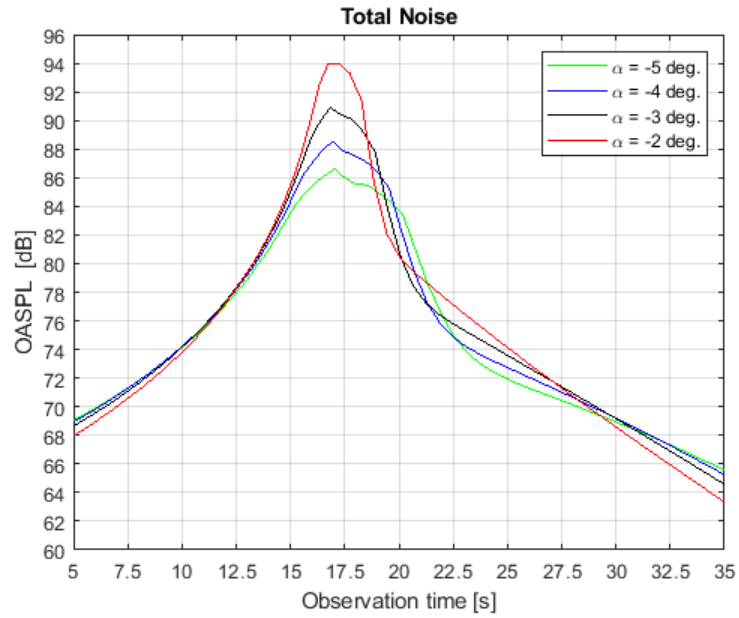


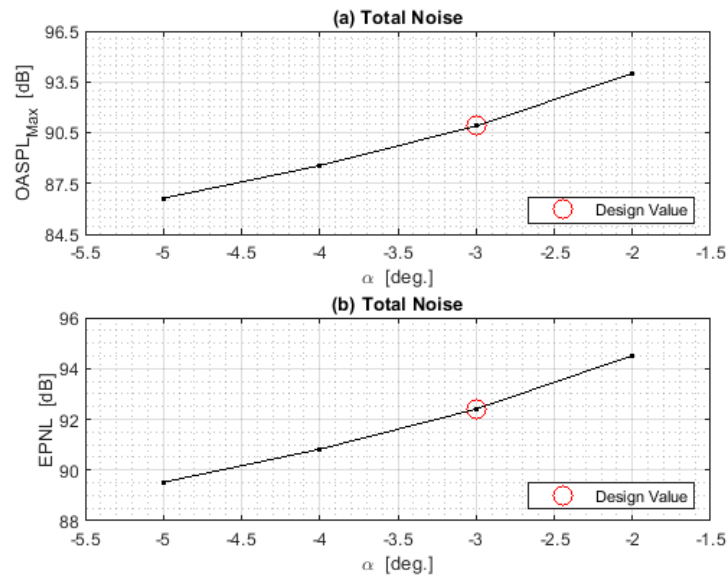
Figure 4.44: Total OASPL values in Approach: (green) $\alpha = -5^\circ$; (blue) $\alpha = -4^\circ$; (black) $\alpha = -3^\circ$ (starting value); (red) $\alpha = -2^\circ$. [ATTILA⁺⁺ v0.8.1]

Table 4.30: Changes in total $OASPL_{Max}$ for different angles of descent. The original input data ($\alpha = -3^\circ$) is used as reference value. [ATTILA⁺⁺ v0.8.1]

α [$^\circ$]	% of Change	$OASPL_{Max}$ [dB]	Diff. [dB]	% of Change
-5	- 66.6	86.62	- 4.27	- 4.698
-4	- 33.3	88.55	- 2.34	- 2.575
-3	+ 0.0	90.89	+ 0.00	+ 0.000
-2	+ 33.3	94.00	+ 3.11	+ 3.422

Table 4.31: Changes in total $EPNL$ for different angles of descent. The original input data ($\alpha = -3^\circ$) is used as reference value. [ATTILA⁺⁺ v0.8.1]

α [$^\circ$]	% of Change	$EPNL$ [dB]	Diff. [dB]	% of Change
-5	- 66.6	89.52	- 2.88	- 3.117
-4	- 33.3	90.82	- 1.58	- 1.710
-3	+ 0.0	92.40	+ 0.00	+ 0.000
-2	+ 33.3	94.51	+ 2.11	+ 2.284

**Figure 4.45:** Changes in total noise for different angles of descent (the red circle marks the starting value): (a) $OASPL_{Max}$; (b) $EPNL$. [ATTILA⁺⁺ v0.8.1]

4.4 Single-event noise contours

A *footprint*, more correctly called *single-event noise contour*, represents the locus of points around the source where the sound level is lower than a predetermined threshold. There is a wide variety of units of measurement that can be used to create these contours, such as the *EPNL*, the *sound exposure level (SEL)* or the maximum recorded *OASPL*.

The improvements provided to ATTILA⁺⁺ have made it possible to predict the perceived noise in a multitude of arbitrary points set by the user. In addition, the accuracy of the calculation has been improved when the microphone (or the aircraft) is placed outside the vertical plane containing the runway. This made it possible to calculate the *EPNL* in a grid of points. Therefore, by exporting the results in MATLAB^[24] it was possible to create the acoustic footprints of the A220-300 both in landing (Figure 4.46) and in take-off (Figure 4.47). The microphones relating to the three certification conditions are also shown. These footprints do not claim to faithfully represent reality, given the large number of hypotheses and approximations made. However, the likelihood of their shapes gives confidence that the most important radiation characteristics (especially the directivity functions) have been correctly represented. As a means of comparison, consider the footprint at take-off shown in Figure 4.48. Although it is only a qualitative representation, it is possible to appreciate the similarity with that generated by ATTILA⁺⁺.

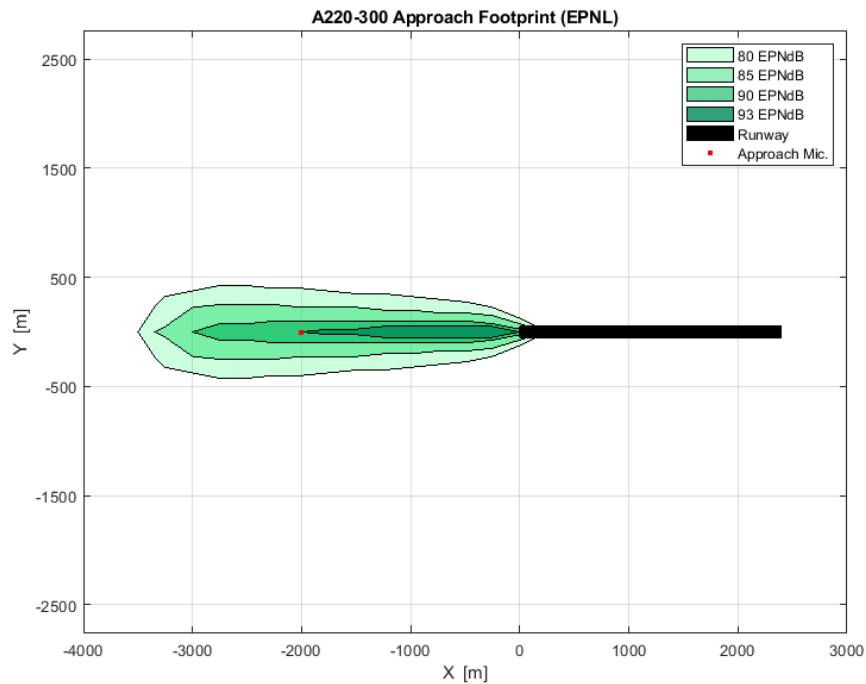


Figure 4.46: Landing footprint of the A220-300. [ATTILA⁺⁺ v0.8.1]

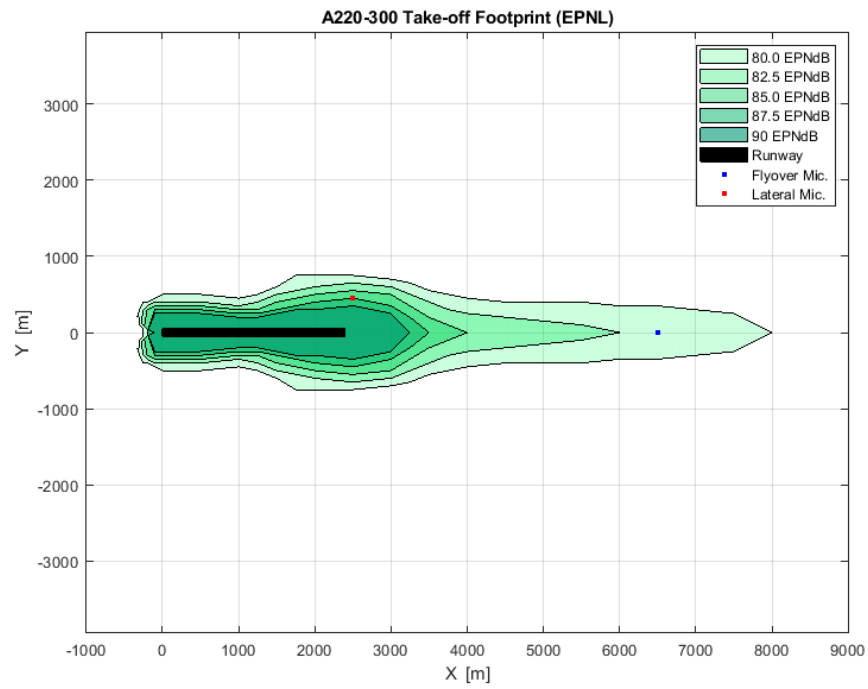


Figure 4.47: Take-off footprint of the A220-300. [ATTILA⁺⁺ v0.8.1]

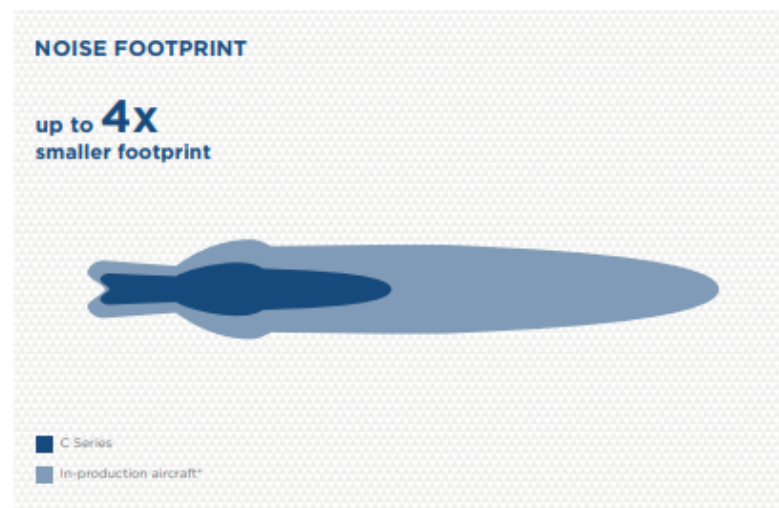


Figure 4.48: Qualitative representation of take-off footprint of the A220-300 ^[37].

5

Conclusions

5.1 Discussion of results

This thesis work was aimed at presenting the research work carried out by the candidate in developing a software for the prediction of aircraft noise. After recalling the main theoretical concepts useful for understanding the problem of sound emissions, Chapter 3 described the computer program ATTILA⁺⁺ developed at the University of Naples “Federico II”. Both the architecture and the functionalities of the software have been extensively described, with reference to the objectives and the requirements set within the ADORNO project. ATTILA⁺⁺, written in C⁺⁺ following the object-oriented programming paradigm (OOP), is currently able to estimate the noise emitted by a turbofan-powered aircraft, for any assigned trajectory and microphone position. In addition, the software is able to include the effects related to the diffusion of acoustic energy in the three-dimensional space, the atmospheric attenuation and the reflection of sound waves on the ground. Compared to the previous MATLAB version of the software, ATTILA⁺⁺ (v0.8.1) offers a wider opportunity to customize both the calculation conditions and the output files containing the results. In particular, the latest ability of the software to manage sources and receivers in a three-dimensional space opens up the possibility of studying the sound footprint left by the aircraft. The code is currently devoid of the ability to estimate the shielding effect and other secondary effects that intervene in the case of a listener placed laterally to the trajectory of the aircraft. As replacement, the program allows to correct the estimated sound pressure levels by means of an additional contribution known as lateral attenuation. Moreover, the program is limited to calculating aerodynamic noise, having to receive engine emissions as additional input.

Chapter 4 presented the results of a series of parametric analyses conducted on a specific regional aircraft. In the first instance, the noise levels produced in the

three phases envisaged by the certification authorities were assessed, verifying that the results coincided with the official values made public by EASA. Subsequently, it was concluded that limited variations in airframe noise had noticeable effects only during the approach to landing. Approach conditions were therefore taken as the main reference for the sensitivity analyses. Each parameter of interest has been varied by keeping the remaining data unchanged. By trying to vary the wing surface, it has been concluded that it is not possible to obtain a significant direct advantage in terms of aerodynamic noise. Much more important achievements could be obtained by working on high-lift devices. In particular, it has been shown that the use of triple-slotted flaps leads to an increase of 3.6 % (+ 3.2 dB) in total airframe noise and of 1.8 % (+ 1.7 dB) in the total *EPNL* compared to single-slotted or double-slotted flaps. Reducing the flap deflection by 10° resulted in a reduction of 0.34 % (− 0.3 dB) in the total *EPNL*. Changes in the overall flap sizes led to changes in the total *EPNL* in the order of 0.1 %. Finally, with reference to the main landing gear, it has been shown that doubling the number of wheels leads to an increase in the *EPNL* equal to 0.53 % (+ 0.5 dB), while halving the diameter allows a saving of 0.26 % (− 0.2 dB). It would therefore seem more advantageous to prefer a smaller number of larger wheels. It should be specified that all values refer to the direct effects of each component, but in reality a modification of one of the design parameters cannot be separated from further modifications involving any other characteristics or performances of the aircraft.

The author is aware of the fact that the results obtained do not faithfully represent reality, for a number of not mutually exclusive reasons. First, the methodologies employed by ATTILA⁺⁺ are based on a few simple geometric information; although they do not exhaustively describe the complexity of the acoustic radiation characteristics of a modern aircraft, they are sufficient to provide reliable estimates in the early design phases. Second, the results of parametric analyses can be considered valid only under the assumption that the real characteristics and sizes of the aircraft under analysis are not too different from those assumed here. Third, the radiation characteristics of the engine have not been estimated with sufficient accuracy.

Although the estimates produced by the software are affected by numerous causes of inaccuracy, the outcome of the work can be considered positive. The main purpose was to demonstrate the potential of ATTILA⁺⁺ and its ability to provide realistic estimates based on a modest number of input parameters that are easy to find even in the early stages of the aircraft design cycle. This was also done by demonstrating its ability to predict the acoustic footprints left by the aircraft during the take-off and landing phases. The obtained numerical results have made it possible to understand the relative weight of each component of the aircraft in the generation of noise. This, combined with the simplicity, the speed and the versatility of the software, opens the door to the integration of the thematic area of aviation acoustics into the aircraft design chain.

5.2 Future developments

In compliance with the specifications provided by the Topic Leader of the ADORNO project, work will be done to improve the technical and functional characteristics of ATTILA⁺⁺. We intend to further increase the versatility and customizability of the calculations, enriching the output content with additional noise metrics. In general, many efforts will be devoted to technically improving the program. In the near future, the software will be provided with the ability to exit clearly on errors. Furthermore, in order to allow an efficient diagnosis of problems, the program will report events and warnings in a log file.

With regard to the predictive capabilities of the software, the most important goal to be achieved is the implementation of an internal method for the evaluation of engine noise. UNINA's group is currently studying the problem of turbofan noise on the basis of ESDU item no. 98008 ^[26]. Subsequently, we intend to extend the applicability of ATTILA⁺⁺ to the case of propeller-driven aircraft, providing an estimate of propeller noise based on the theoretical model contained in ESDU item no. 95029 ^[33]. There is also the intention to introduce a method for estimating the shielding effect. It would improve the accuracy of noise estimations, including an additional effect which is usually taken into account at more advanced design stages than preliminary design. In addition, predicting the engine noise shielded by lifting surfaces would enable the analysis of unconventional aircraft configurations, such as H-tail or U-tail layouts with over-horizontal-tail-mounted engines, or over-wing mounted engines. A suitable solution consists in the adaptation of the methodology illustrated in ESDU item no. 79011 ^[32], which is currently under study.

Last but not least, it has already been scheduled in the context of ADORNO to experimentally validate the results provided by the aforementioned module for the estimation of the shielding effect. The main objective remains to provide partners with a stand-alone software for assessing the acoustic impact of an aircraft and, at the same time, a tool to be integrated into multi-disciplinary design optimization chains.

Bibliography

- [1] Horizon 2020 Programme, *Official Website* (Accessed on 14.06.2020): <https://ec.europa.eu/programmes/horizon2020/en>.
- [2] Horizon 2020, *Work Programme 2018-2020*. Link to PDF (Accessed on 14.06.2020): https://ec.europa.eu/research/participants/data/ref/h2020/wp/2018-2020/main/h2020-wp1820-transport_en.pdf.
- [3] Clean Sky 2 Programme, *Official Website* (Accessed on 14.06.2020): <https://www.cleansky.eu>.
- [4] European Commission, *Clean Sky 2 Joint Technical Programme*. Link to PDF (Accessed on 14.06.2020): https://ec.europa.eu/research/participants/data/ref/h2020/other/guide-appl/jti/h2020-guide-techprog-cleansky-ju_en.pdf.
- [5] Advisory Council on Aviation Research in Europe, *Strategic Research and Innovation Agenda (2012)*. Link to PDF (Accessed on 14.06.2020): <https://www.acare4europe.org/sites/acare4europe.org/files/document/ACARE-Strategic-Research-Innovation-Volume-1.pdf>.
- [6] ADORNO Project - Aircraft Design and nOise RatiNg for regiOnal aircraft, *Official Website* (Accessed on 14.06.2020): <http://www.adorno-project.eu/>.
- [7] University of Naples “Federico II”, *Official Website* (Accessed on 14.06.2020): <http://www.international.unina.it/>.
- [8] MTU Aero Engines, *Official Website* (Accessed on 14.06.2020): <https://www.mtu.de/>.
- [9] LeadTech, *Official Website* (Accessed on 14.06.2020): <http://www.leadtech.it/eng/>.
- [10] V. Trifari, M. Ruocco, V. Cusati, F. Nicolosi, and A. De Marco. Multi-disciplinary analysis and optimization java tool for aircraft design. *ICAS 31st Congress of the International Council of the Aeronautical Sciences, Belo Horizonte, Brazil*, September 2018.
- [11] F. Nicolosi, P. Della Vecchia, V. Trifari, M. Di Stasio, F. Marulo, A. De Marco, V. Marciello, and V. Cusati. Noise, emissions and costs trade factors for regional jet platforms using a new software for aircraft preliminary design. *AIAA Aviation and Aeronautics Forum and Exposition*, June 2020 (doi: <https://doi.org/10.2514/6.2020-2638>).

- [12] C. Casale, T. Polito, V. Trifari, M. Di Stasio, P. Della Vecchia, F. Nicolosi, and F. Marulo. Implementation of a noise prediction software for civil aircraft applications. *AIDAA XXV International Congress, Rome, Italy*, 9-12 September 2019.
- [13] G.J.J. Ruijgrok. *Elements of aviation acoustics*. Delft University Press, 2nd edition, 2004.
- [14] S. Farokhi. *Future Propulsion Systems and Energy Sources in Sustainable Aviation*. John Wiley & Sons, 2020.
- [15] International Civil Aviation Organization (ICAO), *Official Website* (Accessed on 14.06.2020): <https://icao.int>.
- [16] K.D. Kryter. The meaning and measurement of perceived noise level. *Noise Control*, 6(5):12–27, 1960.
- [17] International Civil Aviation Organization (ICAO). *Environmental Protection, Volume I – Aircraft Noise*. ICAO Annex 16, 5th edition, July 2008.
- [18] International Civil Aviation Organization (ICAO). *Environmental Technical Manual on the Use of Procedures in the Noise Certification of Aircraft*. 3rd edition, 2004.
- [19] Federal Aviation Administration (FAA). *Noise standards – Aircraft type and airworthiness certification*. Code of Federal Regulations, January 2003.
- [20] Engineering Sciences Data Unit (ESDU). *The correction of measured noise spectra for the effects of ground reflection, Item no. 94035*. ESDU International plc, London, UK, December 1995.
- [21] M.J. Lighthill. On sound generated aerodynamically i. general theory. *Proceedings of the Royal Society of London. Series A. Mathematical and Physical Sciences*, 211(1107):564–587, 1952.
- [22] M.R. Fink. *Airframe noise prediction method*. FAA-RD-77-29, March 1977.
- [23] A. Filippone. Aircraft noise prediction. *Progress in Aerospace Sciences, Elsevier*, 68:27–63, 2014.
- [24] MathWorks, MATLAB, *Official Website*. (Accessed on 14.06.2020): <https://it.mathworks.com/products/matlab.html>.
- [25] Southwest Research Institute, Numerical Propulsion System Simulation (NPSS), *Official Website*. (Accessed on 14.06.2020): <https://www.swri.org/consortia/numerical-propulsion-system-simulation-npss>.
- [26] Engineering Sciences Data Unit (ESDU). *Prediction of noise generated by fans and compressors in turbojet and turbofan engines, Item no. 98008*. ESDU International plc, London, UK, April 1998.

- [27] Engineering Sciences Data Unit (ESDU), *Official website*. (Accessed on 14.06.2020): <https://www.esdu.com>.
- [28] Engineering Sciences Data Unit (ESDU). *Airframe noise prediction, Item no. 90023*. ESDU International plc, London, UK, November 1990.
- [29] Engineering Sciences Data Unit (ESDU). *Evaluation of the attenuation of sound by a uniform atmosphere, Item no. 78002*. ESDU International plc, London, UK, April 1990.
- [30] Engineering Sciences Data Unit (ESDU). *Estimation of lateral attenuation of air-to-ground jet or turbofan aircraft noise in one-third octave bands, Item no. 82027*. ESDU International plc, London, UK, November 1993.
- [31] M.F. Heidmann. Interim prediction method for fan and compressor source noise. 1975.
- [32] Engineering Sciences Data Unit (ESDU). *Estimation of noise shielding by barriers, Item no. 79011*. ESDU International plc, London, UK, November 1993.
- [33] Engineering Sciences Data Unit (ESDU). *Prediction of near-field and far-field harmonic noise from subsonic propellers with non-axial inflow, Item no. 95029*. ESDU International plc, London, UK, February 1996.
- [34] European Union Aviation Safety Agency (EASA). *No. EASA.IM.A.570 for BD-500 (A220 SERIES)*. Type Certificate Data Sheets for Noise (TCDSN), June 2019.
- [35] Flickr, *A220-300 photo by Rami Khanna-Prade*. Link (Accessed on 14.06.2020): <https://www.flickr.com/photos/ramis-photos/43318611861/in/pool-a220-300/>.
- [36] Wikipedia, *Airbus A220*. Link (Accessed on 14.06.2020): https://it.wikipedia.org/wiki/Airbus_A220.
- [37] Bombardier, *CSeries brochure*. Link to PDF (Archived on 08.09.2015): <https://web.archive.org/web/20150908154642/http://commercialaircraft.bombardier.com/content/dam/Websites/bca/literature/cseries/Bombardier-Commercial-Aircraft-CSeries-Brochure-en.pdf.pdf>.
- [38] Pratt & Whitney, *PW1500G - GTF Commercial Engines*. Link to PDF (Accessed on 14.06.2020): <https://prattwhitney.com/-/media/project/pw/pw-internet/pwu/pwu/products/commercial/pw1500g.pdf?rev=b05b318b0d094c4f9e723690eb2e3a36>.
- [39] MTU Aero Engines, *Pratt & Whitney GTFTM Engines*. Link to PDF (Accessed on 14.06.2020): https://www.mtu.de/fileadmin/EN/7_News_Media/2_Media/Brochures/Engines/PW1000G.pdf.

- [40] GasTurb GmbH, *GasTurb. Official Website* (Accessed on 14.06.2020): <https://www.gasturb.de/>.
- [41] M.S. Howe. Noise produced by a sawtooth trailing edge. *The Journal of the Acoustical Society of America*, 90(1):482–487, 1991.
- [42] T.P. Chong and A. Vathylakis. On the aeroacoustic and flow structures developed on a flat plate with a serrated sawtooth trailing edge. *Journal of Sound and Vibration*, 354:65–90, 2015.